




2019

# The Regulation Of Egfr Signaling And Kras Tumorigenesis By Receptor Palmitoylation

Akriti Kharbanda

University of Pennsylvania, kharbandaakriti@gmail.com

Follow this and additional works at: <https://repository.upenn.edu/edissertations>

 Part of the [Biochemistry Commons](#), [Cell Biology Commons](#), and the [Molecular Biology Commons](#)

---

## Recommended Citation

Kharbanda, Akriti, "The Regulation Of Egfr Signaling And Kras Tumorigenesis By Receptor Palmitoylation" (2019). *Publicly Accessible Penn Dissertations*. 3225.

<https://repository.upenn.edu/edissertations/3225>

This paper is posted at Scholarly Commons. <https://repository.upenn.edu/edissertations/3225>

For more information, please contact [repository@pobox.upenn.edu](mailto:repository@pobox.upenn.edu).

---

# The Regulation Of Egfr Signaling And Kras Tumorigenesis By Receptor Palmitoylation

## **Abstract**

Non-Small Cell Lung Cancer (NSCLC) is often characterized by mutually exclusive mutations in epidermal growth factor receptor (EGFR) or KRAS. The mutual exclusivity of these mutations is due to synthetic lethality, revealing a potential therapeutic vulnerability if possible to selectively activate EGFR in KRAS mutant cells. This thesis work demonstrates a previously unidentified mechanism of EGFR signal regulation through palmitoylation, the addition of the 16-carbon palmitate. The palmitoyltransferase, DHHC20, catalyzes this palmitoylation to Cys1025, Cys1122 and Cys1034 on the C-terminal tail of EGFR. Loss of EGFR palmitoylation leads to hyperactivation of the receptor, but decreased cell growth of KRAS mutant cancer cells. While KRAS is still an elusive therapeutic target, here we report that disrupting EGFR palmitoylation by ablation of DHHC20 or expression of a palmitoylation-resistant EGFR mutant blocks tumorigenesis in a KRAS-driven mouse model of lung adenocarcinoma. Mechanistically, we show that in the presence of oncogenic KRAS, unpalmitoylated, active EGFR increases signaling through the MAP Kinase pathway while simultaneously reducing PI3K/AKT signaling leading to a severe decrease in expression of the central proliferation-associated transcription factor, Myc, similarly as impossible to therapeutically target as KRAS. We find that the dysregulation of EGFR palmitoylation from DHHC20 loss disrupts the delicate balance of MAPK and PI3K signaling leading to detrimental loss of Myc expression and subsequent loss of cell growth. Initially, we discovered that inhibiting EGFR palmitoylation increases sensitivity to the EGFR tyrosine kinase inhibitor, gefitinib, in cell lines specifically harboring mutant KRAS and interestingly, in cells harboring the drug-resistant EGFR gatekeeper mutation through a mechanism that is still unclear. We have now determined that inhibition of DHHC20 induces sensitivity of KRAS mutant cells to a clinically available pan-PI3K inhibitor, Buparlisib, more effective than gefitinib in inducing cell death by directly blocking the residual, necessary PI3K signaling. Thus, this previously unappreciated mechanism of receptor signaling modulation driven by the palmitoyltransferase, DHHC20, can be exploited to treat the currently incurable mutant KRAS NSCLCs.

## **Degree Type**

Dissertation

## **Degree Name**

Doctor of Philosophy (PhD)

## **Graduate Group**

Cell & Molecular Biology

## **First Advisor**

Eric S. Witze

## **Keywords**

EGFR Receptor Signaling, KRAS mutations, Lung Cancer

---

**Subject Categories**

Biochemistry | Cell Biology | Molecular Biology

**THE REGULATION OF EGFR SIGNALING AND KRAS TUMORIGENESIS BY  
RECEPTOR PALMITOYLATION**

Akriti Kharbanda

A DISSERTATION

in

Cell and Molecular Biology

Presented to the Faculties of the University of Pennsylvania

in

Partial Fulfillment of the Requirements for the

Degree of Doctor of Philosophy

2019

**Supervisor of Dissertation**

---

Eric Witze  
Associate Professor of Cancer Biology

**Graduate Group Chairperson**

---

Daniel Kessler  
Associate Professor of Cell and Developmental Biology

**Dissertation Committee**

Donita Brady (Chair)	Presidential Professor of Cancer Biology
Brian Keith	Professor and Dean of Biomedical Studies
Ronen Marmorstein	George W. Raiziss Professor
Costantinos Koumenis	Richard H. Chamberlain Professor of Research Oncology

## ACKNOWLEDGMENTS

First and foremost, I would like to express my deepest gratitude to **Dr. Eric Witze**, my mentor, for his patient guidance, encouragement and dedication to this research. I attribute much of my personal and scientific professional growth to you. Thank you for allowing me to chart my own translational path and for supporting my goals even though they did not always match yours.

I would like to express my greatest appreciation to my first scientific mentor, **Dr. Donald Kufe**, for endowing me with a true passion for science. Without his training and valuable guidance, I would not have gotten through my doctorate let alone even pursued the degree in the first place. Thank you for everything, Dr. Kufe!

I would like to extend my sincere thanks to **Dr. David Feldser** for his valuable training, constructive advice, insightful suggestions and important contributions throughout the course of this project.

I am indebted to my thesis committee, **Dr. Donita Brady, Dr. Brian Keith, Dr. Ronen Marmorstein and Dr. Costas Koumenis**, for the countless discussions, valuable suggestions and positive critiques that helped me finish this work to its fullest potential.

Special thanks **to my lab mates**, past and present.

My fellow Witze lab graduate students, thank you for the undying encouragement day in and day out. We made it together and I'm proud of all of us.

Kristin, you were truly the finest teacher for a new graduate student. I learned everything from you and could only hope throughout that I would become at least half the scientist you are. Thank you for your mentorship!

Nancy, you have been a nurturing and supportive colleague for the last two years. I am so very grateful for your kindness, support and assistance.

Thank you to the **Humans of BRB 7**. I would like to say that I had the most entertaining group of people surrounding me on a daily basis. So many adventures and stories to continuously laugh and reminisce about for the rest of my life. Truth be told, you all made losing my neurons worthwhile. Thank you for the unrelenting encouragement and making everyday enjoyable.

I would also wish to thank **Dr. Veronique Giroux** who was instrumental for my growth as a good scientist. Thank you for the unwavering guidance, support and entertaining conversations Vero!

**To Mom and Dad:** Words that can convey my gratitude to you do not exist. The closest thing I can say is that I would physically, mentally, emotionally would not be here without your support.

Mom, thank you for always being there to listen to me relentlessly rant about every little unfortunate event that is basically described as adult life. Thank you for being my doctor, psychiatrist and pharmacist all in one. Thank you for the words of wisdom that you bestowed on me when I was young and stupid that now came in handy at the darkest of times. I love you Mom!

Dad, you said it. Pagal Hone Do. You warned me not to do what I was going to do, but still supported me in every step I ever took, good or bad. Here I am, as pagal as can be, but always filled with pride that I followed my father's footsteps. This degree is as much yours if not more than it ever was mine. You are my superhero and I am truly excited to be Dr. Kharbanda Jr. I love you Papa!

**To my brother Anshul:** The only one who has and still believes that I am a hard worker and smart enough to be here. Thank you for continuously telling me that I could make it to when I needed to hear it most and for standing by my side even when I was a wreck.

**To Papa and Mummy Nair, and Appupa and Dadima:** Again, I do not have words to express the gratitude I have in my heart for your unconditional support. Thank you for your countless prayers, love, and blessings throughout this process. Appupa, your words of encouragement this last December kept me on my two feet. I would not have been brave enough to continue if it weren't for your wisdom and love. I love you all!

**To my brother-in-law Shrey:** You are my brightest star. Thank you for all the laughs and hugs and yes, the Playstation as well. You helped tame the stressful beast!

**To my husband Mohnish:** I think the only person who realizes the extent of the trauma of getting through a doctorate degree is the significant other and that is because the significant other is equally bearing the trauma. Thank you for being patient, endearing, responsible and my strong rock through the last few years. Thank you for cooking me dinner, giving me massages, making my coffee in the morning and basically doing all my chores for me. Thank you for loving me unconditionally, through my anger and frustration and stress and lack of sleep. I couldn't have done this without you. I love you Momo, today tomorrow and always.

To the sister I made in graduate school, **Sanika:** I don't have words to describe the mess I would be without you. You have stood by me through thick and thin; through rejections, failures and slippery ice ☺ and through all my personal mishaps. I thank God for the day I met you and our adventures together: hiking, eating, studying, stressing, laughing, dancing, singing, driving. I would not be standing here alive if it weren't for you. You pulled me through. I love you Sani!

To my fellow **BGS classmates**: It is decreed official, we are the most amazing class that the program will ever see. We had a great time together where ever and whenever we got together. From LIT Thursday Night HHs at Harvest to Pig Roasts to Super Bowl Parties to Piñata Fests and Halloween Extravaganzas and Migas and Ritas. You never forget the people with whom you went through your PhD, and I don't plan on forgetting any of you. Thanks for the comradery and support.

I dedicate this thesis to my cousin, **Ayesha**, who passed away at the age of 17 from lymphoma. You are the reason I strive to find a way. One day, we will, I promise. RIP  
beautiful child.



# ABSTRACT

## THE REGULATION OF EGFR SIGNALING AND KRAS TUMORIGENESIS BY RECEPTOR PALMITOYLATION

Akriti Kharbanda

Eric Witze

Non-Small Cell Lung Cancer (NSCLC) is often characterized by mutually exclusive mutations in epidermal growth factor receptor (EGFR) or KRAS. The mutual exclusivity of these mutations is due to synthetic lethality, revealing a potential therapeutic vulnerability if possible to selectively activate EGFR in KRAS mutant cells. This thesis work demonstrates a previously unidentified mechanism of EGFR signal regulation through palmitoylation, the addition of the 16-carbon palmitate. The palmitoyltransferase, DHHC20, catalyzes this palmitoylation to Cys1025, Cys1122 and Cys1034 on the C-terminal tail of EGFR. Loss of EGFR palmitoylation leads to hyperactivation of the receptor, but decreased cell growth of KRAS mutant cancer cells. While KRAS is still an elusive therapeutic target, here we report that disrupting EGFR palmitoylation by ablation of DHHC20 or expression of a palmitoylation-resistant EGFR mutant blocks tumorigenesis in a KRAS-driven mouse model of lung adenocarcinoma. Mechanistically, we show that in the presence of oncogenic KRAS, unpalmitoylated, active EGFR increases signaling through the MAP Kinase pathway while simultaneously reducing PI3K/AKT signaling leading to a severe decrease in expression of the central proliferation-associated transcription factor, Myc, similarly as impossible to therapeutically target as KRAS. We find that the dysregulation of EGFR palmitoylation from DHHC20 loss disrupts the delicate balance of MAPK and PI3K signaling leading to detrimental loss of Myc expression and subsequent loss of cell growth. Initially, we discovered that inhibiting EGFR palmitoylation increases sensitivity to the EGFR tyrosine

kinase inhibitor, gefitinib, in cell lines specifically harboring mutant KRAS and interestingly, in cells harboring the drug-resistant EGFR gatekeeper mutation through a mechanism that is still unclear. We have now determined that inhibition of DHHC20 induces sensitivity of KRAS mutant cells to a clinically available pan-PI3K inhibitor, Buparlisib, more effective than gefitinib in inducing cell death by directly blocking the residual, necessary PI3K signaling. Thus, this previously unappreciated mechanism of receptor signaling modulation driven by the palmitoyltransferase, DHHC20, can be exploited to treat the currently incurable mutant KRAS NSCLCs.

# TABLE OF CONTENTS

<b>ACKNOWLEDGMENTS</b> .....	<b>II</b>
<b>ABSTRACT</b> .....	<b>VI</b>
<b>CHAPTER 1: INTRODUCTION</b> .....	<b>1</b>
<b>Genesis</b> .....	<b>1</b>
<b>The Epidermal Growth Factor Receptor (EGFR)</b> .....	<b>2</b>
<b>KRAS and Myc: Critical Nodes in Cancer</b> .....	<b>9</b>
<b>Palmitoylation</b> .....	<b>18</b>
<b>Mouse Models of Lung Adenocarcinoma</b> .....	<b>29</b>
<b>References</b> .....	<b>33</b>
<b>CHAPTER 2: INHIBITION OF DHHC20 MEDIATED EGFR PALMITOYLATION CREATES A DEPENDENCE ON EGFR SIGNALING.</b> .....	<b>41</b>
<b>Abstract</b> .....	<b>41</b>
<b>Results</b> .....	<b>44</b>
<b>Discussion</b> .....	<b>65</b>
<b>Materials and Methods</b> .....	<b>74</b>
<b>References</b> .....	<b>81</b>
<b>CHAPTER 3: INDUCED SENSITIVITY TO EGFR INHIBITORS IS MEDIATED BY PALMITOYLATED CYSTEINE 1025 OF EGFR AND REQUIRES ONCOGENIC KRAS.</b> .....	<b>85</b>
<b>Abstract</b> .....	<b>85</b>
<b>Introduction</b> .....	<b>86</b>
<b>Results</b> .....	<b>87</b>
<b>Discussion</b> .....	<b>99</b>
<b>Materials and Methods</b> .....	<b>102</b>

<b>References .....</b>	<b>105</b>
<b>CHAPTER 4: BLOCKING EGFR PALMITOYLATION SUPPRESSES PI3K SIGNALING AND MUTANT KRAS LUNG TUMORIGENESIS .....</b>	<b>108</b>
<b>Abstract.....</b>	<b>108</b>
<b>Introduction.....</b>	<b>109</b>
<b>Results .....</b>	<b>110</b>
<b>Discussion .....</b>	<b>130</b>
<b>Materials and Methods.....</b>	<b>138</b>
<b>References .....</b>	<b>147</b>
<b>CHAPTER 5: DISCUSSION .....</b>	<b>151</b>
<b>Overview .....</b>	<b>151</b>
<b>Challenges .....</b>	<b>156</b>
<b>Future Ideas .....</b>	<b>176</b>
<b>Concluding Remarks.....</b>	<b>182</b>
<b>References .....</b>	<b>183</b>

# CHAPTER 1: Introduction

## Genesis

The epidermal growth factor receptor (EGFR) and its downstream signaling has been studied for decades establishing a textbook understanding of how EGFR signaling is modulated and how EGFR mutant disease arises. Similarly, KRAS signaling and mutant KRAS disease has been equally well-studied. Despite all this knowledge and subsequent clinical advances made in personalized therapy, there is still a highly remarkable unmet clinical need to treat KRAS-driven non-small cell lung cancer (NSCLC), which still remains refractory to pharmacological inhibition. In fact, NSCLC remains the leading cause of cancer related death with a mortality rate of 1.6 million annual deaths worldwide, especially for those with a KRAS mutation. **(1)** Upon entering graduate school, I believed that I understood EGFR and KRAS signaling to the fullest extent. However, I discovered that there was still much to learn. Some well-studied post-translational modifications of EGFR include phosphorylation of the C-terminal tyrosines and N-terminal glycosylation. Palmitoylation of EGFR had never been studied. I sought to determine the role of EGFR palmitoylation and as a cancer biologist, to determine how palmitoylation of EGFR affected receptor signaling capacity in a disease setting. I found an exciting role of EGFR palmitoylation in governing mutant KRAS tumorigenesis. The goal quickly became to identify a targetable means to manipulate EGFR palmitoylation to eradicate mutant KRAS NSCLC. I trust that this thesis can convince the scientific community of the extraordinary ability of palmitoylation to regulate EGFR signaling. I hope the proposed mechanism will cultivate new therapeutic strategies to revolutionize outcomes in patients with KRAS-driven NSCLC in the near future.

# The Epidermal Growth Factor Receptor (EGFR)

## Regulation of EGFR

Receptor tyrosine kinases (RTK) are widely deregulated in cancer, including breast, lung, pancreatic and colon cancer. Furthermore, increased RTK signaling contributes to a variety of human malignancies. Members of the ErbB family play critical roles in response to extracellular growth cues and initiating downstream signaling cascades through effector pathways **(2-4)**. The epidermal growth factor receptor (EGFR) is one of four members of the ErbB family and is known to facilitate tumorigenesis and cancer progression.

Almost all cell types, except hematopoietic cells, possess EGFR or another ErbB family member to maintain normal developmental and maturation processes. EGFR is structurally composed of an extracellular ligand binding domain, a transmembrane region, a tyrosine kinase domain, and an unstructured C-terminal tail that harbors receptor auto-phosphorylation sites **(5)**. Ligands including the epidermal growth factor, EGF, bind to the extracellular domain of EGFR leading to a conformational change that facilitates homo- and heterodimerization with members of the ErbB family **(5)**. Subsequently, tyrosine kinase activity of the receptor is initiated leading to auto-phosphorylation of C-terminal tyrosines. The phosphorylated tyrosine residues serve as docking sites for adaptor proteins that link the receptor to downstream signaling pathways including Ras-Raf-MEK-ERK, PI3K-AKT, Src and JAK-STAT culminating in the regulation of cell migration, proliferation and survival **(5)**.

EGFR signaling is in part mediated by receptor clathrin-mediated endocytosis. In response to stimulation, EGFR is trafficked through early and late endosomes in route to lysosomes for signal termination and ubiquitin-mediated receptor degradation, and/or

recycling. Studies have suggested that activated EGFR can continue to signal from endosomes, indicating that there may be pathways that actively require EGFR endocytosis (6). Furthermore, studies have shown the distinct localization of EGFR in the nucleus and the presence of this nuclear EGFR correlates with the proliferation status of cells in certain tissues, such as the regenerating liver. There is now evidence to support a role of nuclear EGFR as a transcription factor to activate genes required to regulate the cell cycle (7). Despite the decades of study on EGFR receptor, there are still pieces to the complex signaling scheme that further investigation.

### **EGFR and Lung Cancer**

Lung cancer is the leading cause of cancer related mortality in the United States, with an estimated 234,030 new cases and 154,050 deaths in 2018. About 85% of lung cancers are non-small cell lung cancers (NSCLC). The largest subset of NSCLC, lung adenocarcinoma (LUAD), is the most common type of lung cancer seen in non-smokers and is particularly aggressive. LUAD is characterized by many driver mutations. The most frequent mutation being an activating mutation in EGFR closely followed by an activating mutation in KRAS. These two oncogenic mutations in NSCLC are mutually exclusive, they do not exist together. Activating and amplifying EGFR mutations are involved in progression of triple-negative breast cancer (TNBC), pancreatic and colorectal cancer, and glioblastoma multiforme. However, due to the integral connection between EGFR mutations and lung cancer progression, LUAD is often used to study EGFR and the molecular mechanisms that drive EGFR-driven tumorigenesis.

In the clinic, patients diagnosed with LUAD are tested for these two particular driver mutations so that therapy can be effectively chosen. If a patient has an EGFR or another receptor, such as ALK, mutation, patients are treated with targeted therapy in

the form of tyrosine kinase inhibitors (TKIs) as first-line treatment. Second-line therapy is using TKIs in combination with radiation or chemo. Finally, when all else fails, patients are enlisted into clinical trials for new targeted therapies being developed. Contrastingly, if a patient has a KRAS mutation, the only first-line therapy available is chemotherapy or a suitable clinical trial. There are no targeted therapies currently available for mutant KRAS LUAD. As such, if a patient has a KRAS mutation, survival prognosis is poor.

### **EGFR Oncogenic Mutations and Tyrosine Kinase Inhibitors (TKIs)**

As discussed, dysregulation of EGFR is a common event in cancer, specifically LUAD. Mutations causing amplification or constitutive activation of EGFR that enhance signaling and drug resistance have been identified in breast and lung cancer **(3)**. Activating EGFR point mutations in exon 21, such as L858R, and deletions of exon 19 are often predictors of response to EGFR TKI therapy with Gefitinib or Erlotinib **(8)**. While most EGFR mutations commonly reside within the extracellular (EGFR-vIII) and kinase (L858R, T790M) domains, recent studies identified EGFR mutations within the C-terminal tail **(9)**. Deletion of EGFR exons 25-27 was recently identified in lung cancer and glioblastoma multiforme **(10-12)**. Studies showed that ectopic expression of EGFR lacking exons 25 and 26 promotes anchorage-independent colony formation and increases ligand-independent EGFR and AKT activation. Furthermore, deletion of exons 25-27 confers EGFR TKI sensitivity in glioblastoma xenograft assays **(10,12)**. However, the mechanism of regulation of EGFR through these sites and how loss of these sites leads to constitutive receptor activation remained unknown.

Although patients with NSCLCs harboring activating EGFR mutations initially respond well to EGFR TKIs, the majority of these patients relapse within 10 to 16 months of treatment **(13,14)**. In over half of these patients, resistance to EGFR TKI



therapy is associated with the acquisition of a secondary T790M mutation in the EGFR tyrosine kinase domain. The T790M mutation alters interaction of reversible TKIs with the ATP-binding pocket **(8,15)**. Research focus has shifted to clinically validating a new generation of EGFR TKIs, such as Afatinib, that irreversibly inhibit the EGFR kinase domain as new first-line therapy **(16-17)**. Recently, there has been development of new mutant selective pyrimidine-based third-generation EGFR-TKIs, which irreversibly block T790M-mutant and Exon19 deletion-mutant of EGFR, revealing the potential to overcome drug resistance. However, acquired resistance to these new EGFR TKIs after prolonged use is effusively predicted **(18)**. Significant efforts are still underway to define first-line therapeutic strategies that maximize patient survival; potentially, combining EGFR TKIs with new targeted agents or targeting alternative pathways that feed into mutant EGFR dependency.

### **EGFR Downstream Pathways**

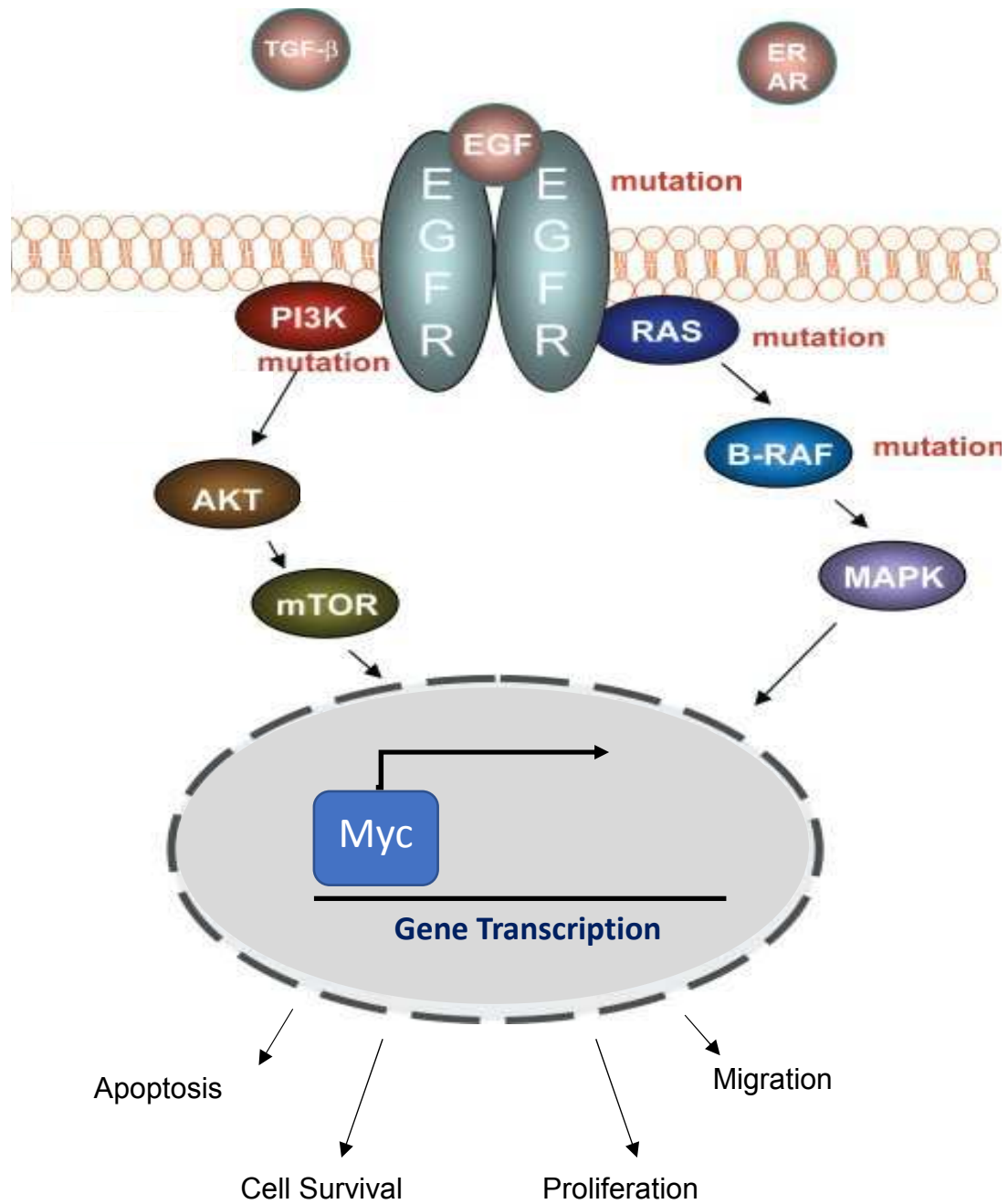
The phosphorylated tyrosine residues of EGFR serve as docking sites for adaptor proteins which link the receptor to downstream signaling pathways, mainly Ras-Raf-MEK-ERK (MAPK) and PI3K-AKT pathway **(5)**. The adaptor protein Grb2 and the guanine nucleotide exchange protein, Sos, link active EGFR to RAS. RAS initiates a cascade through several MEK protein kinases ultimately leading to the phosphorylation of MAPK, also known as ERK. Activated ERK then translocates to the nucleus to transactivate transcription factors leading to reprogramming of the transcriptional profile of the cell to promote growth, differentiation or mitosis **(19)** (Figure 1).

Similarly, activated EGFR directly stimulates the PI3K catalytic subunit, p110alpha bound to EGFR via the regulatory subunit, p85 or other less prevalent adapter molecules. Active PI3K then facilitates conversion of several phospholipid

components in the plasma membrane leading to phosphorylation of AKT at threonine 308 (T308) priming and partially activating AKT. Phosphorylation of AKT at serine 473 (S473) in the hydrophobic carboxy-terminal motif anchored in the plasma membrane by mTOR kinase leads to full activation of AKT. Fully active AKT initiates substrate-specific phosphorylation events in the cell promoting growth, survival, transcription, and apoptosis programs **(20)**.

Ligand binding to EGFR stimulates a multitude of other signaling cascades perhaps to a lesser extent or in conjunction with RAS/MAPK and/or PI3K/AKT activation. A few examples of these parallel signaling cascades are the JAK/STAT pathway and the PLC-1-PKC pathways. Similar to the main signaling cascades, the Janus Kinases (JAKs) transmit their signal through a cascade of phosphorylation events to eventually activate the Signal Transducer and Activator of Transcription (STAT) proteins. STATs translocate to the nucleus where they act as transcription factors. The growth factor ligands or signals to activate the PLC-gamma-1/PKC pathway are slightly different in that the main goal of this pathway is to induce intracellular calcium release. As expected, this cascade is necessary for vasculogenesis, fibroblast transformation, muscle fiber contraction and neuronal activity. EGFR or another dimerized ErbB family receptor phosphorylates PLC-1 at specific tyrosines. Once the receptor recruits PLC-1 to the plasma membrane and activates the protein, PLC-1 hydrolyzes PIP2 in the membrane into free intracellular 1,4,5-triphosphate (IP3) and diacylglycerol (DAG). These secondary messengers, IP3 and DAG, bind to IP3-receptors at the endoplasmic reticulum to induce intracellular calcium release **(21)**. This multitude of complex cascades clearly demonstrates the powerful capacity of one receptor, EGFR, to combine and transmit a complex array of signals through protein cross-talk culminating at the appropriate growth response.

In human cancers, both the MAPK and the PI3K-AKT pathways are commonly mutated and these mutations are sufficient for cell transformation. Mutations in KRAS, predominantly an amino acid substitution at codon 12 or 13, lead to upregulation of the KRAS/MAPK signaling and ERK activation to drive cell division. Similarly, the PI3K pathway is often mutated in the p110 $\alpha$  catalytic subunit (*PIK3CA*) in multiple domains, such as E545K in the helical domain and H1047R in the catalytic domain, leading to activation of AKT and promoting cell survival **(22)**. While mutations in RAS are common in cancer, it has been challenging to therapeutically target RAS directly. The initial consideration for anti-RAS therapy were developing GTP antagonists, which failed because of the RAS nucleotide-binding pocket's very high affinity for GTP. As such, efforts have been made to target the analogous ATP-binding pocket of RAS downstream effector kinases, but these therapies often lead to paradoxical activation of neighboring proliferation pathways or drug resistance **(23)**. PI3K inhibitors, in turn, are currently used in the clinic and more PI3K inhibitors are under clinical investigation. However, PI3K inhibition has been challenging due to the compensatory effect of the various isoforms of the catalytic subunit of PI3K, p110. As a result, single-agent clinical efficacy has been modest at best **(24)**. Efforts are being directed towards investigating PI3K inhibitors in combination with different therapeutic agents.



**Introduction Figure 1:** Simplified EGFR signaling pathway. Ligands are EGF, TGF- $\beta$ , and Epiregulin (ER). The two main pathways are the PI3K/AKT/mTOR and RAS/RAF/MAPK cascades which transmit extracellular stimuli into the cell to promote cell survival and proliferation. Activating mutations in EGFR and downstream effectors (red) lead to lung tumorigenesis. Both pathways lead to regulation of the cell proliferation associated transcription factor, Myc. Figure modified from (66).

# KRAS and Myc: Critical Nodes in Cancer

## Understanding KRAS

The RAS family of proteins encompass three members, NRAS, HRAS and KRAS, encoded for by oncogenes of the same name. Oncogenic NRAS and HRAS mutations exist in various tumor types, however, KRAS is the most commonly mutated member of the RAS family. In fact, *KRAS* was one of the first human genes to be labeled as a putative oncogene and is now known as one of the most frequently mutated oncogenes in cancer. The *RAS* genes encode small GTPases, which are turned on and off by transitioning between GDP or GTP-bound states in response to stimulation of receptors, such as EGFR. The GTPases are composed of: (i) an N-terminal lobe or the effector lobe, which has two switch regions to modulate RAS binding to effectors and regulators downstream, such as RAF and more recently suggested, PI3K. (ii) The catalytic domain of Ras proteins, which shares more than 90% sequence identity across the three family members. And (iii) The C-terminal lobe containing the hypervariable region (HVR), which as suggested is the most variable between the RAS family members and is particularly involved in RAS membrane association and localization (25). The association of RAS to the membrane is critical for its function because at the membrane RAS can bridge extracellular cues from receptors into the important cellular events, such as cell growth, proliferation, differentiation, and survival.

The variation in the HVR between NRAS, HRAS and KRAS defines the unique compartmentalization and membrane localization that may explain specificity in the functions between the three family members. Every RAS protein contains a cysteine in the HVR that is farnesylated, the addition of a 15-carbon hydrophobic fatty acid chain, during post-translational processes. HRAS and NRAS are also palmitoylated on other

HVR cysteine residues. The *KRAS* oncogene encodes two isoforms of KRAS, KRAS-4a and KRAS-4b, through mRNA splice variation. Interestingly, only KRAS-4a is palmitoylated in addition to the C-terminal farnesylation whereas the KRAS-4b HVR has a strong positive charge allowing a favorable interaction with the negatively charged phospholipids in the plasma membrane. As will be discussed in the next section, palmitoylation is the addition of a 16-carbon hydrophobic fatty acid chain, which is very similar to farnesylation except for the fact that palmitoylation is reversible whereas farnesylation is not. These are two dedicated localization signals driving RAS to the membrane, but the reversibility of palmitoylation also allows for removal of RAS from the membrane when the protein needs to be recycled or degraded **(26)**.

### **KRAS Mutations**

Given the cell proliferation driving events following RAS activity, it is no surprise that alterations in *RAS* are responsible for the transition of healthy cells to malignant cells, defined by uncontrolled growth. In addition to the frequent mutation of *RAS* genes occurring in many type of cancers, there are molecular alterations of many other components downstream of RAS, such as RAF **(27)**. Early studies on the RAS family of proteins clearly indicated that different human tumor types showed preferential oncogenic activation of a specific RAS. NRAS mutations occur at a high-frequency in acute leukemias and neuroblastomas. HRAS mutations are common in thyroid and bladder cancers. KRAS mutations occur at a very high frequency in pancreatic, colon and lung cancer, whereas in these tumor types HRAS and NRAS mutations are extremely rare **(28)**. Both KRAS splice variants are conserved across mammalian genomes and are ubiquitously expressed in normal tissue types, but studies indicate that KRAS-4a and KRAS-4b also act differently in different physiological contexts. For

example, some studies demonstrated that KRAS-4a is expressed at greater levels than KRAS-4b in colorectal-derived tumor cell lines and in primary human colorectal adenocarcinoma tissues **(29)**. More importantly, in vivo *lung* oncogenesis may be mediated by mutant KRAS-4a whereas mutant KRAS-4b alone is insufficient to initiate tumorigenesis **(26)**. However, as both KRAS-4a and KRAS-4b are oncogenic when *KRAS* is mutated, there is no evidence to suggest that one splice variant is more oncogenic than the other.

As mentioned, mutations in *KRAS* frequently define some of the cancers that are particularly aggressive, including Pancreatic Ductal Adenocarcinoma (PDAC), colorectal cancer (CRC) and NSCLC. Studies indicate that *KRAS* mutations occur early in PDAC progression and in fact, *KRAS* mutations might be the driving mutation in PDAC tumorigenesis followed by loss of the tumor suppressor p53 for the transition from premalignant lesions to adenocarcinoma. Although not as evidenced as in PDAC studies, studies of CRC have suggested that *KRAS* mutations may also be early events driving progression from premalignant polyps to full-blown CRC. Regardless, *KRAS* mutations are detected in 45% of all CRC diagnoses samples showing that *KRAS* is clearly an important protein for tumor development **(30)**. NSCLCs also display a high frequency of *KRAS* mutations, specifically about 25-30% of all NSCLCs patients show indication of a *KRAS* mutation. As formerly discussed, most *KRAS* mutations occur in codon 12 or 13 where the glycine (G) coded for in either codon is mutated to code for commonly aspartate (D), valine (V) or cysteine amongst others. Particularly, G12C, G12V and G12D account for about 80% of all *KRAS* mutations especially in generation of NSCLCs **(27)**. These mutations result in a conformation of *KRAS* that lead to stabilization of GTP binding to the small GTPase. The GTP cannot be hydrolyzed to

GDP thereby leaving KRAS in a constitutively active state driving constitutive activation of the downstream MAPK cascade.

### **Targeting KRAS**

Due to the clear relationship between KRAS mutations and progression of aggressive malignancies, many have sought to generate therapies that block KRAS activity. However, direct pharmacologic inhibition of KRAS at the nucleotide-binding pocket has been extremely difficult compared to inhibiting other kinases with a similar ATP-binding pocket. This is due to the extremely high affinity of GTP to RAS in stoichiometric ranges far below the efficacious concentrations of a small molecule in a human body.

Alternatively, the community shifted gears to work towards indirectly targeting steps of RAS activation particularly its necessity to be at the plasma membrane. As farnesylation of the HVR of RAS is one of the membrane localization signals, efforts were directed towards generating inhibitors to block RAS farnesylation. This effort brought about the discovery of the farnesyltransferase protein that catalyzes the modification and generation of farnesyltransferase inhibitors (FTIs). However, it was found that FTIs did not inhibit the activity of the most commonly mutated RASs in tumors, KRAS and NRAS, due to the presence of other compensating transferases, such as the geranylgeranyltransferase, and other compensating, membrane-localizing lipid modifications, such as palmitoylation **(31)**.

Many groups have recently discovered and developed small molecule modulators of RAS using the protein crystal structure as a guide. Some of these modulators are able to bind RAS and block necessary protein-protein interactions, such as the interaction with the guanine exchange factor, SOS, or the interaction with RAF. However, these small molecules have other impediments, such as their weak affinity to



RAS, their lack of selectivity to specific RAS family members and the lack of specificity to mutant RAS especially. More recent efforts are geared toward the development of highly selective and potent inhibitors of different downstream RAS effectors, such as RAF, MEK, ERK, PI3K and AKT inhibitors, but the hurdle here is the possible activation of compensatory pathways or generation of secondary mutations with prolonged use of these inhibitors.

While targeting RAS itself or specific RAS effector pathways is one rational therapeutic strategy, an alternative approach is to exploit the concept of synthetic lethality, in which vulnerable gene products are identified that when inhibited cause cell death only in the presence of an oncogenic mutation. Thereby, manipulating synthetic lethal targets in cancer may reduce the potential for side effects as cells harboring oncogenic mutations will be particularly sensitive to the manipulation compared to normal cells that don't have the mutation. Many groups have shifted their focus to identifying these synthetic lethal targets in mutant KRAS conditions. In KRAS-mutant tumors, oncogenic KRAS signaling alters the state of the cell by inducing KRAS effector signaling, adapting to oncogenic stress, and reprogramming of transcription and the metabolism **(32)**. The key to synthetic lethality is identifying these reprogrammed targets that when inhibited will disrupt this new KRAS-driven cell state and subsequently impair the proliferation of these KRAS-mutant cells.

Studies have shown that KRAS mutant cells acquire an increased dependence on RTK signaling pathways. Interestingly, specifically in NSCLC, mutations in the RTK, EGFR, are mutually exclusive with mutations in KRAS. Contrastingly, mutations in PI3K are not mutually exclusive with either EGFR or RAS. The explanation canonically understood for the mutual exclusivity is that both components signal in the same or

overlapping pathways, and hence are functionally redundant. However, more recent studies show that oncogenic mutations in both EGFR and KRAS in the same cell leads to cellular death. Activating EGFR<sup>L858R</sup> mutation was expressed in lung adenocarcinoma cells harboring an activating KRAS<sup>G12D</sup> mutation and vice versa. Co-expression of the two activating mutations led a significant decrease in lung adenocarcinoma cell viability **(33)**. This inhibition of growth due to perturbation of both these genes has been identified as synthetic lethality. Synthetic lethality explains the mutually exclusivity of EGFR and KRAS mutations and why the presence of both mutations is selected against in tumor development. However, the underlying molecular mechanisms that cause this synthetic lethality are still unknown **(33)**. The presence of mutant EGFR has proven to be a potential vulnerability in the mutant KRAS cell state, however, this vulnerability still poses a major challenge in terms of therapy. The challenge resides in developing a drug that will activate rather than inhibit EGFR in mutant KRAS tumor cells.

Despite the valiant efforts being made, there are still no clinically available drugs with anti-cancer efficacy that target RAS proteins directly or act on RAS-driven human cancers. Tumors harboring RAS mutations still remain the most difficult to treat, are usually excluded from targeted therapy treatment and represent a poor survival prognosis.

### **New Understanding of Oncogenic KRAS Signaling**

The RAS community understands that Ras GTPases function as binary molecular switches, cycling between inactive GDP-bound and active GTP-bound states. In the basal state, Ras is predominantly GDP bound but activation of a receptor tyrosine kinases (RTK) recruits guanine nucleotide exchange factors (GEF), such as SOS, to promote the exchange of bound GDP for GTP on nearby Ras molecules. The oncogenic

mutations of *RAS* lead to constitutively active *RAS* with an impaired rate of GAP-mediated GTP hydrolysis and consequently deregulated *RAS* signaling. In this case, it is commonly assumed that mutant *KRAS* is active and no longer requires the activity of an RTK, such as EGFR. In fact, clinical studies show that having oncogenic *KRAS* mutations predict resistance to TKIs; hence, treatment options for *KRAS* mutant cancers do not include the use of TKIs. However, a new understanding of mutant *RAS* regulation has recently surfaced. Although there is a mutation in one allele of *RAS* rendering it mutant, the remaining 2 isoforms of *RAS* remain wildtype and subject to regulation by GAPs and GEFs. These isoforms are thereby contributing to the overall *RAS* signaling output. Recent studies have discovered distinct roles for oncogenic and wildtype *RAS* in regulating signaling in cancer cells harboring oncogenic *RAS* mutations. They show that oncogenic *RAS* regulates the basal signaling, but unexpectedly wildtype *RAS* regulates the growth factor dependent signaling. Thereby, although oncogenic *RAS* is constitutively activating MAPK signaling, activation of EGFR, for example, can further enhance this signaling by stimulating GTP loading onto wildtype *RAS*. Furthermore, the study suggests that oncogenic *RAS* mediates a feedback suppression of RTKs whereas the wildtype *RAS* activates the upstream signaling in the form of compensation. These results support the idea of targeting oncogenic *KRAS* in combination with an EGFR inhibitor in *KRAS* mutant NSCLC (34). This approach will simultaneously block EGFR-mediated activation of wildtype *KRAS* signaling and the sustained MAPK signaling from oncogenic *KRAS*.

### **The Final Destination: Myc**

The ultimate destination of an RTK signal cascade is the nucleus, which results in the signal being read and understood by the transcriptional machinery of the cell.

Depending on the signal, the protein that has finally reached the nucleus acts on transcription factors, which can then adjust transcription of certain genes based on what the signal has transmitted. Upon ligand binding, whether that be epidermal growth factor (EGF) or transforming growth factor- $\alpha$  (TGFA) or epiregulin (EREG), EGFR signals heavily through the RAS/MAPK. The final kinase in the cascade is the extracellular signal-regulated kinase (ERK). ERK has the capacity to translocate to the nucleus and phosphorylate many cell proliferation-associated transcription factors, such as cAMP-response element (CREB), c-Fos and c-Myc. After activation, many of these transcription factors can amplify transcription of their own representative genes in a self-regulatory loop. By altering the levels and activities of transcription factors, ERK eventually leads to altered transcription of genes that are important for the cell cycle and thereby cell growth.

One of the most vital cell proliferation associated transcription factors downstream of the MAPK cascade is c-Myc. The proto-oncogene, *myc*, is at the center of many growth associated signaling pathways and is an immediate early response gene downstream of many RTKs. The regulation of *myc* expression is tightly controlled by a number of mechanisms involving many transcriptional regulatory motifs found within its proximal promoter region. Also, the *myc* mRNA and Myc protein are similarly tightly regulated as the dysregulation of Myc is the beginning of many cellular disabilities. The Myc protein contains an N-terminal transcriptional regulatory domain, a nuclear localization signal and a C-terminal region with a basic DNA binding domain with a helix-loop-helix dimerization motif. Myc dimerizes with another helix-loop-helix protein, Max, to bind DNA. Upon dimerization, Myc-Max binds DNA at specific E-box binding motifs (5'-CACGTG-3') and recruit complexes composed of other transcription factors and histone modifying proteins to repressively or actively control gene transcription **(35)**. Myc-binding

sites are amazingly conserved among different cell types and Myc binds a similar population of high-affinity targets in both tumor and primary cells. Myc-target genes belong to diverse functionally categories, including tissue remodeling, growth ligands and receptors, metabolism and other transcription factors **(36)**.

In cancer cells, *myc* activation can result from constitutive activation of a pathway, such as pathways that regulate B-catenin and APC. B-catenin is a coactivator for the transcription factor, Tcf, which directly activates *myc* transcription, when the negative control on  $\beta$ -catenin by APC is removed. Additionally, *myc* activation can result from direct alterations to the *myc* gene, such as amplifications or chromosomal translocations. For example, *myc* is consistently altered by chromosomal translocation in Burkitt lymphomas and multiple myelomas, and is one of the most highly amplified oncogene amongst many human cancers, including lung, breast and colon carcinomas. Interestingly, inhibition of PI3K leads to *myc* amplification as a form of drug resistance, indicating that Myc is downstream of PI3K in tumorigenesis. Myc expression is estimated to be elevated or signaling deregulated in up to 70% of human cancers. Particularly, high levels of Myc expression have been linked to aggressive triple negative breast cancer (TNBC) **(37)**. Scientific models of Myc-mediated tumorigenesis suggest that established tumors have an oncogene addiction to Myc making Myc a strong candidate to target for cancer therapeutics.

As Myc is a vulnerable drug target, many forms of inhibitors have been developed and are currently being aggressively clinically tested. Approaches to inhibit Myc activity include inhibiting Myc expression, interrupting Myc-Max dimerization, inhibiting Myc-Max DNA binding, and interfering with key Myc target genes, such as c-Jun **(35)**. Directly inhibiting Myc or the Myc-Max dimerization has proved to be difficult

due to an abnormally large protein-protein interface of the heterodimer and the lack of a defined ligand-binding domain. Thereby, focus has shifted towards impeding Myc-dependent transcription and/or blocking activity of *myc* co-activator proteins. Studies discovered that bromodomain (BRD)-containing proteins from the BET family, including BRD4, act as regulatory factors of Myc. BET inhibition by the developed bromodomain inhibitor, JQ1, has shown to downregulate *myc* transcription and genome-wide downregulation of Myc target genes. JQ1 has shown efficacy in murine models of multiple myeloma and Burkitt's lymphoma, and has proved effective in other in vivo preclinical studies **(38)**. Furthermore, BET bromodomain inhibition has recently proved to be efficacious in GEMM of mutant KRAS NSCLC **(39)**. The preliminary success of JQ1 in the disruption of cancer progression constitutes the great therapeutic value of inhibiting Myc. Hence, although direct inhibition of KRAS has remained a challenge in the drug discovery field, inhibiting or deregulating the ultimate destination of RAS signaling, Myc, may prove to be more fruitful.

## **Palmitoylation**

### **What is Palmitoylation?**

Palmitoylation, the most common form of protein acylation, is a post-translation protein lipid modification that requires the formation of a thioester bond between a cysteine thiol side chain and the saturated 16-carbon fatty acid, palmitic acid.

Palmitoylation may also occur through a covalent attachment of palmitic acid to serine or threonine residues of proteins although this is much less frequent than cysteine palmitoylation. Unlike the other lipid modifications, such as myristoylation, prenylation, farnesylation, and addition of cholesterol, palmitoylation is reversible as the thioester bond is readily reactive **(40)**. Palmitic acid modifies mainly membrane associated

proteins, both integral and peripheral membrane proteins. A meta-analysis of various studies produced a collection of approximately 2,000 mammalian proteins that have been shown to be palmitoylated and this collection is called the palmitoylome. About 40% of synaptic proteins were found in the palmitoylome (41), understandably so as palmitoylation of mammalian proteins was first discovered in neurons. The discovery in neurons, where specific proteins must locate to the plasma membrane during synapse formation, led to an understanding of the primary function of palmitoylation, localizing and associating proteins to membranes.

As the scientific community began to appreciate the significance of lipid modifications to specific proteins in cellular signaling pathways, the study of palmitoylation became a focus. Now, the recognized functions of palmitoylation are to regulate protein localization, trafficking, stability, segregation to membrane compartments, and protein-protein interactions (40). The reversibility and hydrophobicity of palmitoylation is the key to these functional roles of palmitoylation in the cell. The addition of palmitic acid to proteins increases their hydrophobicity, which contributes to the membrane association of these proteins. The reversibility permits rapid cycling of palmitoylation and depalmitoylation which allows proteins to be easily shuttled between the plasma membrane and the Golgi apparatus, where these proteins are modified, to regulate many cellular functions.

### **Emerging Regulatory Roles of Acylation**

For many years, palmitoylation was known to simply regulate subcellular trafficking of proteins to membrane compartments. Recent studies have shown that there are many more regulatory roles to acylation, including palmitoylation, and that palmitoylation of proteins can affect cellular signaling processes. Studies have shown

that the major signaling protein, Wingless/Integrated (Wnt), is modified by a 16-carbon cis-unsaturated fatty acid called palmitoleic acid on a serine. This type of lipid modification is called palmitoleoylation **(42)**. Wnt signaling is evolutionarily conserved from metazoans to humans. It is critical during development and functions to regulate tissue homeostasis. Canonically, signaling is initiated when the secreted, lipid-modified Wnt glycoprotein interacts with the extracellular N-terminal cysteine-rich domain (CRD) of the Frizzled (Fzd) G-Protein coupled receptor (GPCR). Fzd then directly interacts with the cytoplasmic phosphoprotein, Dishevelled (Dsh). In the canonical Wnt signaling pathway, Dsh, through interaction with other proteins in a complex, can block the degradation of  $\beta$ -catenin. As a result,  $\beta$ -catenin accumulates in the cytoplasm and translocates to the nucleus to activate transcription of genes associated with body axis patterning, cell fate specification, cell proliferation and cell migration **(43)**.

Palmitoleoylation of Wnt is critical for its secretion to the extracellular environment as a paracrine or autocrine ligand and for its activity. Further study showed that the high-affinity interaction between Wnt and Fzd occurs at two distinct contact sites, one being a protein–fatty acyl interface and the other a canonical protein–protein interface. The protein-fatty acyl interaction is required for efficient activation of Fzd by Wnt. A recent study has discovered that the palmitoleic acid modification of Wnts can be recognized by multiple CRDs from multiple Fzd receptors at one time. Furthermore, the acyl modification allows for the bridging of two CRD monomers showing that the binding of lipid-modified Wnt mediates Fzd receptor dimerization **(44)**. The study proves the existence of this new acylated Wnt-Fzd interface by isolating a crystal structure of the human Fzd5 CRD bound to a 16-carbon cis-unsaturated fatty acid in a lipid binding groove with a U-shaped geometry. Moreover, this crystal structure revealed a dimeric arrangement of the Fzd5 CRD with both monomers containing the lipid-binding groove



**(44)**. This study represents that fatty acid modifications of proteins are recognized by specific flexible cavities which facilitate specific protein-protein interactions and this interaction can stimulate downstream signaling.

A more recent study showed that the tyrosine kinase, c-Abl, has a binding pocket for the hydrophobic myristoyl group on the N-terminus and the loss of this myristoylation leads to dramatically higher kinase activity compared to the myristoylated c-Abl **(45)**. This suggests that myristoylation of c-Abl is required to regulate the activity of c-Abl. This demonstrates a new role for myristoylation, the addition of a 14-carbon saturated fatty acid, involving the regulation of a cell signaling molecule. c-Abl is a modular signaling protein that has many roles, including the regulation of the actin cytoskeleton and the integration of DNA damage responses in the nucleus. Abl is mostly well-known in the context of Bcr-Abl. A reciprocal translocation of genetic material on chromosome 9 and chromosome 22 leads to the generation of a stunted chromosome named the Philadelphia chromosome (Ph). The Ph contains a fusion gene encoding the fusion protein, Bcr-Abl. As a result of the fusion, Bcr-Abl becomes an oncogenic tyrosine kinase that is constitutively active uncontrollably driving myeloid progenitor cell transformation leading to initiation and progression of chronic myelogenous leukemia (CML). Clinically, treatment of CML has been revolutionized due to the development of the ATP-competitive inhibitors for the Abl kinase domain, such as the renowned imatinib (Gleevec). Imatinib works in part by trapping the Abl kinase active site in a specific inactive conformation and has been revolutionary in the treatment of CML.

c-Abl is closely related to the Src family of kinases which are regulated by phosphorylation at a conserved tyrosine in the C-terminal tail of the protein. This phosphorylation causes self-association with the kinases SH2 domain. This leads to a

series of intra-kinase conformational changes that result in an inactive conformation of the activation loop. Ligand binding to the SH2 domain interferes with this inactive conformation and allows for activation of the kinase. This allows for controlled regulation of signals and prevents unrestrained catalytic activity in a form of autoinhibition. c-Abl kinase is regulated in a similar intramolecular interaction, but the SH2 domain-phosphorylated tail association is replaced by an interaction of the N-terminal myristoyl group with the kinase domain through a hydrophobic binding pocket at the base of the kinase domain **(45)**.

The mechanism of myristoylation of the N-terminal tail looping around and binding to an orthotopic binding pocket is specific to c-Abl and an Abl-paralog, Arg. This myristoyl group binding helps stabilize the inactive form of c-Abl. The other Src family kinases, such as c-Src, are myristoylated at the N-terminal domain, however, this myristoylation functions canonically by only allowing c-Src to localize to the plasma membrane. In both c-Src and c-Abl, the inactivation to activation of the kinases are coupled with conformational changes in the kinase domain with which the mouth of the kinase domain is either flexed or open. In c-Abl, the myristoyl group helps stabilize the inactive form of c-Abl. Gleevec has been shown to be very selective to c-Abl which is why it has been so effective in treating and often resulting in remission. Now, it has been established that this drug specificity comes from the interaction of inactive c-Abl with the myristoylated N-terminal tail. When the myristoylation is released from its binding pocket, the kinase domain of c-Abl conforms into a different activation structure distinct from other Src kinases and Gleevec has a specific binding motif in that particular activation structure **(46)**. This study shows that myristoylation, which is concurrent to palmitoylation, has the ability to regulate kinase activity by associating to the kinase domain at a specific motif and can thereby affect the binding and efficacy of a kinase

inhibitor. With this discovery, there is now a scientific initiative to identify new signaling roles for acylation, especially palmitoylation, that can lead to the development of new therapeutic approaches for palmitoylation dependent diseases, including cancer.

### **Regulation of Palmitoylation**

Although palmitoylation was discovered in 1979, the enzymes that catalyze protein palmitoylation were only discovered recently in 2002. Palmitoylation is regulated by two classes of enzymes, the DHHC (Asp-His-His-Cys) domain containing protein acyl-transferases or palmitoyltransferases (PAT), which mediate the addition of palmitate to target substrates, and the acyl-protein thioesterases (APT) which remove palmitate (47). The DHHC proteins were first discovered in yeast, *Saccharomyces Cerevisiae*, as a Ras palmitoyltransferase and then an ankyrin-repeat-containing protein and a SNARE protein. In mammals, DHHC proteins were also originally identified and studied in neuronal cells as many SNAP and SNARE proteins are palmitoylated to associate with plasma membrane at synapse formation (48). There are increasing examples of the critical role for protein palmitoylation in cell signaling. Protein palmitoylation plays a role in determining receptor levels and localization in neurons and immune cells. For example, the turnover of glutamate receptors at neuronal synapses is promoted by depalmitoylation of the postsynaptic density protein (PSD-95) in response to glutamate receptor activity. Twenty-three PATs have been identified in mammals and some have been shown to have biomedical relevance as their palmitoylated substrates are involved in the pathogenesis of neurological disorders, such as Huntington's disease (DHHC17) and schizophrenia (DHHC8) (49). However, many DHHC enzymes have not been studied and their substrates have not been identified.

## Palmitoylation in Cancer

Palmitoylation and the DHHC proteins have not to date been well-studied in the context of development or progression of cancer. Recently, studies have discovered that these enzymes modulate the function and location of important oncoproteins and tumor suppressors. Subsequently, analysis of The Cancer Genome Atlas (TCGA) revealed that alterations in expression and function of several of these PATs occurs in a variety of cancers **(48, 51, 52)**. The role of palmitoylation in cancer has mostly focused on the palmitoylation of HRAS and NRAS **(52)**. A cycle of palmitoylation and depalmitoylation of RAS proteins in mammalian cells regulates the trafficking of these proteins between intracellular compartments and the plasma membrane, where RAS is required to be for activity. As previously discussed, this modification of RAS led to development of, albeit unsuccessful, farnesyltransferase inhibitors (FTIs) to attempt inhibition of RAS acylation and thereby RAS localization to the plasma membrane.

Recently, studies have linked palmitoylation in a functional capacity driving tumorigenic signaling pathways. Mutations in the Notch signaling pathway have a strong relationship with human T lymphoblastic leukemias (T-ALL) genesis, and have been shown to be involved in solid tumor progression, such as breast, lung, gastric and liver cancer. As previously discussed, disruptions in Wnt signaling are heavily implicated in carcinogenesis of colorectal cancer through loss of APC. Palmitoylation of Wnt ligands are critical to their function as they are required to localize to the membrane to be secreted or to crosstalk with their receptors **(42)**. New findings demonstrate that the cycle of palmitoylation and depalmitoylation of Notch and Wnt is a major mechanism of asymmetric cell division maintaining Notch and Wnt-associated protein dynamics and cellular functions **(53)**. A disruption in this cycle leads to altered or restricted Notch and

Wnt signaling eventually causing transformation. Study of palmitoylation is becoming more prevalent in the context of carcinogenesis however, more work is required to prove the necessity of therapeutically targeting palmitoylation or acylation in general.

### **Palmitoylation Assays**

At its discovery, protein palmitoylation was the first example of a covalent lipid modifications of proteins in eukaryotic cells. In the following years, many more lipid modifications of proteins, such as myristoylation, prenylation, farnesylation and cholesterol addition, were discovered and shown to have a regulatory function. Protein palmitoylation was also thought to have various regulatory functions in the cell. However, a key difference between palmitoylation and the other forms of lipid modifications is that palmitoylation is reversible. Furthermore, despite the many scientific technological advancements, antibodies detecting palmitoylated proteins have not been generated, unlike the readily available antibodies detecting phosphorylated proteins. Therefore, tools to study palmitoylation are limited and difficult to perform **(54)**. The first stipulated qualitative method to measure protein palmitoylation was in vivo metabolic radiolabeling of proteins with tritiated palmitate, [ $H^3$ ]-palmitate, and then detection by fluorography **(55)**. Although effective to identify palmitoylated proteins and assess the palmitoylation level of a certain protein in living cells, the method is excruciatingly long and often does not produce a quantifiable result. New methods of a similar nature use metabolic incorporation of alkynyl fatty acid analogues, such as 17-octadecynoic acid (17-ODYA). After metabolic labeling, the extent of proteins labeled with the azido-group containing palmitoyl group is monitored by simple copper-catalyzed click chemistry to azide-linked reporter tags, such as rhodamine-azide or biotin-azide. The labeled palmitoylated proteins are then separated using SDS-PAGE or affinity enriched for mass

spectrometry-based proteomics. This method is faster and is especially useful for monitoring the on-off rates of palmitoylation using a pulse-chase approach **(56)**, but still not easy to quantify.

The generation of a new method called the acyl-biotin exchange (ABE) method made it possible to study protein palmitoylation faster and in a quantifiable way. The in vitro ABE method rapidly replaced the traditional metabolic labeling methods. In this method, cell lysates are first subjected to N-ethylmaleimide (NEM) treatment which blocks any free thiols on available proteins. Then the lysates are subjected to hydroxylamine (HAM) which cleaves the cystein-palmitoyl thioester linkages on palmitoylated proteins. The newly freed thiols on the originally palmitoylated proteins are then labeled with biotin-HPDP (Biotin-HPDP-N-[6-(Biotinamido)hexyl]-3'-(2'-pyridyldithio)propionamide). The biotin-HPDP labeled proteins are then affinity-purified with streptavidin-agarose beads and subjected to SDS-PAGE analysis with western blotting for suspected palmitoylated proteins or high-throughput, tandem mass spectrometry **(57)**. The work in this thesis primarily utilized the ABE method followed by mass spectrometry or immunoprecipitation of the protein of interest.

## **DHHC20**

Our lab discovered that the melanoma cell adhesion molecule (MCAM) is depalmitoylated in response to Wnt5a, which promotes melanoma cell invasion. **(58)**. A previous proteomic study of WM239A melanoma cells identified only two PAT, DHHC20 and DHHC5. We proceeded to study DHHC20 by genetic means and discovered that it palmitoylates MCAM. Although most PAT activity has been observed in the post-translational modifying compartments, such as the Golgi and endoplasmic reticulum, studies have shown that human DHHC20 also displays distinct plasma membrane

localization. In fact, DHHC20 is one of only three out of the 23 palmitoyltransferases that localizes to the membrane, the other two being DHHC5 and DHHC21 **(59)**. This localization at the membrane allows DHHC20 to access and associate with membrane localized proteins, such as receptor tyrosine kinases. Thus began the journey to understand this palmitoyltransferase and how it functions to palmitoylate receptors on the plasma membrane.

Studies have shown that DHHC20 has a tissue-specific expression pattern. These studies observed that DHHC20 was expressed at high levels in the testis, placenta, thyroid, colon and prostate, at lower levels in the brain, heart, liver, lungs, thymus, leukocytes, ovary and breast, and not expressed at all in skeletal muscle and the small intestine **(60)**. Another study performed quantitative PCR analysis of DHHC20 expression level in normal human tissue versus tumors. These studies demonstrated that DHHC20 expression is significantly upregulated in breast, colon, lung and prostate tumors in comparison with organ-matched normal tissues **(61)**. Furthermore, they found that many potential targets of DHHC20 are potentially transforming when constitutively activated in breast cancer and several other potential targets of DHHC20 have elevated expression and activity in colorectal carcinomas **(61)**. Analysis of The Cancer Genome Atlas (TCGA) reveals that alterations in DHHC20 expression including deletions, amplifications and mutations occur in cancers of the breast, lung and prostate. Many studies have determined that expression of DHHC20 is sufficient to cause cellular transformation. A group mutated the catalytic cysteine in DHHC20 to a serine, DHHS20, rendering it catalytically inactive. They showed that NIH3T3 cells expressing the catalytically inactive DHHS20 were unable to grow in soft agar, whereas cells expressing DHHC20 were able to. Soft agar growth depicts an anchorage-independent growth pattern which is characteristic of cellular transformation and cellular transformation is the

first step to malignancy. Therefore, this study proved that overexpression of catalytically active DHHC20 causes transformation of NIH3T3 cells in vitro **(61)**. Taken together, these findings show that human DHHC20 is expressed in a tissue-specific manner and is upregulated in certain tumor tissues correlating with the expression of its tumorigenic intracellular targets. These results associate DHHC20 with the development of human cancer setting a strong precedence to study DHHC20 and its enzymatic targets.

The recent publication of the first three-dimensional structure of DHHC20 sparked a new interest in the palmitoylation field. The structure explains how DHHC proteins function and offers a map to efficiently design drugs against DHHC20. This study describes the DHHC20 structure as being the canonically known 4-pass transmembrane protein but with a newly discovered hydrophobic cavity formed by the transmembrane domain where the acyl chain logically binds. The active site containing the DHHC motif is at the membrane-cytosol interface of the cavity. The active site of the enzyme then catalyzes the thioester-exchange to targets by using fatty acyl-coenzyme A. This transmembrane cavity with the cytosolic active site explains why cysteines of proteins that are in or close to the membrane are ideal candidates for palmitoylation **(62)**. These structures were published at a time when the entire field of protein palmitoylation suffers from the lack of small molecule probes and inhibitors for the DHHC family proteins, including efficient antibodies to experimentally study. Thus, this new understanding of the shape of DHHC20 is a starting point to develop therapeutic inhibitors using a structure-guided approach.



# Mouse Models of Lung Adenocarcinoma

## The Origins

The analyzes of genetics on many cancers and their experimental study from the last two decades has taught us one important lesson about cancer: specific cancer types most often depend on the dysregulation of only a limited set of signaling cascades, which are often unique for a particular tumor type. A few examples of cancer types in fact show an extremely high incidence for a distinct driver mutation, e.g. BCR-ABL translocations in chronic myeloid leukemia (CML), KRAS mutations in pancreatic cancer or BRAF mutations in melanoma. With this lesson learned, the scientific community was able to generate mouse models that recapitulated most of the unique characteristics of the desired tumor type simply by introducing a number of tumor-specific driver mutations into the appropriate target cell that represents the desired tumor type. In this manner, the community was able to ask and answer questions pertaining to the influence of individual mutations on tumor development and progression. The generation of these mouse models has been a critical achievement for the targeted drug development field as it is clear that it was impossible to perform efficacy studies in human patients.

Initially, the mouse model community generated tools to derive and culture embryonic stem cells followed by mutating specific genes in those derived mouse blastocytes using SV40 viral DNA. Finally, through germline transmission, transgenic mice harboring specific mutations were generated (63). Today, we have tools available to conditionally activate or inactivate genes in distinct cell types at any desired moment using small molecules, such as doxocycline or tamoxifen. We have methods to regulate expression of introduced genes or shRNAs against genes of interest using small molecules. We can mark the switched cells using fluorescent reporters, such as green

fluorescent protein (GFP). We can even read out distinct signaling pathways using either fluorescent or bioluminescent reporters and conduct lineage tracing of stem cells from a chosen tissue. With the development of these new genetically engineered mouse models (GEMMs) of cancer, we have a newfound facility to quickly assess the contribution of distinct mutation combinations to tumor development and design appropriate targeted therapy.

### **The Model of Choice**

Many or most of the driver mutations found in human NSCLC have been introduced into the mouse individually and in combination with others. Some examples of the driver mutations introduced include Kras, Braf, Egfr, Lkb1, Rac1, NfkappaB, and p53. The combinations of driver mutations have been particularly revealing as they have allowed the community to study the interdependencies of driver mutations leading to altered disease phenotypes, making the mouse models more and more similar to human disease. Most of the successful mouse models of lung cancer have focused on the adenocarcinoma subtype of NSCLCs made by using a Lox-Stop-Lox (LSL) conditional KrasG12D mutation genetically engineered into the endogenous Kras locus leaving one allele to be wildtype Kras. With the introduction of viral, whether that be adenoviral or lentiviral, Cre recombinase into the desired cells of LSL-KrasG12D mice, the mutant KrasG12D allele is expressed at relatively endogenous levels. The advantage of the control of the endogenous locus allows for the closest recapitulation of spontaneous human tumor initiation and the subsequent processes pertaining to tumor progression, making the study of human cancer much easier **(64)**. However, a disadvantage of the LSL-KrasG12D/+ model is the low frequency of activation, which results in a low probability of and delayed tumor initiation.

The activation of the oncogenic KrasG12D is sufficient to initiate tumorigenesis. However, an additional deletion or point mutation of tumor suppressor, p53, significantly enhances tumor progression, leading to a more rapid development of adenocarcinomas with features of a more advanced disease. The deletion of *p53* is achieved by genetically engineering two loxP sites flanking the mouse *Trp53* gene at its endogenous locus. The mice are then cross-bred with the LSL-KrasG12D containing mice to generate mice that will activate KrasG12D and delete *p53* by introduction of viral Cre recombinase at the same time. This model has several advantages over the LSL-KrasG12D alone mice, including rapid tumor progression, access to large tumors for further tissue processing, short survival of mice for faster experiments, and a metastatic potential to study metastases into the liver and kidneys **(65)**.

To add an additional means of efficient scientific study, the mouse field generated a triple conditional mouse by adding a yellow fluorescent protein (YFP) reporter allele (*Rosa26*<sup>LSL-YFP</sup>). In the triple conditional mouse, the introduction of viral Cre recombinase will express KrasG12D, delete *p53* and express YFP in the same cell at the same time. Therefore, with the addition of the YFP reporter, the cells infected with viral Cre recombinase are marked and can be followed using immunofluorescence and immunohistochemistry techniques. Although the YFP mark does not prove that the cells are expressing KrasG12D and have *p53* deleted, it allows for recognition of all the infected cells, allowing quantification of the viral efficacy. The efficiency of Cre recombinase to recombine DNA has been well-studied and established. Therefore, it can be fairly assumed that in all the infected cells marked with YFP Cre recombinase has allowed expression of KrasG12D and deletion of p53.

## Administration of Cre Recombinase

Initially, Cre recombinase was administered using the replication-deficient adenoviruses expressing Cre (Adeno-Cre). There are a few advantages to using adenoviruses. For example, it is fairly easy to generate a high and reproducible titer. However, a disadvantage to adenovirus is that it can only be used to introduce Cre. Recently, lentiviruses are used to administer Cre (Lenti-Cre) because lentiviruses can integrate into the genome of infected cells. With the ability to integrate into the genome, lentiviruses can be used to further modify tumors with stable expression of cDNAs to overexpress, or short-hairpin RNAs to silence, genes of interest **(66)**.

In order to recapitulate lung adenocarcinoma, Lenti-Cre has to be administered directly to the lung so that Cre recombinase can allow expression of KrasG12D and deletion of *p53* specifically in lung cells. To deliver Lenti-Cre to the lung, a method called intratracheal intubation (IT) is used. The advantages of IT are that the viral administration is directly into the lung with reproducibility of delivery to ensure consistency in number of tumors between experiments. However, the disadvantages of IT include the requirement of specialized equipment and significant technical training. If IT is performed incorrectly, the trachea of the mouse can be ruptured, the mouse can die from asphyxiation, pleural effusion and/or the virus can be delivered down the esophagus to the incorrect location **(65)**.

IT is performed under anesthetized mice between ages 6-12 weeks. After anesthetization, the mouse is propped up to open the mouth and the tongue is displaced to the side. A light shined under the throat of the mouse is used to identify the trachea, which is situated above the esophagus. A catheter is inserted into the trachea and the virus composed in phosphate-buffered saline solution is injected into the catheter. The

mouse then inhales the solution into the lungs. The mice are allowed to recover from the anesthesia and kept in an appropriate environment for 12-16 weeks to allow tumor initiation and progression. To isolate the tumors, after 12-16 weeks, the mice are euthanized and the whole lungs are isolated for analysis.

## References

1. Ferlay J, et al. Cancer incidence and mortality worldwide: sources, methods and major patterns in GLOBOCAN 2012. *Int J Cancer*. **136(5)**:359–86, 2015.
2. Lemmon, M.A., Schlessinger, J., and Ferguson, K.M. The EGFR family: not so prototypical receptor tyrosine kinases. *Cold Spring Harbor Pers. Bio*. **6**, a020768, 2014.
3. Roskoski, R., Jr. ErbB/HER protein-tyrosine kinases: Structures and small molecule inhibitors. *Pharmacological Research : the official journal of the Italian Pharmacological Society*. **87**, 42-59, 2014.
4. Walton, G.M., Chen, W.S., Rosenfeld, M.G., and Gill, G.N. Analysis of deletions of the carboxyl terminus of the epidermal growth factor receptor reveals self-phosphorylation at tyrosine 992 and enhanced in vivo tyrosine phosphorylation of cell substrates. *JBC*. **265**, 1750-1754, 1990.
5. Seshacharyulu, P., Ponnusamy, M.P., Haridas, D., Jain, M., Ganti, A.K., and Batra, S.K. Targeting the EGFR signaling pathway in cancer therapy. *Expert Opinion on Therapeutic Targets* **16**, 15-31, 2012.
6. Tomas A, Futter CE, Eden ER. EGF receptor trafficking: consequences for signaling and cancer. *Trends Cell Biol*. **24(1)**:26-34, 2014.
7. Shiaw-Yih Lin, Keishi Makino, Weiya Xia, Angabin Matin, Yong Wen, Ka Yin Kwong, Lilly Bourguignon & Mien-Chie Hung. Nuclear localization of EGF

- receptor and its potential new role as a transcription factor. *Nature Cell Biology*. **3** :802–808, 2001.
8. Normanno N, De Luca A, Bianco C, Strizzi L, Mancino M, Maiello MR, Carotenuto A, De Feo G, Caponigro F, Salomon DS. Epidermal growth factor receptor (EGFR) signaling in cancer. *Gene*. **366**:2–16, 2006.
  9. Pines, G., Kostler, W.J., and Yarden, Y. Oncogenic mutant forms of EGFR: lessons in signal transduction and targets for cancer therapy. *FEBS Letters* **584**, 2699-2706, 2010.
  10. Cho, J., Pastorino, S., Zeng, Q., Xu, X., Johnson, W., Vandenberg, S., Verhaak, R., Cherniack, A.D., Watanabe, H., Dutt, A., *et al*. Glioblastoma-derived epidermal growth factor receptor carboxyl-terminal deletion mutants are transforming and are sensitive to EGFR-directed therapies. *Cancer Research* **71**, 7587-7596, 2011.
  11. Ekstrand, A.J., Sugawa, N., James, C.D., and Collins, V.P. (1992). Amplified and rearranged epidermal growth factor receptor genes in human glioblastomas reveal deletions of sequences encoding portions of the N- and/or C-terminal tails. *Proceedings of the National Academy of Sciences*. **89**, 4309-4313, 1992.
  12. Imielinski, M., Berger, A.H., Hammerman, P.S., Hernandez, B., Pugh, T.J., Hodis, E., Cho, J., Suh, J., Capelletti, M., Sivachenko, A., *et al*. Mapping the hallmarks of lung adenocarcinoma with massively parallel sequencing. *Cell* **150**, 1107-1120, 2012.
  13. Siegel R, Naishadham D, Jemal A. Cancer Statistics. *Ca Cancer J Clin*. **63**:11–30, 2013.
  14. Chen Z, Fillmore C, Hammerman P, Kim C, Wong K-K. Non-small-cell lung cancers: a heterogeneous set of diseases. *Nat Rev Cancer*. **14**:535–546, 2014.

15. Jorissen R, et al. Epidermal growth factor receptor: mechanisms of activation and signalling. *Exp Cell Res.* **284**:31–57, 2003.
16. Maione P, Rossi A, Bareschino M, Sacco PC, Schettino C, Casaluce F, Sgambato A, Gridelli C1. Irreversible EGFR inhibitors in the treatment of advanced NSCLC. *Curr Pharm Des.* **20(24)**:3894-900, 2014.
17. Hirsh V. Next-Generation Covalent Irreversible Kinase Inhibitors in NSCLC: Focus on Afatinib. *BioDrugs.* **29(3)**:167-83, 2015.
18. Morgillo F, Della Corte CM, Fasano M, Ciardiello F. Mechanisms of resistance to EGFR-targeted drugs: lung cancer. *ESMO Open.* **1(3)**, 2016.
19. Zhang W and Liu HT. MAPK signal pathways in the regulation of cell proliferation in mammalian cells. *Cell Research.* **(12)**, 9–18, 2002.
20. Hemmings BA, Restuccia DF. PI3K-PKB/Akt pathway. *Cold Spring Harb Perspect Biol.* **4(9)**, 2012.
21. Wee P, Wang Z. Epidermal Growth Factor Receptor Cell Proliferation Signaling Pathways. *Cancers (Basel).* **9(5)**:52, 2017.
22. Burke JE, Williams RL. Dynamic steps in receptor tyrosine kinase mediated activation of class IA phosphoinositide 3-kinases (PI3K) captured by H/D exchange (HDX-MS). *Adv Biol Regul.* **53(1)**:97-110, 2013.
23. Baines AT, Xu D, Der CJ. Inhibition of Ras for cancer treatment: the search continues. *Future Med Chem.* **3(14)**:1787-808, 2011.
24. Massacesi C, Di Tomaso E, Urban P, et al. PI3K inhibitors as new cancer therapeutics: implications for clinical trial design. *Onco Targets Ther.* **9**:203-10, 2016. Mayukh Chakrabarti, Hyunbum Jang, and Ruth Nussinov. Comparison of the Conformations of KRAS Isoforms, K-Ras4A and K-Ras4B, Points to

- Similarities and Significant Differences. *The Journal of Physical Chemistry*. **120** (4), 667-679, 2016.
25. To MD, Wong CE, Karnezis AN, Del Rosario R, Di Lauro R, Balmain A. Kras regulatory elements and exon 4A determine mutation specificity in lung cancer. *Nat Genet*. **40(10)**:1240-4, 2008.
26. Stolze B, Reinhart S, Bullinger L, Fröhling S, Scholl C. Comparative analysis of KRAS codon 12, 13, 18, 61, and 117 mutations using human MCF10A isogenic cell lines. *Sci Rep*. **5**:8535, 2015.
27. Castellano E, Santos E. Functional specificity of ras isoforms: so similar but so different. *Genes Cancer*. **2(3)**:216-31, 2011.
28. Tsai FD, Lopes MS, Zhou M, et al. K-Ras4A splice variant is widely expressed in cancer and uses a hybrid membrane-targeting motif. *Proc Natl Acad Sci U S A*. **112(3)**:779-84, 2015.
29. Fernández-Medarde A, Santos E. Ras in cancer and developmental diseases. *Genes Cancer*. **2(3)**:344-58, 2011.
30. Ahmed A. Samatar & Poulikos I. Poulikakos. Targeting RAS–ERK signalling in cancer: promises and challenges. *Nature Reviews Drug Discovery*. **13**: 928–942, 2014.
31. Aguirre AJ, Hahn WC. Synthetic Lethal Vulnerabilities in *KRAS*-Mutant Cancers. *Cold Spring Harb Perspect Med*. **8(8)**, 2018.
32. Unni AM, Lockwood WW, Zejnullahu K, Lee-Lin SQ, Varmus H. Evidence that synthetic lethality underlies the mutual exclusivity of oncogenic *KRAS* and *EGFR* mutations in lung adenocarcinoma. *Elife*. **4**, 2015.



33. Young A1, Lou D, McCormick F. Oncogenic and wild-type Ras play divergent roles in the regulation of mitogen-activated protein kinase signaling. *Cancer Discov.* **3(1)**:112-23, 2013.
34. Dang CV. MYC on the path to cancer. *Cell.* **149(1)**:22-35, 2012.
35. Fernandez PC, Frank SR, Wang L, et al. Genomic targets of the human c-Myc protein. *Genes Dev.* **17(9)**:1115-29, 2003.
36. Palaskas N, Larson SM, Schultz N, Komisopoulou E, Wong J, Rohle D, Campos C, Yannuzzi N, Osborne JR, Linkov I, et al. 18F-fluorodeoxy-glucose positron emission tomography marks MYC-overexpressing human basal-like breast cancers. *Cancer Res.* **71**:5164–5174, 2011.
37. Delmore JE, Issa GC, Lemieux ME, et al. BET bromodomain inhibition as a therapeutic strategy to target c-Myc. *Cell.* **146(6)**:904-17, 2011.
38. Shimamura T, Chen Z, Soucheray M, et al. Efficacy of BET bromodomain inhibition in Kras-mutant non-small cell lung cancer. *Clin Cancer Res.* **19(22)**:6183-92, 2013.
39. Aicart-Ramos, C., Valero, R.A., and Rodriguez-Crespo, I. Protein palmitoylation and subcellular trafficking. *Biochimica et biophysica acta* **1808**, 2981-2994, 2011.
40. Sanders SS, Martin DD, Butland SL, Lavallée-Adam M, Calzolari D, Kay C, Yates JR, Hayden MR. "Curation of the Mammalian Palmitoylome Indicates a Pivotal Role for Palmitoylation in Diseases and Disorders of the Nervous System and Cancers". *PLoS Computational Biology.* **11 (8)**, 2015.
41. Nile AH, Hannoush RN. Fatty acylation of Wnt proteins. *Nat Chem Biol.* **12**:60–69, 2016.
42. Holstein TW. The evolution of the Wnt pathway. *Cold Spring Harb Perspect Biol.* **4**, 2012.

43. Nile AH, Mukund S, Stanger K, Wang W, Hannoush RN. Unsaturated fatty acyl recognition by Frizzled receptors mediates dimerization upon Wnt ligand binding. *Proc Natl Acad Sci U S A*. **114(16)**:4147-4152, 2007.
44. Hantschel O1, Nagar B, Guettler S, Kretzschmar J, Dorey K, Kuriyan J, Superti-Furga G. A myristoyl/phosphotyrosine switch regulates c-Abl. *Cell*. **112(6)**:845-57, 2003.
45. Bhushan Nagar, Oliver Hantschel, Matthew A. Young, Klaus Scheffzek, Darren Veach, William Bornmann, Bayard Clarkson, Giulio Superti-Furga and John Kuriyan. Structural Basis for the Autoinhibition of c-Abl Tyrosine Kinase. *Cell*. **112**, 859–871, 2003.
46. Conibear, E., and Davis, N.G. Palmitoylation and depalmitoylation dynamics at a glance. *Journal of cell science* **123**, 4007-4010, 2010.
47. Linder ME, Deschenes RJ. New insights into the mechanisms of protein palmitoylation. *Biochemistry*. **42**: 4311–4320, 2003.
48. Guan X, Fierke CA. Understanding Protein Palmitoylation: Biological Significance and Enzymology. *Sci China Chem*. **54(12)**:1888-1897, 2011.
49. Greaves, J., and Chamberlain, L.H. DHHC palmitoyl transferases: substrate interactions and (patho)physiology. *Trends in biochemical sciences* **36**, 245-253, 2011.
50. Young A, Lou D, McCormick F. Oncogenic and wild-type Ras play divergent roles in the regulation of mitogen-activated protein kinase signaling.
51. Swarthout, J.T., Lobo, S., Farh, L., Croke, M.R., Greentree, W.K., Deschenes, R.J., and Linder, M.E. DHHC9 and GCP16 constitute a human protein fatty acyltransferase with specificity for H- and N-Ras. *JBC*. **280**, 31141-31148, 2005.

52. Stypulkowski E, Asangani IA, Witze ES. The depalmitoylase APT1 directs the asymmetric partitioning of Notch and Wnt signaling during cell division. *Sci Signal.* **11(511)**, 2018.
53. Resh MD. Covalent lipid modifications of proteins. *Curr Biol.* **23(10)**:R431-5, 2013.
54. Linder M, Deschenes R. Protein palmitoylation. *Methods.* **40(2)**:125-6, 2006.
55. Martin BR. Nonradioactive analysis of dynamic protein palmitoylation. *Curr Protoc Protein Sci.* **73**, 2013.
56. Wan J1, Roth AF, Bailey AO, Davis NG. Palmitoylated proteins: purification and identification. *Nat Protoc.* **2(7)**:1573-84, 2007.
57. Wang, W., Runkle, K.B., Terkowski, S.M., Ekaireb, R.I., and Witze, E.S. Protein Depalmitoylation Is Induced by Wnt5a and Promotes Polarized Cell Behavior. *JBC.* **290**, 15707-15716, 2015.
58. Fukata Y1, Fukata M. Protein palmitoylation in neuronal development and synaptic plasticity. *Nat Rev Neurosci.* **11(3)**:161-75, 2010.
59. Ohno Y, Kihara A, Sano T, Igarashi Y. Intracellular localization and tissue-specific distribution of human and yeast DHHC cysteine-rich domain-containing proteins. *Biochim Biophys Acta.* **17614**:474–483, 2006.
60. Draper JM, Smith CD. DHHC20: a human palmitoyl acyltransferase that causes cellular transformation. *Mol Membr Biol.* **27(2-3)**:123-36, 2010.
61. Rana MS, Kumar P, Lee CJ, Verardi R, Rajashankar KR, Banerjee A. Fatty acyl recognition and transfer by an integral membrane S-acyltransferase. *Science.* **359(6372)**, 2018.

62. Frese K.K., Tuveson D.A. Maximizing mouse cancer models. *Nat. Rev. Cancer.* **7**, 645–658, 2007.
63. Jackson E.L., Willis N., Mercer K., Bronson R.T., Crowley D., Montoya R., Jacks T., Tuveson D.A. Analysis of lung tumor initiation and progression using conditional expression of oncogenic K-ras. *Genes Dev.* **15**, 3243–3248, 2001.
64. DuPage M, Dooley AL, Jacks T. Conditional mouse lung cancer models using adenoviral or lentiviral delivery of Cre recombinase. *Nat Protoc.* **4(7)**:1064-72, 2009.
65. Naldini L, et al. In vivo gene delivery and stable transduction of nondividing cells by a lentiviral vector. *Science.* **272**:263–267, 1996.
66. Schuch G, Kobold S and Bokemeyer C. Evolving role of cetuximab in the treatment of colorectal cancer. *Cancer Management and Research.* **1**: 79-88, 2009.

## **CHAPTER 2: INHIBITION OF DHHC20 MEDIATED EGFR PALMITOYLATION CREATES A DEPENDENCE ON EGFR SIGNALING.**

Kristin B. Runkle, Akriti Kharbanda, Ewa Stypulkowski, Xing-Jun Cao, Wei Wang, Benjamin A. Garcia, Eric S. Witze. Inhibition of DHHC20 mediated EGFR palmitoylation creates a dependence on EGFR signaling. *Mol. Cell.* **62**, (2016). Reprinted with the copyright permission of Elsevier Publishing.

### **Abstract**

Inappropriate activation of the receptor tyrosine kinase EGFR contributes to a variety of human malignancies. Here we show a mechanism to induce vulnerability to an existing first line treatment for EGFR driven cancers. We find that inhibiting the palmitoyltransferase DHHC20 creates a dependence on EGFR signaling for cancer cell survival. The loss of palmitoylation increases sustained EGFR signal activation and sensitizes cells to EGFR tyrosine kinase inhibition. Our work shows that the reversible modification of EGFR with palmitate “pins” the unstructured C-terminal tail to the plasma membrane; impeding EGFR activation. We identify by mass spectrometry palmitoylated cysteine residues within the C-terminal tail where mutation of the cysteine residues to alanine is sufficient to activate EGFR signaling promoting cell migration and transformation. Our results reveal that the targeting of a peripheral modulator of EGFR signaling, DHHC20, causes a loss of signal regulation and susceptibility to EGFR inhibitor induced-cell death.

### **Introduction**

Receptor tyrosine kinases (RTK) are widely deregulated in cancer and increased RTK signaling contributes to a variety of human malignancies. Members of the ErbB

family play critical roles in responding to extracellular cues and initiating downstream signaling cascades through effector pathways (Lemmon et al., 2014; Roskoski, 2014; Walton et al., 1990). The epidermal growth factor receptor, EGFR, is one of four members of the ErbB family and is known to facilitate tumorigenesis and cancer progression. EGFR is structurally comprised of an extracellular ligand binding domain, a transmembrane region, a tyrosine kinase domain, and an unstructured C-terminal tail that harbors receptor auto-phosphorylation sites (Seshacharyulu et al., 2012). Ligands including the epidermal growth factor, EGF, bind to the extracellular domain of EGFR causing a conformational change that facilitates homo- and heterodimerization with members of the ErbB family (Seshacharyulu et al., 2012). Dimerization induces activation of the tyrosine kinase activity of the receptor leading to auto-phosphorylation of C-terminal tyrosines. The phosphorylated tyrosine residues serve as docking sites for adaptor proteins that link the receptor to downstream signaling pathways including Ras-Raf-MEK-ERK, PI3K-AKT, Src and JAK-STAT culminating in the regulation of cell migration, proliferation and survival (Seshacharyulu et al., 2012). Spatial and temporal control of EGFR signaling is mediated by receptor endocytosis. In response to EGF, EGFR is trafficked through early and late endosomes in route to lysosomes for signal termination and receptor degradation, in a process that serves as a well-regulated mechanism for tempering signaling responses.

Dysregulation and inappropriate activation of EGFR is a common event in cancer and increased expression and mutations in EGFR that enhance signaling and resistance to therapy have been identified in breast and lung cancer (Roskoski, 2014). While EGFR mutations commonly reside within the extracellular (EGFR-vIII) and kinase domains (L858R, T790M), recent studies identified EGFR mutations within the C-terminal tail (Pines et al., 2010). Deletion of EGFR exons 25-27 was found in lung cancer and

glioblastoma multiforme (Cho et al., 2011; Ekstrand et al., 1992; Imielinski et al., 2012). Ectopic expression of EGFR lacking exons 25 -26 promotes cell transformation and increases EGFR and AKT activation (Imielinski et al., 2012); however the mechanisms involved remain unknown.

Palmitoylation is the reversible modification of cysteine residues with a 16-carbon fatty acid which regulates protein localization, trafficking, stability and protein-protein interactions (Aicart-Ramos et al., 2011). Palmitoylation is regulated by two classes of enzymes, the DHHC domain containing protein acyl-transferases (PAT) which mediate the addition of palmitate to target substrates, and the acyl-protein thioesterases (APT) which remove palmitate (Conibear and Davis, 2010). Twenty three PATs have been identified in mammals and alterations in the expression and function of several PATs have been observed in cancer (Conibear and Davis, 2010; Greaves and Chamberlain, 2011; McCormick et al., 2008).

The role of palmitoylation in cancer has mostly focused on the palmitoylation of H-Ras and N-Ras which facilitates Ras localization to the plasma membrane and is required for activity (Swarthout et al., 2005). Analysis of The Cancer Genome Atlas (TCGA) reveals that alterations in DHHC20 expression including deletions, amplifications and mutations occur in cancers of the breast, lung and prostate. We found that the C-terminal tail of EGFR is palmitoylated by DHHC20. Inhibiting DHHC20 increases EGFR activation and increases the dependency on EGFR signaling for cell survival. We identify cysteine residues 1025, 1034 and 1122 as palmitoylation sites within the C-terminal tail. Mutation of 1025 or 1122 to alanine attenuates EGFR palmitoylation, activates EGFR signaling and increases cell migration and anchorage

independent growth. Finally, our results reveal a mechanism for EGFR activation caused by mutations in the C-terminal tail of EGFR previously identified in lung cancer.

## Results

### **Silencing DHHC20 increases EGFR mediated cell responses**

The palmitoyltransferase DHHC20 is expressed in multiple human breast and lung cancer cell lines and was found to suppress metastatic behavior in melanoma cells (Figure S1) (Wang et al., 2015). Analysis of the TCGA database revealed DHHC20 mRNA is elevated in basal and Her2-enriched breast carcinoma compared to luminal A and B tumors (Figure 1A). In the triple negative breast adenocarcinoma cell line MDA-MB-231 DHHC20 is localized to the plasma membrane and punctate structures adjacent to the nucleus when observed by immunofluorescence (IF) microscopy (Figure 1B). The levels of DHHC20 staining and the abundance of a specific 32kDa band on an SDS PAGE gel were decreased by DHHC20 shRNA (Figure 1 B-C). Expression of a shRNA resistant isoform of DHHC20 showed a consistent staining pattern by IF and the same molecular weight band that was reduced by shRNA, confirming this is the correct size and localization of DHHC20 protein (Figure 1 B-C). Inhibition of DHHC20 induced a change in cell morphology from an elongated spindle shape to a more spread morphology with extensive membrane ruffling in MDA-MB-231 cells (Figure 1D). The change in morphology correlated with a 3-fold increase in chemotaxis towards media containing 10% FBS that was suppressed by stable expression of shRNA resistant DHHC20 (Figure 1E). MDA-MB-231 cells have been shown to express high levels of EGFR which signals to downstream pathways important in cell migration (Price et al., 1999). We therefore asked if EGFR inhibition was sufficient to block the increase in chemotaxis. Treatment with the EGFR inhibitor Gefitinib significantly reduced



chemotaxis in cells expressing DHHC20 shRNA (shDHHC20) by approximately 50%, but had a minimal effect on the chemotaxis of control shRNA cells (Figure 1F).

The relatively short exposure to Gefitinib that inhibited cell migration did not affect cell viability in the MDA-MB-231 cells that are normally insensitive to Gefitinib (Figure S2). We next asked if silencing DHHC20 increased the cytotoxic effects of Gefitinib at longer time points. Treating MDA-MB-231 cells with

Gefitinib for 72 hours increased cell death in DHHC20 shRNA cells (22.1%) compared to control shRNA cells (6.9%) (Figure 1G). Similar results were observed using SW1573 lung adenocarcinoma cells (Figure 1G, Figure S3). The small molecule 2-bromo-palmitate (2BP) inhibits palmitoyltransferases (Figure S4) (Jennings et al., 2009). We therefore asked if 2BP produced an effect on Gefitinib sensitivity similar to silencing DHHC20. Treatment of MDA-MB-231 cells with 500nM 2BP resulted in 4.9% cell death after 72 hours. When treated in combination with 10 $\mu$ M Gefitinib the percentage of cell death increased (26.2%) compared to Gefitinib alone (13.3%) (Figure 1H). Increasing the concentration of 2BP to 5 $\mu$ M in combination with Gefitinib elevated the percentage of dead cells (48.9%) compared to 5 $\mu$ M 2BP alone (10.9%) (Figure 1H).

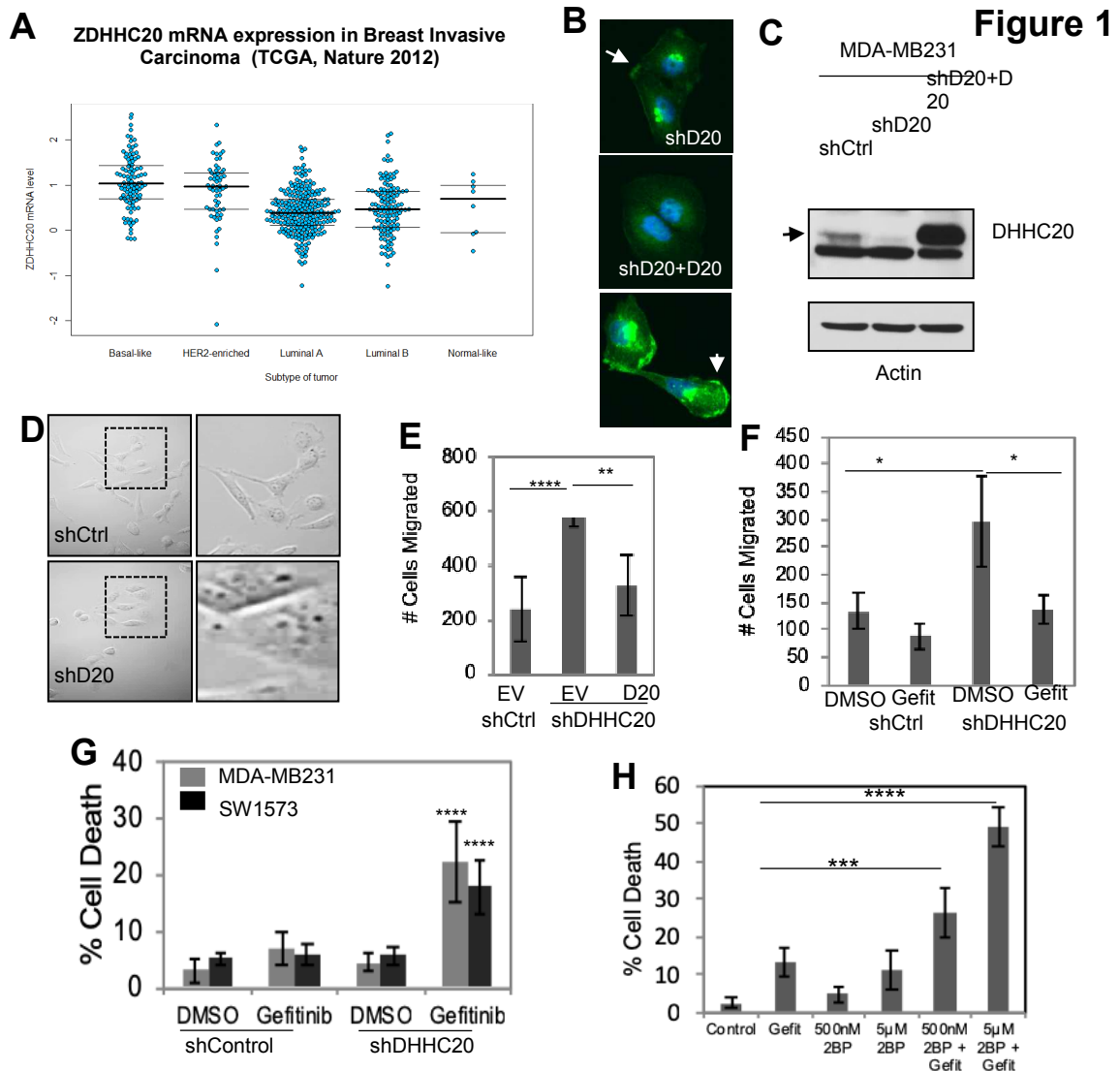


**Figure 1. Silencing DHHC20 increases EGFR-dependent cell migration and enhances Gefitinib-induced cytotoxicity.** (A) DHHC20 mRNA expression is altered in human breast cancer subtypes. The TCGA database was used to analyze global patterns of ZDHC20 expression in human breast invasive carcinoma; Basal-like (n=98), HER2-enriched (n=58), Luminal A (n=230), Luminal B (n=125) and Normal-like (n=8). (B-C) DHHC20 expression is silenced with shRNA. MDA-MB-231 shControl, shDHHC20 and shDHHC20+DHHC20 stable cell lines were generated by lentiviral infection. (B) Immunofluorescence staining of DHHC20 (green) and DAPI (blue) show expression of DHHC20 at the plasma membrane (arrow) and perinuclear region. (C) Immunoblotting with a DHHC20 specific antibody shows inhibition of the DHHC20 band (arrow). (D) Silencing DHHC20 in MDA-MB-231 cells induces cell spreading with increased membrane ruffling. (E) Knockdown of DHHC20 increases chemotaxis towards DMEM + 10% FBS which is rescued by expression of shRNA resistant DHHC20 (mean +/-StDev). (F) EGFR signaling is required for the increased chemotaxis of shDHHC20 cells. Migration of MDA-MB-231 shControl and shDHHC20 cells in the presence of DMSO or 10µM Gefitinib was determined using a transwell chemotaxis assay (mean +/-StDev). (G) Gefitinib increases cytotoxicity in DHHC20 silenced cells. MDA-MB-231 (gray bars) and SW1573 (black bars) cells were treated with DMSO or 10µM Gefitinib and cell viability was measured by Trypan Blue (mean +/-StDev). (H) Blocking palmitoylation with 2BP increases Gefitinib induced cytotoxicity. MDA-MB-231 cells were treated with 10µM Gefitinib alone or in combination with 500nM or 5µM 2BP and cell viability was measured by Trypan Blue (mean +/-StDev)

## **Inhibition of DHHC20-mediated palmitoylation increases EGF-induced EGFR activation**

The increased sensitivity to Gefitinib shown by silencing DHHC20 suggests that decreased DHHC20 expression increases the dependence of cells on EGFR signaling. Under resting conditions the activation state of EGFR in shDHHC20 cells measured by phosphorylation of EGFR (tyrosines 1068, 1148 and 1173) and the downstream signaling component AKT (serine 473) was similar to control cells (Figure 2A). However, upon EGF stimulation silencing DHHC20 dramatically increased the amplitude and duration of EGFR activation (Figure 2A). Furthermore, the level of phosphorylated AKT in shDHHC20 cells was elevated and sustained through the four hour time course of EGF treatment compared to shControl cells (Figure 2A). In contrast to AKT phosphorylation the levels of phosphorylated ERK were higher in resting DHHC20 shRNA expressing cells relative to the shControl cells and did not increase further with EGF stimulation (Figure 2A). These results are rescued by expression of shRNA resistant DHHC20 (Figure S5A). Similar results were observed in SW1573 lung adenocarcinoma cells (Figure S5B).

We next asked if inhibition of DHHC20 increased the sensitivity to EGF stimulation compared to control cells. Cells were treated with varying concentrations of EGF and phosphorylation of EGFR and AKT was measured. While phosphorylated EGFR was detected in shControl cells at EGF concentrations as low as 10ng/ml, EGFR was activated in shDHHC20 cells at 5ng/ml of EGF (Figure S6). Although the level of EGFR was elevated by 2-fold in the DHHC20 shRNA cells the ratio of phosphorylated EGFR/total EGFR was increased by nearly 6-fold indicating a higher level of receptor activation (Figure S6). The elevated level of EGFR activation in shDHHC20 cells

suggested higher doses of Gefitinib might be required to inhibit EGFR signaling. Although the shDHHC20 cells had a much higher amount of activated EGFR, treatment with 0.1  $\mu$ M Gefitinib reduced EGFR and AKT phosphorylation to the same level in both the control and the DHHC20 shRNA expressing cells (Figure 2B). The increase in cell death with Gefitinib treatment in shDHHC20 cells may be the result of the greater overall decrease in EGFR signaling. Unexpectedly, ERK phosphorylation was not inhibited by Gefitinib suggesting ERK is activated through an alternative signaling pathway. However, inhibition of EGFR expression by shRNA reduced ERK activation in DHHC20 silenced cells demonstrating it is dependent on EGFR (Figure 2C).

We next asked if acute inhibition of palmitoylation with 2BP increases EGFR activation and downstream signaling. After 1 hour AKT activation rapidly increased in cells treated with 500nM 2BP which returned to basal levels by 12 hours (Figure 2D). In contrast, ERK activation in response to 2BP was induced later, at 6 hours, and was maintained throughout the 24 hour time course (Figure 2D). In the presence of EGF, treatment with 2BP increased the phosphorylation of EGFR compared to vehicle control (Figure 2E).

**Figure 2**

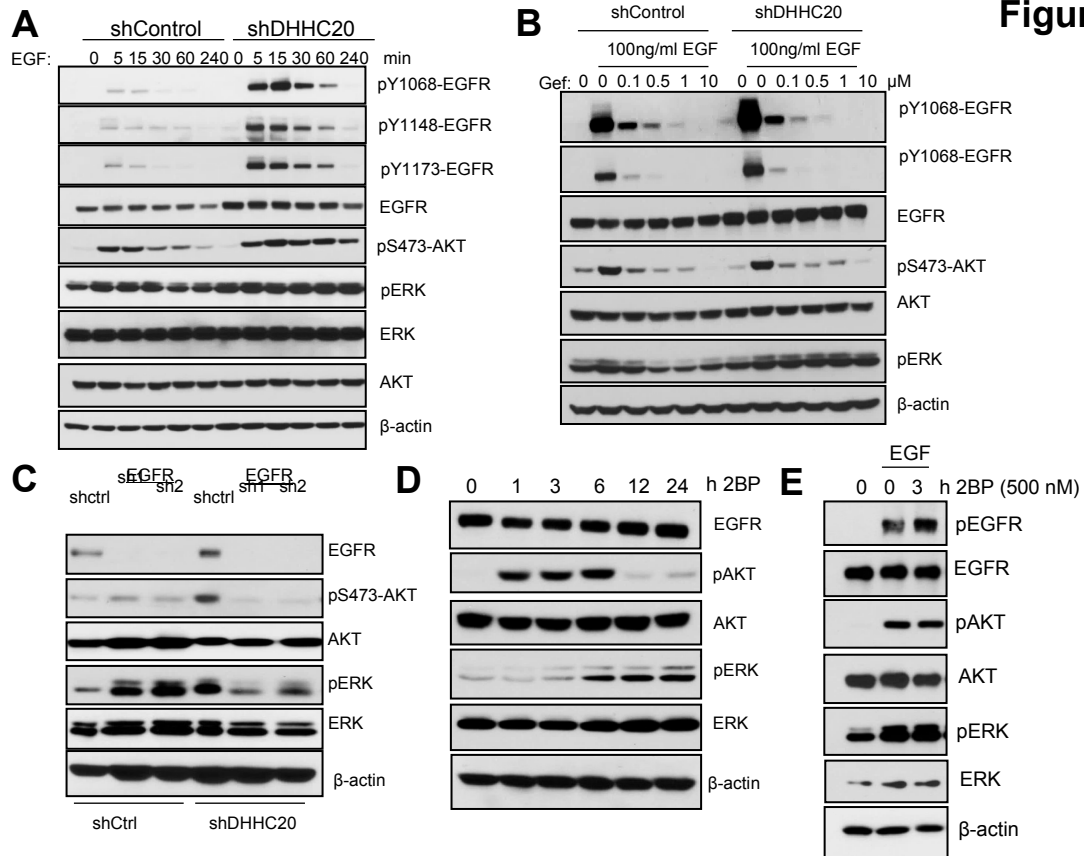


**Figure 2. DHH20 knockdown increases EGFR activation and signaling.** (A) Silencing DHH20 in MDA-MB-231 cells increases EGFR expression and the phosphorylation of EGFR and AKT. Serum starved MDA-MB-231 shControl and shDHH20 cells were treated with 100ng/ml EGF for the indicated time points and protein expression was determined by SDS-PAGE. (B) Gefitinib inhibits activation of EGFR and AKT. MDA-MB-231 cells were serum starved in the presence of 10 $\mu$ M gefitinib, treated with EGF for 15 minutes and activation of EGFR, AKT, and ERK was determined by SDS-PAGE. (C) The increased phosphorylation of ERK observed in DHH20 silenced cells is dependent on EGFR signaling. MDA-MB-231 shControl and shDHH20 cells were infected with shRNA targeting EGFR. Cells were serum starved and activation of ERK and AKT was analyzed by SDS-PAGE. (D) 2BP increases AKT and ERK activation. MDA-MB-231 cells were treated with 500nM 2BP and the activation of AKT and ERK was analyzed by SDS-PAGE. (E) 2BP increases EGF-induced EGFR activation. MDA-MB-231 cells were serum starved, treated with 500nM 2BP for 3 hours and then stimulated with EGF for 15 minutes. Activation of EGFR, AKT, and ERK was analyzed by SDS-PAGE.

## **Inhibition of DHHC20 expression disrupts EGFR endocytic trafficking**

Ubiquitylation of EGFR serves as an endosomal trafficking signal to facilitate lysosomal degradation (Katzmann et al., 2002). Cells expressing shDHHC20 had higher levels of ubiquitylated EGFR compared to shControl cells (Figure 3A). IF staining was used to examine the effect of DHHC20 expression on the endocytic trafficking of EGFR. In resting cells EGFR is predominantly localized at the plasma membrane in both shControl and shDHHC20 cells (data not shown). Upon EGF stimulation of shControl cells EGFR was internalized and clustered around the perinuclear region of the cell containing the lysosomal membrane protein LAMP-1 (Figure 3B). In contrast, in shDHHC20 cells the internalized vesicles maintained a peripheral distribution and failed to localize with LAMP-1 positive vesicles after 15 minutes of EGF stimulation (Figure 3B). Expression of shRNA resistant DHHC20 partially restored the wild type perinuclear localization and lysosomal targeting of EGFR in response to EGF (Figure 3B). In shDHHC20 cells, EGFR containing vesicles localized to the cell periphery and lacked markers of early (EEA1, Rab5) or late (Rab7) endosomes within 15 minutes of EGF stimulation (Figure S7A-F). Additionally, EGFR localization did not overlap with the recycling endosome marker Rab11 indicating that the aberrant EGFR trafficking was not the result of increased receptor recycling (Figure S7G). Live imaging of fluorescently tagged EGF indicates EGF is internalized in DHHC20 cells similar to control cells. After internalization, the localization of the EGF containing endosomes in the DHHC20 shRNA expressing cells is static at the periphery of the cell (Figure 3C). This is in contrast to control cells where EGF is rapidly trafficked to lysosomes (Figure 3C). To determine if the altered trafficking is specific to EGFR, cells were labelled with fluorescently tagged transferrin. We found that unlike EGF the trafficking of the endocytosed transferrin is

similar between DHHC20 silenced cells and control cells and the accumulation of enlarged endosomes that formed with EGF did not form with transferrin (Figure S8).

After internalization EGFR is thought to continue to signal until the receptor is sequestered into multivesicular bodies (MVB). Endosome specific signaling to ERK and AKT has been demonstrated for EGFR following the endosomal recruitment of scaffold proteins such as Grb2 (Murphy et al., 2009). We asked if the increased amount of EGFR in the endosomal pool actively signals in shDHHC20 cells by examining endogenous Grb2 localization by IF. After 15 minutes of EGF treatment the EGF containing endosomes in the DHHC20 silenced cells localized with very high levels of Grb2 compared to control cells that contained low levels of endosomally localized Grb2 (Figure 3D). These findings suggest that the accumulation of endosomal EGFR likely contributes to the sustained signaling responses observed in shDHHC20 expressing cells.

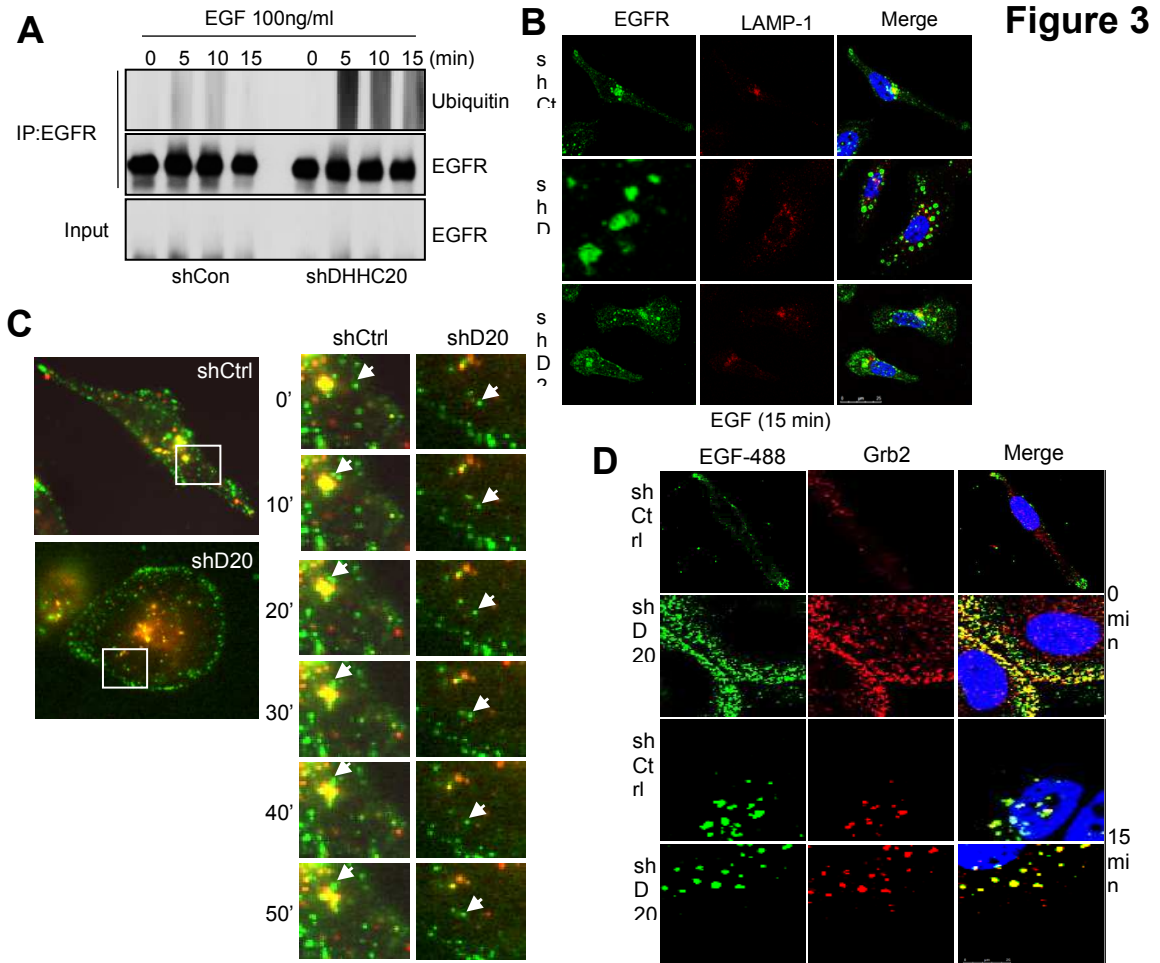


**Figure 3. Silencing DHHC20 expression disrupts EGFR endocytic trafficking.**

(A) Ubiquitination of EGFR is increased in shDHHC20 cells in response to EGF. Serum starved MDA-MB-231 cells were treated with 100ng/ml EGF and EGFR was immunoprecipitated using anti-EGFR (sc-120). Ubiquitylation was determined by SDS-PAGE. (B) Silencing DHHC20 decreases EGF-induced EGFR trafficking to LAMP-1 positive lysosomes, which is rescued by exogenous expression of DHHC20. MDA-MB-231 shControl, shDHHC20 and shDHHC20+DHHC20 cells were treated with EGF for 15 minutes and stained for EGFR (green), LAMP-1 (red) and DAPI (blue). Confocal images were obtained and colocalization of EGFR and LAMP-1 was measured by Mander's Overlap Coefficient; shControl (0.403), shDHHC20 (0.242), shDHHC20+DHHC20 (0.395). (C) Live cell trafficking of EGF to lysosomes is disrupted in shDHHC20 cells. MDA-MB-231 shControl and shDHHC20 cells were incubated with 50nM LysoTracker (red) and 25µg/ml Alexa-fluor488 labeled EGF (green) and images were obtained every 10 seconds for 20 minutes. (D) Silencing DHHC20 increases Grb2 localization to EGF-positive endosomes. MDA-MB-231 shControl and shDHHC20 cells were incubated with Alexa-fluor488 labeled EGF (green), fixed and stained for Grb2 (red) and DAPI (blue). Confocal images were obtained and colocalization between EGFR and LAMP-1 was measured by Mander's Overlap Coefficient; shControl (0.627), shDHHC20 (0.723).



## **DHHC20 palmitoylates EGFR within the C-terminal tail**

Since EGFR was recently reported to be palmitoylated, we asked if EGFR is the target of DHHC20 (Bollu et al., 2015). To detect palmitoylated EGFR we performed an *in vitro* acyl-biotinyl exchange (ABE) assay on MDA-MB-231 cells. The ABE assay removes palmitate from cysteine residues with hydroxylamine followed by substitution with biotin. In the presence of hydroxylamine, EGFR was detected in the streptavidin pull-down fraction compared to the negative control without hydroxylamine indicating the presence of palmitoylated EGFR (Figure 4A). Treatment with 2BP effectively inhibited EGFR palmitoylation (Figure 4B). Palmitoylation of EGFR in MDA-MB-231 cells was also observed by metabolically labelling cells with palmitic acid azide as a second approach to confirm EGFR palmitoylation (Figure 4C). Silencing DHHC20 reduced EGFR palmitoylation indicating that DHHC20 is required for wild type levels of EGFR palmitoylation (Figure 4C). Overexpression of DHHC20 was sufficient to increase EGFR palmitoylation in HEK293T cells expressing wild type (WT) EGFR compared to vector control cells (Figure 4D). Consistent with palmitoylation inhibiting EGFR signaling, when protein depalmitoylation is blocked with the small molecule Palmostatin B EGFR palmitoylation is increased and EGFR and AKT phosphorylation is inhibited (Figure S9A, B).

EGFR contains nine cysteine residues within the intracellular domain, six of which are located within the tyrosine kinase domain and three within the C-terminal tail (Figure 4F). An EGFR truncation mutation which deletes amino acids 1024-1186 including the three cysteine residues within the C-terminal tail completely abolished EGFR palmitoylation in HEK293T cells ectopically expressing DHHC20, indicating that the palmitoylated cysteine residues are located within the C-terminal tail (Figure 4D).

To identify the specific palmitoylated residues by mass spectrometry (MS) the palmitoylated peptides were purified by ABE followed by alkylation with iodoacetamide (Figure 4E). When analyzed by MS the intracellular palmitoylated cysteine residues were detected as carbamidomethyl (CAM) modified and the unmodified cysteine residues in the cytosolic domains that were blocked with NEM were detected as NEM modified based on the mass difference between NEM and CAM (Figure 4E, F). Cysteine residues C915, C926 in the kinase domain were detected only as NEM modified indicating the absence of the palmitoyl modification (Figure 4F, G). However, peptide ions were identified with both NEM and CAM modifications for both C1025 and C1034 in the C-terminal tail (Figure 4H-L, data not shown). This indicates both C1025 and C1034 sites exist in both palmitoylated and unpalmitoylated states in the cell. The large size of the tryptic peptide containing cysteine residue C1122 prevented the identification of the peptide by MS.

**Figure 4**

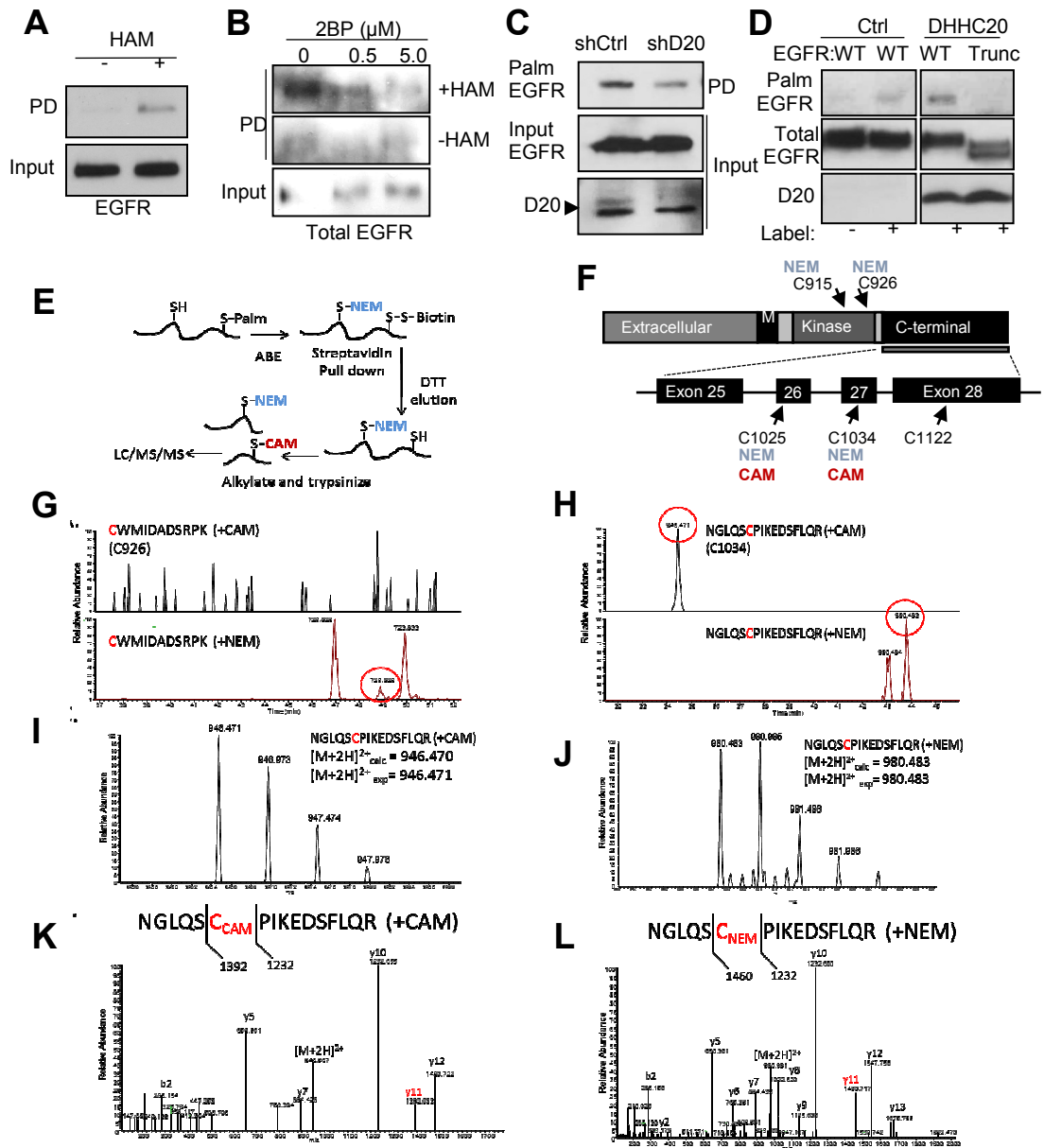


**Figure 4. DHH20 palmitoylates EGFR within the C-terminal tail.** (A) EGFR is palmitoylated. EGFR palmitoylation in MDA-MB-231 cells was determined using an acyl-biotinyl exchange (ABE) assay followed by immunoblotting for EGFR. (B) The palmitoyltransferase inhibitor 2BP reduces EGFR palmitoylation. MDA-MB-231 cells were treated with 2BP for 24 hours and EGFR palmitoylation was determined by ABE. (C) Silencing DHH20 decreases EGFR palmitoylation in MDA-MB-231 cells. Palmitoylation of endogenous EGFR was determined by metabolic labeling. (D) DHH20 palmitoylates the C-terminal tail of EGFR. HEK293T cells transiently expressing full length EGFR (WT) or a C-terminal tail truncation mutant (Trunc) and either empty vector control (EV) or DHH20. Palmitoylation of EGFR was determined by metabolic labelling. (E) Experimental strategy for detecting EGFR palmitoylation by mass spectrometry. (F) Schematic of EGFR including the exons and cysteine residues located within the C-terminal tail and kinase

domain. Numbering corresponds to human EGFR excluding the signal sequence. Cysteines 751, 757, 773 and 794 located in the kinase domain are not shown. (G) Selected ion chromatograms of the  $[M+2H]^{2+}$  peptide (CWMIDADSRPK) with both potential carbamidomethylation (CAM, +57 Da) and N-Ethylmaleimide (NEM, +125 Da) modifications of cysteine 926. As can be seen in the chromatograms, only a peak for the CWMIDADSRPK (+NEM) peptide was found, and no peaks for CWMIDADSRPK (+CAM) were observed. (H) Selected ion chromatograms of the  $[M+2H]^{2+}$  peptide (NGLQSCPIKEDSFLQR) with both potential carbamidomethylation (CAM, +57 Da) and N-Ethylmaleimide (NEM, +125 Da) modifications of cysteine 1034. As can be seen in the chromatograms, both peaks for NGLQSCPIKEDSFLQR (+NEM) and NGLQSCPIKEDSFLQR (+CAM) were observed (~ 10 min retention time shift between the species). (I) Full mass spectrum of the parent ion corresponding to the NGLQSCPIKEDSFLQR (+CAM), and accurate mass confirms the correct assignment. (J) Full mass spectrum of the parent ion corresponding to the NGLQSCPIKEDSFLQR (+NEM), and accurate mass confirms the correct assignment. (K) MS/MS spectrum of the  $[M+2H]^{2+}$  peptide NGLQSCPIKEDSFLQR (+CAM), with highlighted fragment ion indicating the CAM modification on the Cys residue 1034. (L) MS/MS spectrum of the  $[M+2H]^{2+}$  peptide NGLQSCPIKEDSFLQR (+NEM), with highlighted fragment ion indicating the NEM modification on the cysteine residue 1034.

## **Mutation of palmitoylated cysteine residues increases EGFR interaction with Grb2**

To determine the molecular mechanism by which EGFR palmitoylation regulates its signaling activity cysteine residues 1025, 1034 and 1122 were mutated to alanine either alone or in combination. When expressed in MDA-MB-231 cells the C1025A, C1122A and double cysteine mutants correctly localized to the cell membrane and were indistinguishable from WT EGFR (Figure 5A). In contrast to the other mutants the C1034A mutation could be detected by indirect IF microscopy in only a small number of rounded cells that contained very high levels of phosphorylated ERK compared to cells expressing wild type EGFR (Figure 5B). The morphology and high levels of phosphorylated ERK in the C1034A expressing cells could indicate either a block in mitosis or induction of cell death. As a result, the C1034A mutant could not be detected by immunoblotting and we were therefore unable to examine this mutation in palmitoylation and signaling assays. In all the subsequent experiments we discuss the C1025 and C1122 sites with the knowledge that C1034 is possibly if not likely palmitoylated. Mutation of either C1025 or C1122 markedly reduced EGFR palmitoylation compared to the wild type receptor in HEK293T cells, but mutation of both cysteine residues was not sufficient to completely eliminate palmitoylation indicating these residues are at minimum required for wild type EGFR palmitoylation levels (Figure 5C). This raised the question of whether there are mutations in cancer that delete any of the inhibitory cysteine residues that would indicate a biological function for EGFR palmitoylation.

A mutation identified in lung cancer that deletes exons 25-26 increases EGFR phosphorylation, downstream signaling to AKT, and anchorage independent growth (Figure 5D) (Imielinski et al., 2012). Since this mutation removes cysteine1025, we

asked if mutating this residue is sufficient to increase anchorage independent growth. When NIH 3T3 cells expressing WT or the EGFR cysteine mutants were grown in soft agar the exon 25-26 deletion increased the number of colonies by 2.4 fold compared to cells expressing WT EGFR (Figure 5D, Figure S10). The C1025 and C1025/C1122 mutants significantly increased colony formation compared to WT EGFR by 1.7 and 1.9 fold respectively (Figure 5D). The C1122 single mutant did not have a significant effect on colony formation. Furthermore cells expressing EGFR C1025A or C1025A/C1122A migrate significantly faster than cells expressing WT EGFR (Figure 5E). We conclude that the loss of palmitoylation at these cysteine residues is important for the increased migration observed with DHHC20 shRNA and the cell transformation previously described for the exon 25-26 deletion seen in lung cancer patients. However, the sites are not equivalent in promoting EGFR mediated cell behavior since C1025A has a stronger effect on colony formation and migration than C1122A.

To determine if the accumulation of EGFR and the high endosomal localization of Grb2 observed in DHHC20 silenced cells was caused specifically by decreased EGFR palmitoylation the EGFR C1025/1122A mutant was examined in NIH 3T3 cells. Similar to what was observed in shDHHC20 cells the C1025/1122A mutant receptor accumulated in peripherally localized endosomes that did not colocalize with LAMP-1 (Figure 5F). Furthermore, there was an increase in Grb2 staining in cells expressing C1025/1122A compared to cells expressing the WT receptor (Figure 5G).

To study the mechanism of receptor activation in greater detail we examined activation mediated Grb2 binding to the EGFR mutants. Immunoprecipitation of WT and mutant EGFR revealed an increase in the interaction of the C1025A mutant with Grb2 compared to WT EGFR (Figure 5H-I). However, EGFR C1122A and C1025A/C1122A

did not increase the interaction with Grb2 indicating that palmitoylation of C1025 is unique in its ability to attenuate Grb2 binding. Grb2 binding with the exon 25-26 deletion mutant was higher compared to WT EGFR and is strikingly similar to what was observed with the C1025A mutant, providing further evidence that the pathway activation caused by the exon 25-26 deletion is through decreased palmitoylation at C1025 (Figure 5H-I).

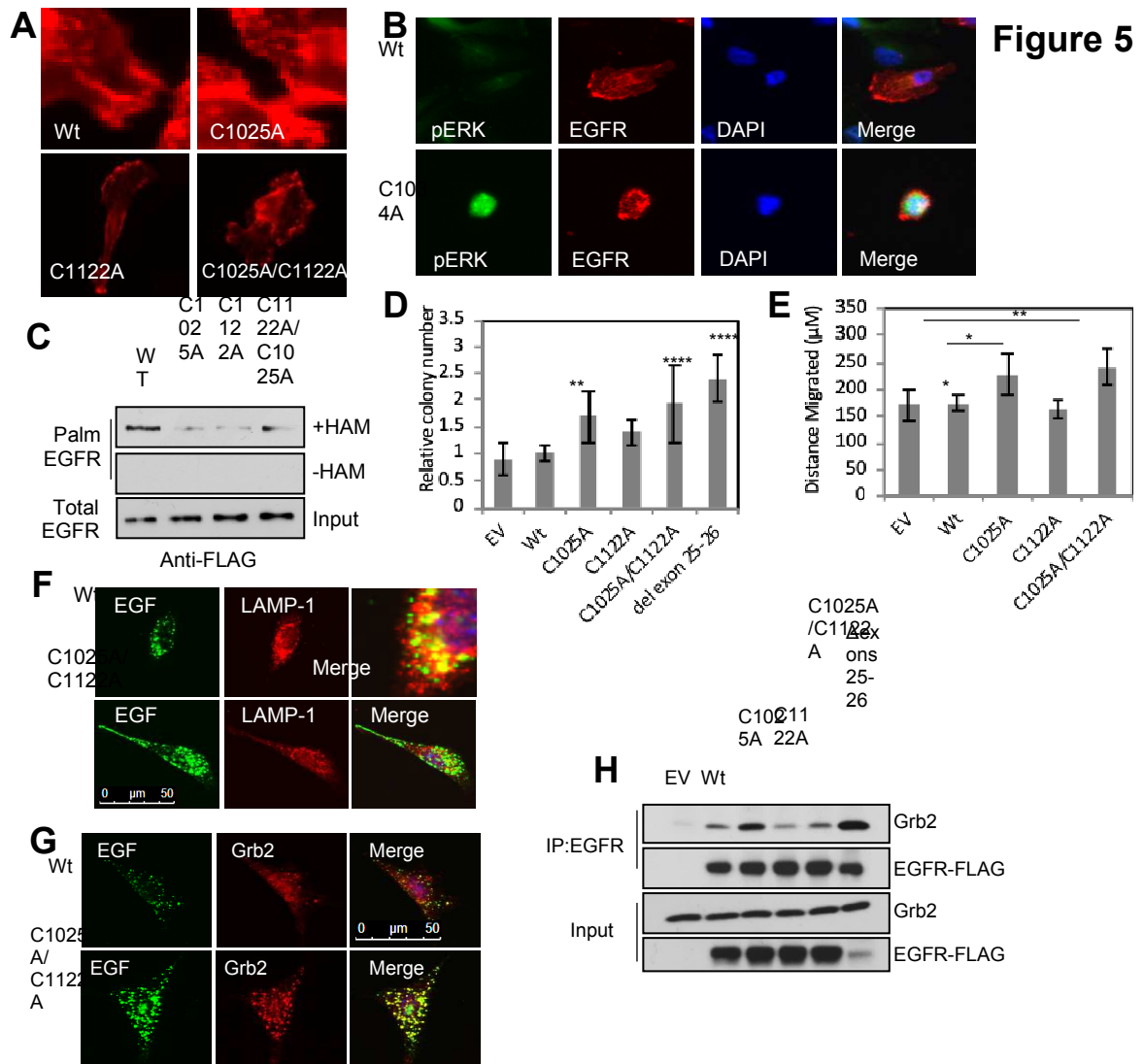


**Figure 5. Mutation in C1025 and C1122 activates EGFR, promotes cellular transformation and increases cell migration.** (A) Mutation of cysteines 1025 and 1122 does not alter receptor localization. MDA-MB-231 cells were transfected with the indicated EGFR constructs, fixed and stained for FLAG-tagged EGFR (red). (B) Expression of EGFR-C1034A in MDA-MB-231 cells increases ERK phosphorylation. Cells were fixed and stained for pERK (green), FLAG-EGFR (red) and DAPI (blue). (C) Mutation of EGFR cysteine residues 1025, 1122 and 1025/1122 decreases EGFR palmitoylation. HEK293T cells were transfected with DHHC20 and the indicated EGFR constructs. Palmitoylation of EGFR cysteine mutants was determined by ABE. (D) Mutation of EGFR C1025, C1025/C1122 and deletion of exons 25-26 increases colony formation in soft agar. NIH 3T3 cells expressing EGFR constructs were plated in soft agar and colonies were counted at 8 weeks. Expression levels of each mutant are shown in Figure S10 (mean  $\pm$  StDev). (E) Mutation of EGFR C1025 and C1025/C1122 increases cell migration. NIH 3T3 cells expressing EGFR constructs were scratched and migration was measured at 8 hours (mean  $\pm$  SEM). (F-G) Mutation of EGFR C1025/C1122 delays EGFR endocytosis and increases the localization of Grb2 to EGF-positive endosomes. NIH 3T3 cells expressing doxycycline inducible EGFR constructs were serum starved in the presence of 1 $\mu$ g/ml doxycycline, treated with EGF-alexafuor488 for 15 min, fixed, and stained for LAMP-1 (F) or Grb2 (G). (H) Mutation of EGFR C1025 increases the interaction between Grb2 and EGFR. HEK293T cells were transfected with EGFR constructs and EGFR was immunoprecipitated with anti-EGFR (sc-120 AF488). The binding of EGFR to Grb2 was determined by SDS-PAGE.



## **EGFR palmitoylation promotes the turnover of activated EGFR and association of the C-terminal tail with the plasma membrane.**

We examined the activation of the palmitoylation defective EGFR mutants to further understand the mechanism by which palmitoylation suppresses EGFR activation. We first asked if the cysteine point mutations phenocopy the increase in EGFR activation observed with DHHC20 shRNA. When transiently expressed in NIH 3T3 cells EGFR mutants C1025A, C1122A and C1025A/C1122A increased the basal phosphorylation of EGFR at Tyr1068, Tyr1148, and Tyr1173 and phosphorylation of AKT compared to the WT receptor under serum starved conditions (Figure 6A). When cells expressing mutant EGFR were treated with 10 $\mu$ M Gefitinib the activation of AKT was inhibited, but ERK activation was unaffected (Figure S11). Taken together, the high basal EGFR tyrosine phosphorylation observed in the EGFR mutants in conjunction with Grb2 binding being specific to the C1025 mutant indicates that tyrosine phosphorylation is not sufficient to promote Grb2 binding.

To determine how palmitoylation of EGFR is regulated we examined the levels of palmitoylated and dually palmitoylated/phosphorylated EGFR in response to EGF stimulation. Palmitoylated WT EGFR is detected in resting cells and increases modestly after 5 minutes of EGF stimulation, returning to basal levels by 60 minutes (Figure 6B). To determine the contribution of the individual palmitoylation sites the level of palmitoylated EGFR during EGF stimulation was examined in the EGFR cysteine point mutants. In the C1025A mutant palmitoylated C1122 peaked at 5 minutes post-EGF treatment and subsequently decreased below basal levels at 15 minutes and returned to basal levels at 60 minutes (Figure 6B). Unlike C1122, palmitoylation of C1025 in the

C1122A mutant is below detection in resting cells. After 5 minutes of EGF stimulation C1025 palmitoylation increased and then steadily decreased by 60 minutes (Figure 6B).

We next examined the phosphorylation kinetics of palmitoylated EGFR in response to EGF and found that palmitoylated EGFR is also phosphorylated at tyrosine 1068. However, in contrast to the total level of phosphorylated WT EGFR (input) which is does not decrease until 60 minutes, phosphorylation of palmitoylated WT EGFR rapidly decreased between 5 and 15 minutes (Figure 6C). This suggests the dually phosphorylated and palmitoylated receptor fraction is more rapidly turned over than the phosphorylated unpalmitoylated receptor fraction. In the C1025A mutant palmitoylation is restricted to C1122 and phosphorylation of the palmitoylated receptor peaked at 5 minutes of EGF stimulation, but then decreased down to basal levels by 15 minutes (Figure 6C). In the C1122A mutant the receptor is palmitoylated at C1025 and is only weakly phosphorylated consistent with the palmitoylation of C1025 suppressing EGFR activation. Furthermore, in the C1122A mutant the total receptor phosphorylation (input) is sustained and does not decrease by 60 minutes (Figure 6C). This indicates C1122 palmitoylation promotes receptor turnover. While we can't address the function of cysteine 1034 these results indicate that C1025 and C1122 are palmitoylated in response to EGF with each site having a unique effect on receptor function.

The C-terminal tail is not included in current crystal structures of EGFR and therefore little is known about how it is positioned relative to the kinase domain. Although EGFR is membrane associated, the C-terminal tail is unstructured and thought to extend away from the plasma membrane and into the cytosol. We reasoned that palmitoylation could promote peripheral association of the C-terminal tail with the plasma membrane by burying palmitate in the lipid bilayer. To test this possibility a recognition sequence for

the protease thrombin was inserted in frame between the kinase domain and the C-terminal domain to allow the C-terminal tail to be cleaved from the plasma membrane. Cell lysates were treated either with or without thrombin and the membrane fraction was isolated by centrifugation and analyzed by SDS PAGE. If the C-terminal tail associates with the plasma membrane after proteolytic cleavage then it will be detected by immunoblotting in the membrane fraction with an antibody specific to the C-terminus of EGFR (Figure 6D). Only after thrombin treatment is the 25kDa C-terminal tail detected in the membrane fraction (Figure 6E). The membrane association of the cleaved C-terminal tail is dependent on palmitoylation as inhibition of DHHC20 by shRNA markedly reduces the 25kDa fragment in the membrane fraction (Figure 6E).

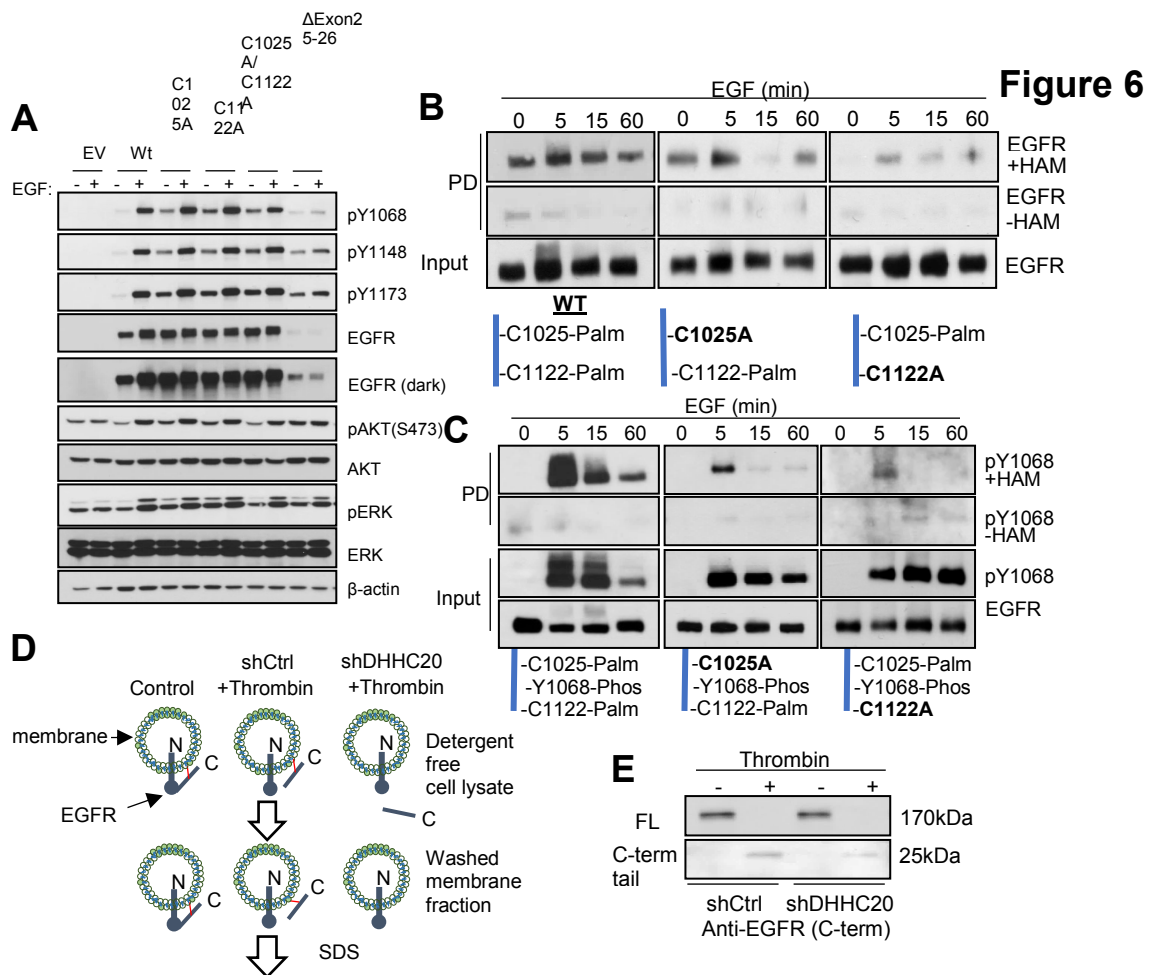


**Figure 6. Palmitoylation regulates the activity of EGFR in response to EGF.** (A) Mutation of EGFR cysteines activates EGFR independent of EGF. NIH 3T3 cells were transfected with EGFR constructs, serum starved, and stimulated with 25µg/ml EGF for 5 minutes where indicated. Activation of EGFR, AKT and ERK was determined by SDS-PAGE. (B) EGFR palmitoylation is increased with EGF stimulation. MDA-MB-231 cells were serum starved, treated with 100ng/ml EGF and palmitoylation was determined by ABE. (C) Palmitoylation of the phosphorylated form of EGFR is reduced in EGFR cysteine mutants C1025A and C1122A. MDA-MB-231 cells stably expressing doxycycline inducible EGFR constructs were serum starved in the presence of 1µg/ml doxycycline, treated with 100ng/ml EGF, and palmitoylation was determined by ABE. (D) Experimental strategy of the thrombin cleavage assay. (E) Palmitoylation pins the C-terminal tail of EGFR to the cell membrane. HEK293T cells transiently expressing EGFR-FLAG containing a thrombin cleavage site (LVPRGS) at Gly959 were lysed in the presence or absence of thrombin protease. The membrane fraction was isolated by centrifugation and EGFR was immunoprecipitated from the membrane fraction. The presence of membrane bound full length (170kDa) EGFR and the cleaved C-terminal tail (25kDa) was determined by SDS-PAGE.

## Discussion

We have identified a mechanism to regulate EGFR activation through palmitoylation of the C-terminal tail of EGFR. We show that EGF induces palmitoylation of EGFR and that palmitoylation facilitates receptor inactivation through two distinct mechanisms. Mutation of cysteines 1025 and 1122 alone and in combination increase the basal phosphorylation of EGFR, ERK, and AKT. However, only mutation of C1025 increases the binding of EGFR with the adapter protein Grb2. Furthermore, EGFR that is palmitoylated on C1025 has very low levels of EGF induced phosphorylation indicating that palmitoylation at C1025 blocks receptor signaling. Mutation of C1122 sustains EGFR phosphorylation in response to EGF and both total and phosphorylated EGFR palmitoylated on C1122 decreases precipitously after 15 minutes of EGF stimulation consistent with a role for palmitoylation at C1122 in promoting receptor turnover. This is consistent with the effects of silencing DHHC20 on EGFR function. When DHHC20 is silenced by shRNA EGFR signaling is increased and sustained, there is increased localization of Grb2 to EGFR positive endosomes, and there are increased levels of total EGFR (Figure 7).

Our findings demonstrate that palmitoylation of EGFR C-terminal cysteines reversibly “pins” the C-terminal tail to the plasma membrane to promote receptor inactivation. Disrupting the membrane association of the C-terminal tail by inhibiting palmitoylation may reduce steric hindrance or provide greater accessibility for adaptor protein binding (Figure 7). Additionally, the interaction between EGFR and endosomal ESCRT complex may require palmitoylation of the EGFR C-terminal tail to facilitate endocytic proper trafficking.

Palmitoylation is required for the endocytic trafficking and downregulation of EGFR. The delayed endocytic trafficking of EGFR observed in DHHC20 silenced cells may account for the elevated level of EGFR expression in these cells. The delay in EGFR endocytosis was recapitulated in the C1025/C1122 mutant supporting that palmitoylation of the receptor is responsible for the trafficking defect. Our findings suggest that delayed endocytic trafficking provides a platform for EGFR to signal within endosomal compartments. In support of this, other studies have shown that activated receptors accumulate in endosomes and can transmit signals that are distinct from those at the plasma membrane due to the endosomal localization of certain essential signaling components (Murphy, PNAS, 2009). Our findings reveal that the endosomal localization of Grb2 is increased when DHHC20 is silenced and when cysteines 1025 and 1122 are mutated. Based on our data we argue that the slower rate of endocytic trafficking in shDHHC20 cells allows for increased receptor signaling on endosomal compartments.

Blocking EGFR palmitoylation genetically by silencing DHHC20 or pharmacologically by treatment with 2BP sensitizes cells to EGFR TK inhibition. While silencing DHHC20 or mutating EGFR C-terminal palmitoylated cysteines increases EGFR activation, Gefitinib effectively reduces receptor phosphorylation to the same level as control cells. This marked decrease in EGFR signaling may be the mechanism leading to the increased toxicity of Gefitinib in DHHC20 silenced cells. The clinical implications of these findings are three-fold. First, the increase in dependency of EGFR signaling when DHHC20 is inhibited by shRNA raises the possibility that patients with inactivation of DHHC20 could show increased responsiveness to EGFR inhibitor therapy. Second, inhibition of DHHC20 with a small molecule could function therapeutically in combination with EGFR inhibitors. Third, the EGFR exon 25-26 deletion mutation identified in lung cancer increased colony formation in soft agar and

the interaction between EGFR and Grb2 similar to what was observed with the C1025A mutant. Therefore, loss of palmitoylation at C1025 may serve as a mechanism for the increased EGFR activation and transforming properties of the deletion mutant. Taken together, these data suggest that targeting of a peripheral modulator of EGFR signaling, DHHC20, in combination with EGFR TK inhibitors may serve as an effective clinical approach to treat cancers such as TNBC that are inherently resistant to EGFR targeted therapy.

**Figure 7**

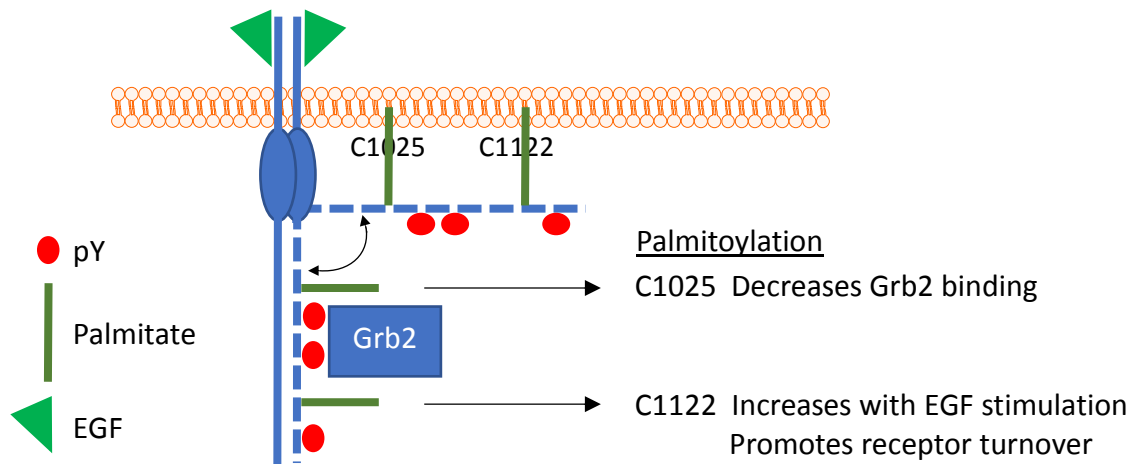
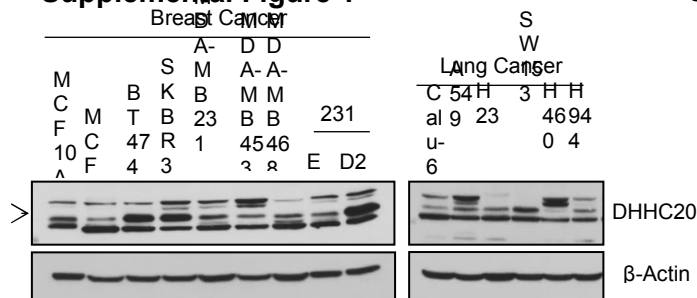


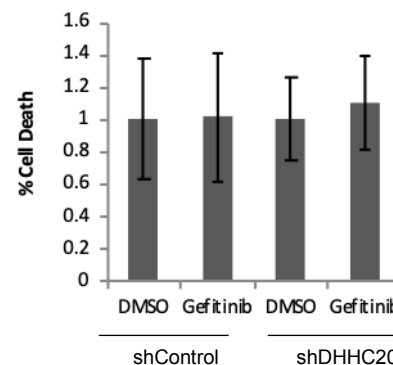
**Figure 7. Mechanistic summary of the effects of palmitoylation on EGFR activation and signaling.** These findings support a model where palmitoylation of the C-terminus of EGFR promotes membrane association. Palmitoylation of EGFR at C1025 impedes the binding of Grb2 to EGFR whereas palmitoylation at C1122 increases with EGF stimulation and promotes receptor turnover.



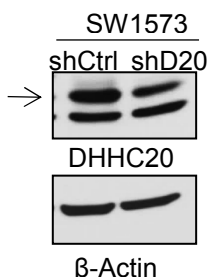
### Supplemental Figure 1



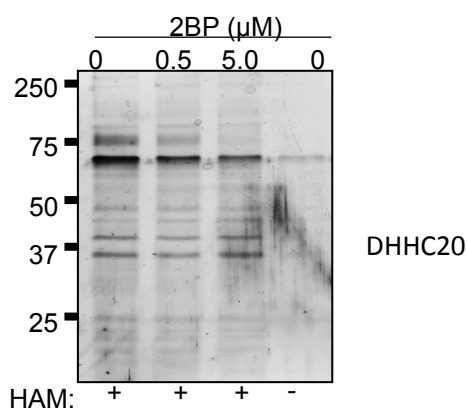
### Supplemental Figure 2



### Supplemental Figure 3



### Supplemental Figure 4



### Supplemental Figure Legends

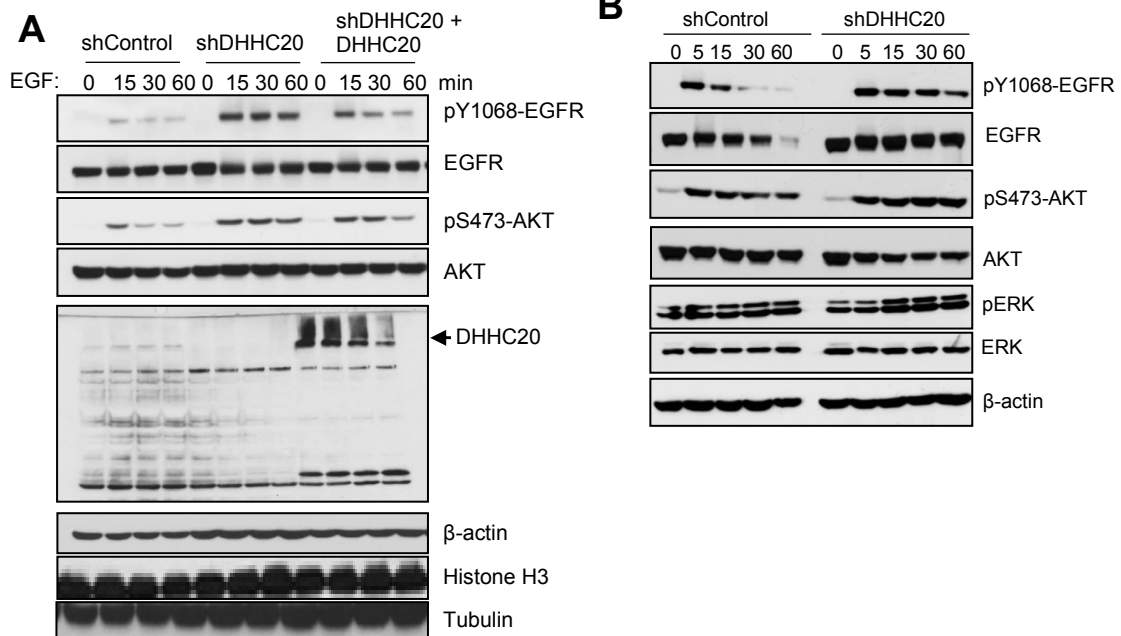
**Figure S1. DHHC20 is expressed in breast cancer and lung cancer cell lines.** Cells were lysed and DHHC20 expression was determined by SDS-PAGE.

**Figure S2. Treatment of MDA-MB-231 shControl and shDHHC20 cells with Gefitinib for 18 hours does not induce cell death.** MDA-MB-231 cells were treated with 10uM gefitinib for 18 hours and the percent cell death was measured by trypan blue staining.

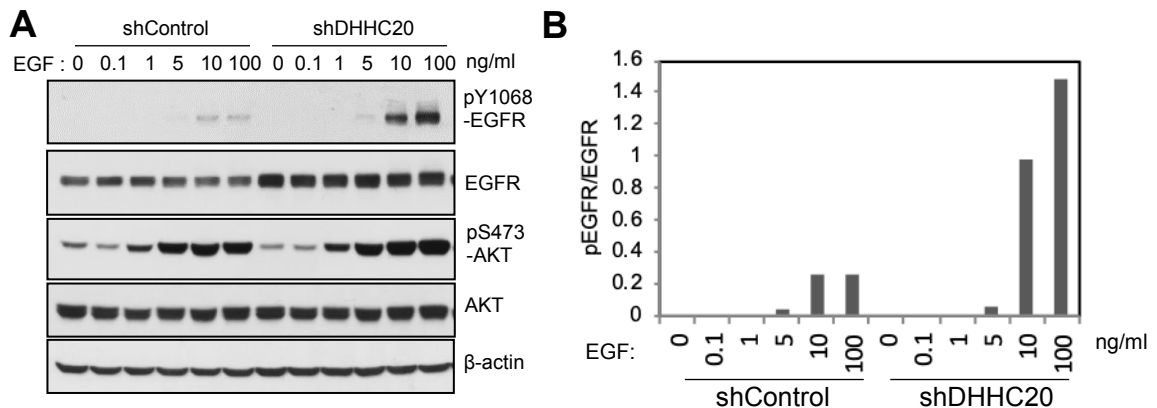
**Figure S3. DHHC20 expression is reduced in SW1573 lung cancer cells by shRNA.** SW1573 cells were infected with shDHHC20 shRNA, selected with puromycin, and protein expression was determined by SDS-PAGE.

**Figure S4. 2BP dose dependently reduces palmitoylation.** MDA-MB-231 cells were treated with 0, 0.5 or 5μM 2BP for 24 hours and palmitoylation was determined by ABE and silver stain.

## Supplemental Figure 5



## Supplemental Figure 6

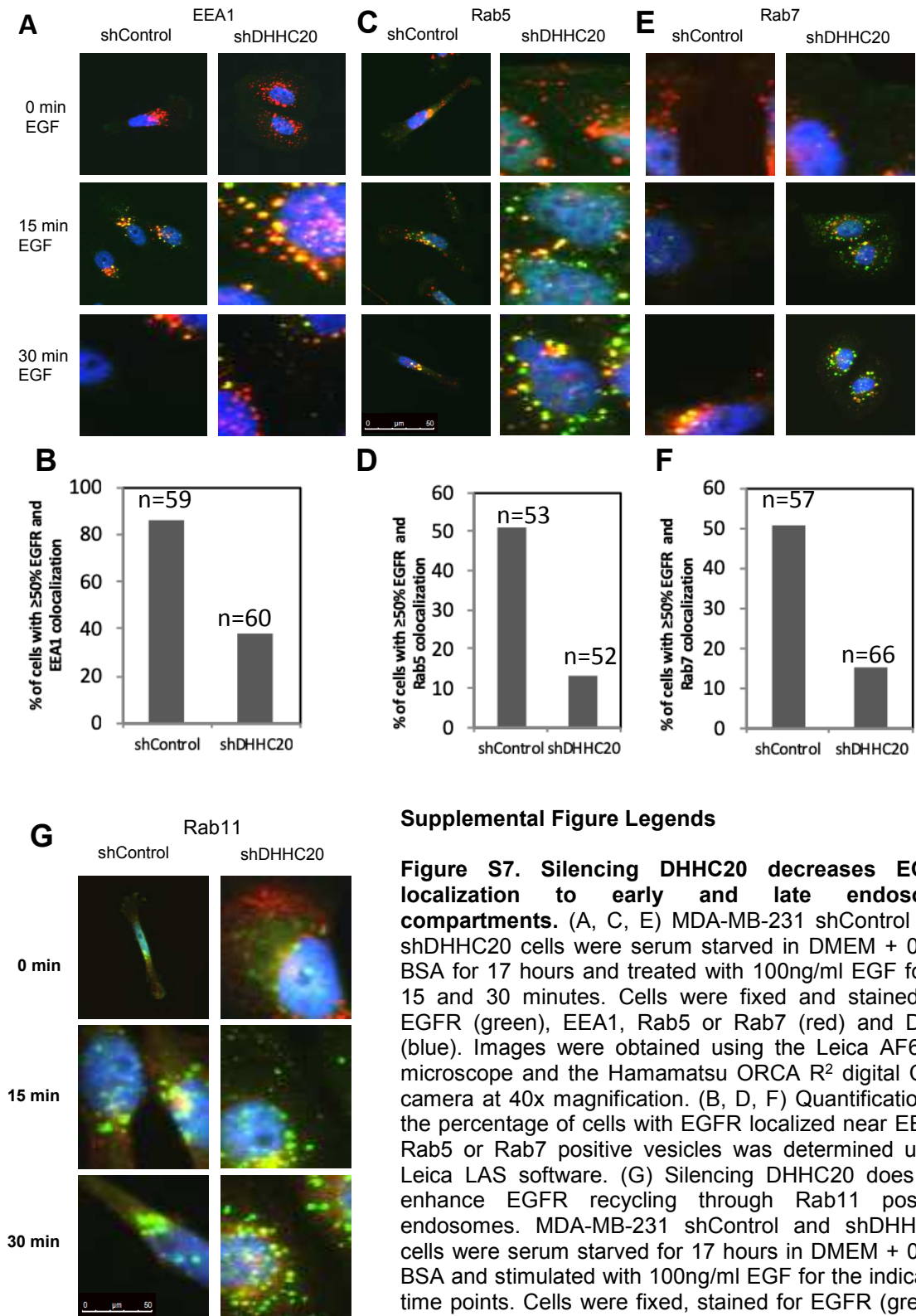


## Supplemental Figure Legends

**Figure S5. Elevated EGFR signaling is specific to DHHC20 inhibition and is conserved in SW1573 cells.** (A) Exogenous expression of DHHC20 partially rescues the elevated EGFR signaling. MDA-MB-231 shControl, shDHHC20 and shDHHC20 cells stably expressing a shRNA resistant DHHC20 construct were serum starved and treated with 100ng/ml EGF for the indicated times. EGFR signaling was determined by SDS-PAGE. (B) EGF-induced activation of EGFR, AKT and ERK is sustained in DHHC20 silenced lung adenocarcinoma cells. SW1573 cells were starved, treated with 100ng/ml EGF for the indicated time points, and activation of EGFR, AKT and ERK was determined by SDS-PAGE.

**Figure S6. Silencing DHHC20 increases EGFR activation in response to low and high doses of EGF.** MDA-MB-231 shControl and shDHHC20 cells were serum starved, treated with EGF at doses ranging from 0ng/ml - 100ng/ml for 15 minutes, and activation of EGFR and AKT was determined by SDS-PAGE. The phosphorylation of EGFR at Y1068 was normalized to total levels of EGFR by densitometry using ImageJ.

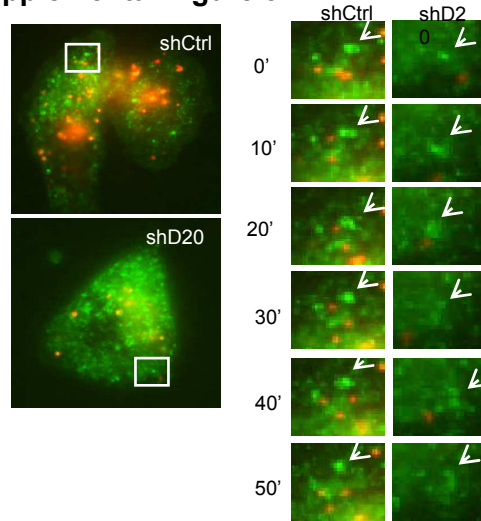
## Supplemental Figure 7



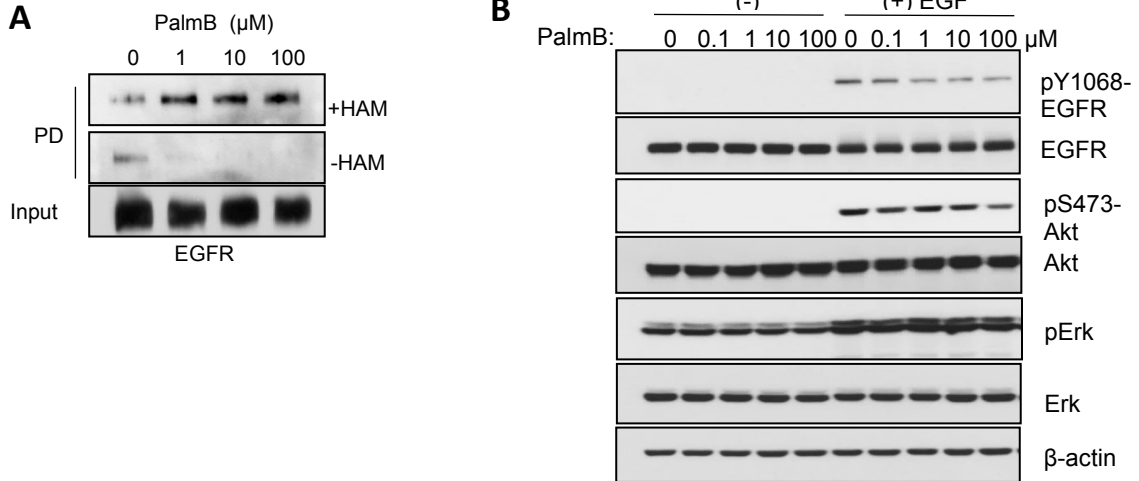
### Supplemental Figure Legends

**Figure S7. Silencing DHHHC20 decreases EGFR localization to early and late endosome compartments.** (A, C, E) MDA-MB-231 shControl and shDHHC20 cells were serum starved in DMEM + 0.2% BSA for 17 hours and treated with 100ng/ml EGF for 0, 15 and 30 minutes. Cells were fixed and stained for EGFR (green), EEA1, Rab5 or Rab7 (red) and DAPI (blue). Images were obtained using the Leica AF6000 microscope and the Hamamatsu ORCA R<sup>2</sup> digital CCD camera at 40x magnification. (B, D, F) Quantification of the percentage of cells with EGFR localized near EEA1, Rab5 or Rab7 positive vesicles was determined using Leica LAS software. (G) Silencing DHHHC20 does not enhance EGFR recycling through Rab11 positive endosomes. MDA-MB-231 shControl and shDHHC20 cells were serum starved for 17 hours in DMEM + 0.2% BSA and stimulated with 100ng/ml EGF for the indicated time points. Cells were fixed, stained for EGFR (green), Rab11 (red) and DAPI (blue) and imaged as in A, C, E.

### Supplemental Figure 8



### Supplemental Figure 9



### Supplemental Figure Legends (Continued)

**Figure S8. DHHC20 expression does not affect the intracellular trafficking of the transferrin.** MDA-MB-231 shControl and shDHHC20 cells were plated onto glass-bottom imaging dishes and starved in DMEM + 0.2% BSA for 17 hours. Cells were treated with 15ng/ml EGF in combination with 2.5 $\mu$ g/ml alexa-fluor488 labeled transferrin and 50nM lysotracker and incubated on ice for 1 hour. Cells were washed with PBS and images were obtained every 10 seconds for 20 minutes using the Leica AF6000 microscope and the Hamamatsu ORCA R<sup>2</sup> digital CCD camera at 40x magnification.

**Figure S9. Inhibition of EGFR depalmitoylation decreases EGFR signaling.** (A) The depalmitoylation inhibitor palmostatin B increases EGFR palmitoylation. MDA-MB-231 cells were treated with 1, 10, 100  $\mu$ M palmostatin B for 15 hours and EGFR palmitoylation was determined by ABE. (B) Inhibiting depalmitoylation with Palmostatin B attenuates EGFR activation. MDA-MB-231 cells were pretreated with the indicated doses of Palmostatin B for 8 hours and serum starved in the presence of Palmostatin B for an additional 17 hours. Cells were treated with 100ng/ml EGF for 15 min, lysed and protein expression and protein phosphorylation was determined by immunoblotting.



## **Materials and Methods**

### **Cell culture and transfection**

MDA-MB-231, HEK293T, and NIH 3T3 cells were cultured in DMEM containing 10% FBS. SW1573 cells were maintained in RPMI containing 10% FBS. All transfections were carried out using TransIT-LT1 (Mirus) according to the manufacturer's instructions.

### **Antibodies**

Anti-DHHC20 and anti-flag M2 antibodies were purchased from Sigma-Aldrich. Anti-pY1068-EGFR, pY1148-EGFR, pY1173-EGFR, EGFR, pERK, ERK, pS473-AKT, AKT,  $\beta$ -actin, EEA1, Rab5, Rab7 and Rab11 were obtained from Cell Signaling Technologies. Anti-LAMP-1 (CD107a) was purchased from BD Pharmigen. EGFR (528) Alexa Fluor 488 and EGFR (sc-120) were purchased from Santa Cruz Biotechnology. Transferrin from Human Serum, Alexa Fluor® 488 Conjugate was purchased from ThermoFisher. Phalloidin-594 and EGFR (528) Alexa Fluor 488 were purchased from Life Technologies.

### **Analysis of TCGA data**

The level of ZDHHC20 mRNA was plotted against the PAM50.SUBTYPE using the beeswarm package in the software program "R". Box plots were created to visualize the median values and quartiles of each subtype. Statistics were calculated using the function aov in "R"; ( $p < 2e-16$ ).

### **Silencing of human DHHC20 and EGFR**

The oligonucleotides for shControl, shDHHC20, and shEGFR constructs were synthesized (Integrated DNA Technologies) and inserted into the pLKO.1 vector.

shControl encodes the non-targeting sequence of *SHC002* (Sigma), the shRNA target sequences of human DHHC20 is 5'- GAGCTCTGCGTGTTTACTATT-3', and the shRNA sequences of EGFR are 5' CACAGTGGAGCGAATTCCTTT 3' (shEGFR 2.4) and 5' GCTGGATGATAGACGCAGATA 3' (shEGFR 3.2). MDA-MB-231 cells were transduced with lentivirus encoding shControl or shDHHC20 and selected by puromycin treatment (1 µg/ml). A shRNA resistant DHHC20 construct was used to rescue expression in shDHHC20 cells. MDA-MB-231 cells transduced with shEGFR lentivirus were harvested 72 hours post infection.

### **Soft Agar Colony Formation**

$5 \times 10^3$  NIH 3T3 cells were suspended in 0.4% agarose and plated onto a 0.8% solidified agarose layer. Colonies were manually counted from triplicate wells at 4 weeks.

### **Cell Viability**

Cells were treated with Gefitinib (10µM) and/or 2BP (500nM and 5µM) for 72hrs and viability was measured by Trypan Blue staining. Quantification was done using a 1-way ANOVA with Tukey's multiple comparison post-test.

### **EGFR signaling**

MDA-MB-231 and SW1573 cells were serum starved for 17 hours in DMEM+0.2% BSA. Cells were stimulated with 100ng/ml of EGF and harvested in RIPA buffer containing 150mM NaF , 2mM Na<sub>3</sub>V0<sub>4</sub>, 1mM PPI, 2µg/ml pepstatin A, 1µg/ml aprotinin and 1µg/ml leupeptin. Activation of EGFR, ERK and AKT was measured by SDS-PAGE.

### **Immunofluorescence microscopy**

MDA-MB231 shControl and shDHHC20 cells were serum starved for 17 hours in DMEM+0.2% BSA, treated with 100ng/ml EGF, and fixed in formalin. Cells were permeabilized in 0.1% triton-X-100, blocked in 5% BSA and primary antibodies were added overnight. Where indicated, cells were incubated with 1µg/ml Alexa-fluor488 labeled EGF for 1 hour on ice and transferred to 37°C for 15 minutes before fixing and adding primary antibodies. Secondary Alexa-Fluor antibodies were used prior to mounting the coverslips with DAPI-containing mounting media. Cells were visualized on a Leica SP8 confocal microscope or a Leica AF6000 microscope. Images were obtained using the Hamamatsu ORCA R<sup>2</sup> digital CCD camera at 40x magnification. Quantification was determined using Perkin Elmer's Volocity software.

### **Live cell microscopy**

MDA-MB-231 shControl and shDHHC20 cells were serum starved in DMEM + 0.2% BSA for 17 hours and incubated with 50nM lysotracker (red) for 30 minutes. The lysotracker was removed and cells were incubated on ice for 30 minutes with 25µg/ml Alexa-fluor488 labeled EGF (green) or 2.5ug/mL Alexa-fluor488 labeled transferrin and 15ng/mL unlabeled EGF . Cells were washed, incubated in HBSS media (HBSS + 1mg/mL glutamine + 1% FBS + 20mM HEPES, pH 7.4), and images were obtained in a 37°C humidified chamber every 10 seconds for 20 minutes using the Leica AF6000 microscope and the Hamamatsu ORCA R<sup>2</sup> digital CCD camera at 40x magnification.

### **Transwell Migration Assay**

MDA-MB231 cells were plated onto the apical chamber of transwell dishes and allowed to migrate for 17 hours towards DMEM containing 10% FBS. Where indicated, cells



were pretreated with DMSO or 10 $\mu$ M Gefitinib for 30 minutes before adding the chemoattractant. Cells were washed in PBS, fixed in methanol and stained with 0.05% Crystal Violet for 40 minutes. Cells on the apical side of the membrane were removed with a Q-tip and cells that had migrated to the basolateral chamber were imaged using the Leica AF6000 microscope. Images were obtained using the Hamamatsu ORCA R<sup>2</sup> digital CCD camera at 10x magnification and counted. Quantification was done using a 1-way ANOVA with a Tukey's multiple comparison post-test.

### **Scratch Assay**

NIH 3T3 cells were plated onto 6-well dishes and scratched at confluence. Images were taken at 0hrs and 8hrs using the Hamamatsu ORCA R<sup>2</sup> digital CCD camera at 4x magnification. Images of four representative areas of each scratch were captured and 4 measurements were taken per image for a total of 12 measurements per scratch. The distance migrated was calculated using Leica Microsystems LAS AF software.

### **Palmitoylation assay with metabolic labelling**

MDA-MB-231 shControl and shDHHC20 cells were treated with 100 $\mu$ M palmitic acid azide in serum free DMEM for 4 hours at 37°C. Cells were washed in PBS and lysed in 200 $\mu$ l buffer (50mM Tris pH 7.5, 1% SDS, and 1 $\mu$ g/ml leupeptin, 1 $\mu$ g/ml aprotinin, 2 $\mu$ g/ml pepstatin A). Lysates were sonicated and centrifuged at 15,000 RPM for 10 minutes. 50 $\mu$ l of lysate was reacted with biotin alkyne using the Click-IT assay in a 200  $\mu$ l final reaction volume. Biotinylated proteins were isolated using streptavidin agarose, washed 5 times in wash buffer (50mM Tris pH 7.5, 0.1%SDS) and palmitoylated EGFR was analyzed by SDS PAGE.

### **Acyl-biotinyl exchange (ABE) assay**

The protocol is adapted from Wan et al., 2007. Cells were harvested in lysis buffer (50mM HEPES pH 7.4, 1% Triton X-100, 150mM NaCl, 5mM EDTA, 50mM N-ethylmaleimide (NEM), 1µg/ml leupeptin, 1µg/ml aprotinin, 2µg/ml pepstatin A). Lysates were clarified by centrifugation at 15,000 RPM for 10 minutes. 1µg of anti-EGFR (sc-120) was added to 200µl of lysate and incubated overnight on ice. 15µl of protein A sepharose was added to lysates and incubated for 2 hours at 4°C. Beads were washed in lysis buffer without NEM. The beads were eluted in 4%SDS buffer+50mM NEM (50mM HEPES pH 7.4, 4% SDS, 150mM NaCl, 5mM EDTA). 10µg of acetylated BSA was added as a carrier to the eluate followed by methanol/chloroform (m/c) precipitation. The dried pellet was resuspended in 40µl 4%SDS buffer+50mM NEM and incubated at room temperature for 1 hour. The samples were m/c precipitated twice then resuspended in 80µl 4%SDS buffer. The samples were split in half and 160µl of hydroxylamine buffer (0.7M hydroxylamine pH 7.4, 50mM HEPES pH 7.4, 0.2% Triton X-100, 150mM NaCl, 5M EDTA) was added to one half of the sample and control 0.2% Triton X-100 buffer (50mM HEPES pH 7.4, 0.2% Triton X-100, 150mM NaCl, 5mM EDTA) was added to the remaining sample and incubated at room temperature for 1 hour. The samples were m/c precipitated and resuspended in 40µl 4%SDS buffer containing 10µM Biotin-HPDP. 160µl of 0.2% Triton X-100 buffer +10µM Biotin-HPDP was added and incubated at RT for 1 hour. The samples were m/c precipitated and resuspended in 20µl of 4%SDS buffer followed by addition of 800µl of 1% Triton X-100 buffer (50µl removed for analysis as “input”). 30µl of streptavidin agarose beads were added to the samples and incubated overnight at 4°C rotating. The samples were washed in 1% Triton-X100 buffer and analyzed by SDS-PAGE.

## **EGFR purification for Mass spectrometry**

HEK293T cells were transfected with EGFR and DHHC20 and EGFR was immunoprecipitated by standard methods using anti-EGFR sc-120. The acyl biotin exchange assay was used to label palmitoylated cysteine residues with 10 $\mu$ M Biotin-HPDP. The biotinylated proteins were isolated with streptavidin beads and eluted with 10 $\mu$ M dithiothriitol to break the Biotin-HPDP disulfide linker. The reduced cysteine residues were blocked with 4mM iodoacetamide and the proteins were digested with trypsin.

## **Nano-LC-MS/MS analysis and data analysis**

Digestion solution was acidified by 5% formic acid, and peptides were desalted prior to LC-MS/MS analysis using in-house C18 STAGE tips as previously described [PMID: 12585499]. Peptide samples were loaded onto a 75  $\mu$ m I.D. x 20 cm fused silica capillary column packed with Reprosil-Pur C18-AQ resin (3  $\mu$ m; Dr. Maisch GmbH, Germany) and resolved by an EASY-nLC 1000 HPLC system (Thermo Scientific) coupled in-line with a Q-Exactive (Thermo Scientific). The HPLC gradient was 2-30% solvent B (A = 0.1% formic acid in water; B = 0.1% formic acid in acetonitrile) for 70 min, followed by 30% to 95% solvent B for 10 min, and then held at 95% solvent B for 10 min, with a constant flow-rate of 300 nL/min. Full MS spectrum scans (m/z 350-1600) were performed at a resolution of 70,000 (at 200 m/z), and the 3 most intense ions were selected for MS/MS performed with high-energy collision dissociation (HCD) with normalized collision energy of 25 at a resolution of 17,500 (at 200 m/z). Five target MS/MS (508.7633, 736.3706, 1103.0043, 1104.0523 and 1470.3366) were set in case they were missed in data-dependent acquisition mode. AGC targets of full MS and MS/MS scans were 1x10<sup>6</sup> and 5x10<sup>4</sup>, respectively. Unassigned charge states and

singly charged species were rejected, dynamic exclusion was set to 30 seconds, and lock mass calibration was implemented using polysiloxane ions 371.10123 and 445.12000. Mascot was used for database searching. Two trypsin miss-cleavage sites were allowed, and precursor ion and fragment ion tolerances were set to 10 ppm and 0.02 Da, respectively. Oxidation (+15.9949) on methionine, carbamidomethylation (+57.0215) and N-ethylmaleimide (125.0477) on cysteine were set as dynamic modifications. A peptide score of 20 was chosen to filter the peptide identification matches. Peptide quantification was performed on the extracted ion chromatograms (XICs) of peptides with all charge states.

### **Thrombin cleavage assay**

HEK293T cells expressing either shControl or shDHHC20 vectors were co-transfected with DHHC20 and either EGFR Wt or EGFR containing a thrombin cleavage sequence (LVPRGS) inserted at Gly959. Cells were harvested 48 hours post-transfection in 250 $\mu$ l of either buffer A (10mM Tris pH 8, 1.5mM MgCl<sub>2</sub>, 10mM KCl, 100 $\mu$ M Palmostatin B, 150mM NaF, 2mM Na<sub>3</sub>VO<sub>4</sub>, 1mM PPI, 2 $\mu$ g/ml pepstatin A, 1 $\mu$ g/ml aprotinin and 1 $\mu$ g/ml leupeptin) or buffer B (10mM Tris pH 8, 1.5mM MgCl<sub>2</sub>, 10mM KCl, 100 $\mu$ M Palmostatin B and 50 units of thrombin). Lysates were disrupted 7 times by passing through a 22 gauge needle and centrifuged at 800xg for 10 minutes. The thrombin containing samples were incubated at room temperature for 1 hour and centrifuged at 45,000 rpm for 30 minutes to isolate the membrane fraction which was then resuspended in RIPA buffer and incubated with anti-flag beads for 1 hour. The beads were washed with lysis buffer and the bound protein was eluted by boiling in SDS-loading buffer. Samples were loaded on an SDS-PAGE gel and membrane bound EGFR was detected using an EGFR antibody.

## References

1. Aicart-Ramos, C., Valero, R.A., and Rodriguez-Crespo, I. (2011). Protein palmitoylation and subcellular trafficking. *Biochimica et biophysica acta* 1808, 2981-2994.
2. Bollu, L.R., Katreddy, R.R., Blessing, A.M., Pham, N., Zheng, B., Wu, X., and Weihua, Z. (2015). Intracellular activation of EGFR by fatty acid synthase dependent palmitoylation. *Oncotarget* 6, 34992-35003.
3. Cho, J., Pastorino, S., Zeng, Q., Xu, X., Johnson, W., Vandenberg, S., Verhaak, R., Cherniack, A.D., Watanabe, H., Dutt, A., *et al.* (2011). Glioblastoma-derived epidermal growth factor receptor carboxyl-terminal deletion mutants are transforming and are sensitive to EGFR-directed therapies. *Cancer research* 71, 7587-7596.
4. Conibear, E., and Davis, N.G. (2010). Palmitoylation and depalmitoylation dynamics at a glance. *Journal of cell science* 123, 4007-4010.
5. Ekstrand, A.J., Sugawa, N., James, C.D., and Collins, V.P. (1992). Amplified and rearranged epidermal growth factor receptor genes in human glioblastomas reveal deletions of sequences encoding portions of the N- and/or C-terminal tails. *Proceedings of the National Academy of Sciences of the United States of America* 89, 4309-4313.
6. Greaves, J., and Chamberlain, L.H. (2011). DHHC palmitoyl transferases: substrate interactions and (patho)physiology. *Trends in biochemical sciences* 36, 245-253.

7. Imielinski, M., Berger, A.H., Hammerman, P.S., Hernandez, B., Pugh, T.J., Hodis, E., Cho, J., Suh, J., Capelletti, M., Sivachenko, A., *et al.* (2012). Mapping the hallmarks of lung adenocarcinoma with massively parallel sequencing. *Cell* 150, 1107-1120.
8. Jennings, B.C., Nadolski, M.J., Ling, Y., Baker, M.B., Harrison, M.L., Deschenes, R.J., and Linder, M.E. (2009). 2-Bromopalmitate and 2-(2-hydroxy-5-nitro-benzylidene)-benzo[b]thiophen-3-one inhibit DHHC-mediated palmitoylation in vitro. *Journal of lipid research* 50, 233-242.
9. Katzmann, D.J., Odorizzi, G., and Emr, S.D. (2002). Receptor downregulation and multivesicular-body sorting. *Nature reviews. Molecular cell biology* 3, 893-905.
10. Lemmon, M.A., Schlessinger, J., and Ferguson, K.M. (2014). The EGFR family: not so prototypical receptor tyrosine kinases. *Cold Spring Harbor perspectives in biology* 6, a020768.
11. McCormick, P.J., Dumaresq-Doiron, K., Pluviose, A.S., Pichette, V., Tosato, G., and Lefrancois, S. (2008). Palmitoylation controls recycling in lysosomal sorting and trafficking. *Traffic* 9, 1984-1997.
12. Murphy, J.E., Padilla, B.E., Hasdemir, B., Cottrell, G.S., and Bunnett, N.W. (2009). Endosomes: a legitimate platform for the signaling train. *Proceedings of the National Academy of Sciences of the United States of America* 106, 17615-17622.

13. Pines, G., Kostler, W.J., and Yarden, Y. (2010). Oncogenic mutant forms of EGFR: lessons in signal transduction and targets for cancer therapy. *FEBS letters* 584, 2699-2706.
14. Price, J.T., Tiganis, T., Agarwal, A., Djakiew, D., and Thompson, E.W. (1999). Epidermal growth factor promotes MDA-MB-231 breast cancer cell migration through a phosphatidylinositol 3'-kinase and phospholipase C-dependent mechanism. *Cancer research* 59, 5475-5478.
15. Roskoski, R., Jr. (2014). ErbB/HER protein-tyrosine kinases: Structures and small molecule inhibitors. *Pharmacological research : the official journal of the Italian Pharmacological Society* 87, 42-59.
16. Seshacharyulu, P., Ponnusamy, M.P., Haridas, D., Jain, M., Ganti, A.K., and Batra, S.K. (2012). Targeting the EGFR signaling pathway in cancer therapy. *Expert opinion on therapeutic targets* 16, 15-31.
17. Swarthout, J.T., Lobo, S., Farh, L., Croke, M.R., Greentree, W.K., Deschenes, R.J., and Linder, M.E. (2005). DHHC9 and GCP16 constitute a human protein fatty acyltransferase with specificity for H- and N-Ras. *J Biol Chem* 280, 31141-31148.
18. Walton, G.M., Chen, W.S., Rosenfeld, M.G., and Gill, G.N. (1990). Analysis of deletions of the carboxyl terminus of the epidermal growth factor receptor reveals self-phosphorylation at tyrosine 992 and enhanced in vivo tyrosine phosphorylation of cell substrates. *The Journal of biological chemistry* 265, 1750-1754.

19. Wang, W., Runkle, K.B., Terkowski, S.M., Ekaireb, R.I., and Witze, E.S. (2015). Protein Depalmitoylation Is Induced by Wnt5a and Promotes Polarized Cell Behavior. *The Journal of biological chemistry* 290, 15707-15716.



## CHAPTER 3: INDUCED SENSITIVITY TO EGFR INHIBITORS IS MEDIATED BY PALMITOYLATED CYSTEINE 1025 OF EGFR AND REQUIRES ONCOGENIC KRAS.

Akriti Kharbanda, Kristin Runkle, Wei Wang, Eric S. Witze. Induced sensitivity to EGFR inhibitors is mediated by palmitoylated cysteine 1025 of EGFR and requires oncogenic Kras. *Biochem Biophys Res Commun.* **493(1)**, (2017). Reprinted with the copyright permission of Elsevier Publishing.

### Abstract

Currently, there are no effective therapeutic strategies targeting Kras driven cancers, and therefore, identifying new targeted therapies and overcoming drug resistance have become paramount for effective long-term cancer therapy. We have found that reducing expression of the palmitoyl transferase DHHC20 increases cell death induced by the EGFR inhibitor gefitinib in Kras and EGFR mutant cell lines, but not MCF7 cells harboring wildtype Kras. We show that the increased gefitinib sensitivity in cancer cells induced by DHHC20 inhibition is mediated directly through loss of palmitoylation on a previously identified cysteine residue in the C-terminal tail of EGFR. We utilized an EGFR point mutant in which the palmitoylated cysteine 1025 is mutated to alanine (EGFR<sup>C1025A</sup>), that results in receptor activation. Expression of the EGFR mutant alone in NIH3T3 cells does not increase sensitivity to gefitinib-induced cell death. However, when EGFR<sup>C1025A</sup> is expressed in cells expressing activated Kras<sup>G12V</sup>, EGFR inhibitor induced cell death is increased. Surprisingly, lung cancer cells harboring the EGFR inhibitor resistant mutation, T790M, become sensitive to EGFR inhibitor treatment when DHHC20 is inhibited. Finally, the small molecule, 2-bromopalmitate, which has been shown to inhibit palmitoyl transferases, acts synergistically with gefitinib to induce cell death in the gefitinib resistant cell line NCI-H1975.

## Introduction

EGFR and other members of the ErbB family of receptor tyrosine kinases (RTKs) play critical roles in reacting to extracellular growth cues by initiating downstream signaling cascades through various effector pathways (1-3). Mutations in EGFR, leading to its constant activation and subsequent uncontrolled cell growth, are detectable in 10% to 30% of tumors from patients with non-small cell lung cancer (NSCLC)(4). Ligand (EGF) binding to EGFR induces receptor dimerization and subsequent auto-phosphorylation of specific tyrosine residues on the C-terminal tail. Activating EGFR point mutations in exon 21, such as L858R, and deletions of exon 19 are often predictors of response to EGFR tyrosine kinase inhibitor (TKI) therapy with gefitinib or erlotinib (5). However, the majority of patients with NSCLCs harboring these activating EGFR mutations relapse within 10 to 16 months of treatment with EGFR TKIs (5-6). In over half of these patients, resistance to EGFR TKI therapy is associated with the acquisition of a secondary T790M mutation in the EGFR TK domain, which alters interaction of reversible TKIs with the ATP-binding pocket (4,7). It is therefore critical to develop strategies to overcome drug resistance. We have recently uncovered a previously unknown regulation of EGFR through EGFR palmitoylation.

Protein palmitoylation is the reversible covalent attachment of a 16-carbon saturated fatty acid palmitate onto cysteine residues. Addition of the large hydrophobic palmitate facilitates association of proteins at the plasma membrane (PM) influencing formation of cell signaling complexes.(8-12) Palmitoylation is mediated by a family of 23 protein acyl-transferases containing a conserved DHHC (aspartic acid, histidine, histidine, cysteine) motif essential for catalysis (13-15). DHHC20 palmitoylates the epidermal growth factor receptor (EGFR) on specific cysteine residues on the C-terminal

tail, suppressing its activation. Unexpectedly, inhibition of DHHC20 in both breast and lung cancer cells increases induction of cell death in response to the EGFR inhibitor gefitinib, despite the fact the cells harbor activated Kras mutations and wild type EGFR (16). Mutations in Kras, predominantly an amino acid substitution at codon 12 or 13, lead to upregulation of the Ras/MAPK signaling and ERK activation, ultimately driving cell division. While mutations in Ras are common in cancer it has been challenging to therapeutically target Ras directly because of the nucleotide-binding pocket's very high affinity for GTP.

Here we report that using a palmitoylation defective EGFR mutant we demonstrate the increased response to gefitinib is mediated by the palmitoylated cysteine residue 1025, but only when in combination with activated Kras. Alternatively, inhibition of DHHC20 also increases sensitivity to gefitinib-induced cell death in cancer cells harboring not only activating EGFR mutations, but also the gefitinib resistant T790M mutation, independent of activated Kras. These results demonstrate a previously unreported mechanism to overcome mutation driven drug resistance by targeting a recently identified modification of EGFR.

## **Results**

### **Increased gefitinib-induced cell death is mediated by the palmitoylation site C1025 on the C-terminal tail of EGFR.**

We reported previously that inhibition of DHHC20 increased the sensitivity of the triple negative breast cancer cell line, MDA-MB-231, to TKI induced cell death (Fig. 1A) (16). Although inhibition of DHHC20 by shRNA leads to an increase in sensitivity to gefitinib-induced cell death, it is still unclear if this effect was directly mediated by inhibiting EGFR palmitoylation or if it is the effect of another unknown target of DHHC20.

We previously showed that EGFR is palmitoylated on the C-terminal tail and that mutating one of the palmitoylated cysteine residues 1025 to alanine is sufficient to reduce receptor palmitoylation, induce receptor autophosphorylation, adaptor binding and downstream signaling to AKT and ERK when transiently expressed in NIH3T3 cells (16). To test if blocking EGFR palmitoylation directly increases gefitinib sensitivity of human cancer cells, we developed a conditional system for expressing wild type EGFR (EGFR<sup>WT</sup>) or palmitoylation defective EGFR with cysteine 1025 mutated to alanine (EGFR<sup>C1025A</sup>) in MDA-MB-231 cells with a tetracycline-inducible promoter. Induction of the cells with doxycycline for 72 hours resulted in protein levels of EGFR<sup>C1025A</sup> is slightly higher than EGFR<sup>WT</sup> consistent with previous findings (Fig. 1B) (16). After 24 hours of doxycycline inductions, cells were treated with gefitinib (5 $\mu$ M) for 72 hours. The percentage of dead cells expressing EGFR<sup>WT</sup> were similar to cells infected with an empty vector control treated with gefitinib (Fig. 1C). Cells expressing the EGFR<sup>C1025A</sup> mutant and treated with DMSO showed similar percentages of cell death as EGFR<sup>WT</sup> expressing cells (Fig. 1C). However, when the EGFR<sup>C1025A</sup> mutant cells were treated with gefitinib, cell death increased to 80.6% compared to the 32.4% in gefitinib treated EGFR<sup>WT</sup> expressing cells (Fig. 1C). One potential damaging outcome when blocking EGFR palmitoylation is increased tumor growth caused by activated EGFR. However, expression of EGFR<sup>C1025A</sup> did not increase growth of the breast cancer cells and in fact significantly reduced cell proliferation compared to cells overexpressing EGFR<sup>WT</sup> (Fig 1D). These results indicate that blocking EGFR palmitoylation at cysteine residue 1025 is sufficient to induce gefitinib sensitivity in triple negative breast cancer cells. This confirms that the increased sensitivity to gefitinib-induced cell death imposed by DHHC20 inhibition via shRNA is caused by loss of EGFR palmitoylation at cysteine residue 1025.

**DHHC20 silencing does not increase gefitinib sensitivity in wild type Kras expressing MCF7 breast cancer cells.**

The MDA-MB-231 breast cancer cells express wild type EGFR, but harbor an activating mutation in Kras (Kras<sup>G12D</sup>). We asked if a similar sensitivity to gefitinib is observed in cancer cells expressing wild type Kras upon DHHC20 silencing. Silencing DHHC20 in the breast cancer cell line MCF7 harboring a mutation in the PI3K pathway (PIK3CA<sup>E545K</sup>) had no effect on gefitinib-induced cell death consistent with a requirement for oncogenic Kras (Fig. 1A). However, similar to the slowed growth upon expression of EGFR<sup>C1025A</sup> in MDA-MB-231, inhibiting DHHC20 in MCF7 cells did slow cell growth, suggesting that DHHC20 plays a role in proliferation in the presence of a PIK3CA mutation (Fig. 1B). Inhibiting DHHC20 did modestly increase phosphorylation of both ERK and AKT, suggesting that the loss of DHHC20 promotes the signaling of the constitutively active mutant PIK3CA (Supp. Fig. 1B). We next examined the gefitinib sensitivity of downstream EGFR signaling in shControl and shDHHC20 expressing cells. Treatment of MCF7 cells with 5  $\mu$ M gefitinib decreased pERK only when DHHC20 was silenced by shRNA, but pAKT was only slightly inhibited by gefitinib in the MCF7 shDHHC20 cells (Supp. Fig. 1B).

Since MCF7 cells were still not sensitive to gefitinib-induced cell death after DHHC20 inhibition we asked if non-transformed cells were also resistant. When DHHC20 was inhibited in MCF10A cells, there was no increase in the sensitivity to gefitinib-induced cell death after 72 hours of treatment (Fig. 2C). Furthermore, inhibition of DHHC20 in MCF10a cells had no effect on cell growth (Fig. 2D), indicating that DHHC20 is not essential for normal cell growth. We also examined the gefitinib sensitivity of downstream EGFR signaling in shControl and shDHHC20 expressing

MCF10a cells. Treatment with 5  $\mu$ M gefitinib decreased pEGFR and pERK in both shControl and shDHHC20 cells as expected because gefitinib will inhibit EGFR in these non-transformed cells (Supp. Fig. 1C). These results thus far indicate that inhibition of DHHC20 only increases sensitivity to gefitinib-induced cell death in cancer cells with activating mutations in Kras.

**Figure 1**

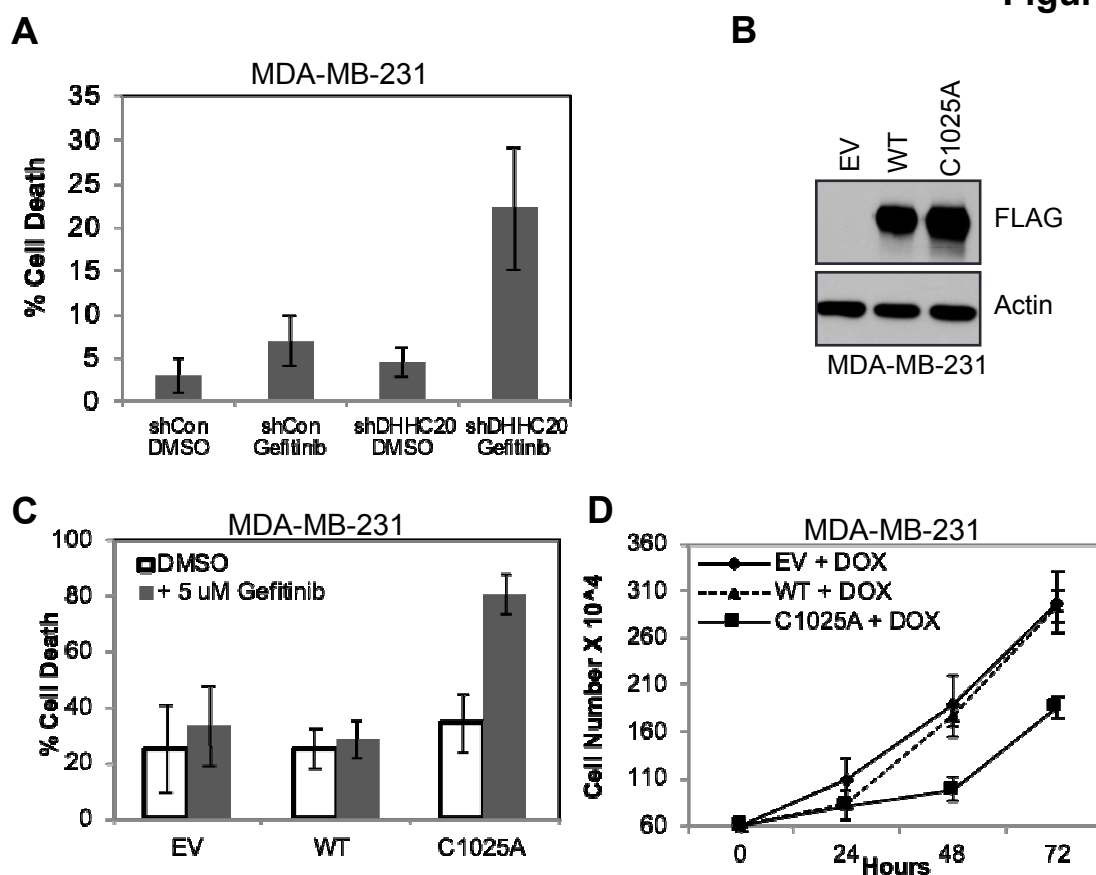


**Figure 1. Expression of palmitoylation defective EGFR<sup>C1025A</sup> mediates gefitinib-induced cytotoxicity.** (A) Gefitinib increases cytotoxicity in DHHC20 silenced Kras mutant cells MDA-MB-231. (B) MDA-MB-231 (Kras<sup>G13D</sup>) cells stably expressing inducible EGFR<sup>WT</sup> or EGFR<sup>C1025A</sup> or empty vector control (EV) were treated with doxocycline (1μg/ml) for 15 hours. Immunoblotting with anti-FLAG shows induced expression of FLAG tagged EGFR<sup>WT</sup> and EGFR<sup>C1025A</sup>. (C) Cells were treated with doxocycline (1μg/ml) every 24 hours and with DMSO or 5 μM gefitinib at 24 hours post-seeding. Expression of EGFR<sup>C1025A</sup> induced sensitivity to gefitinib. Cell viability was measured by Trypan Blue staining at 72 hours post-treatment (mean +/-StDev). (D) Induced expression of EGFR<sup>C1025A</sup> in MDA-MB-231 cells reduces cell growth.

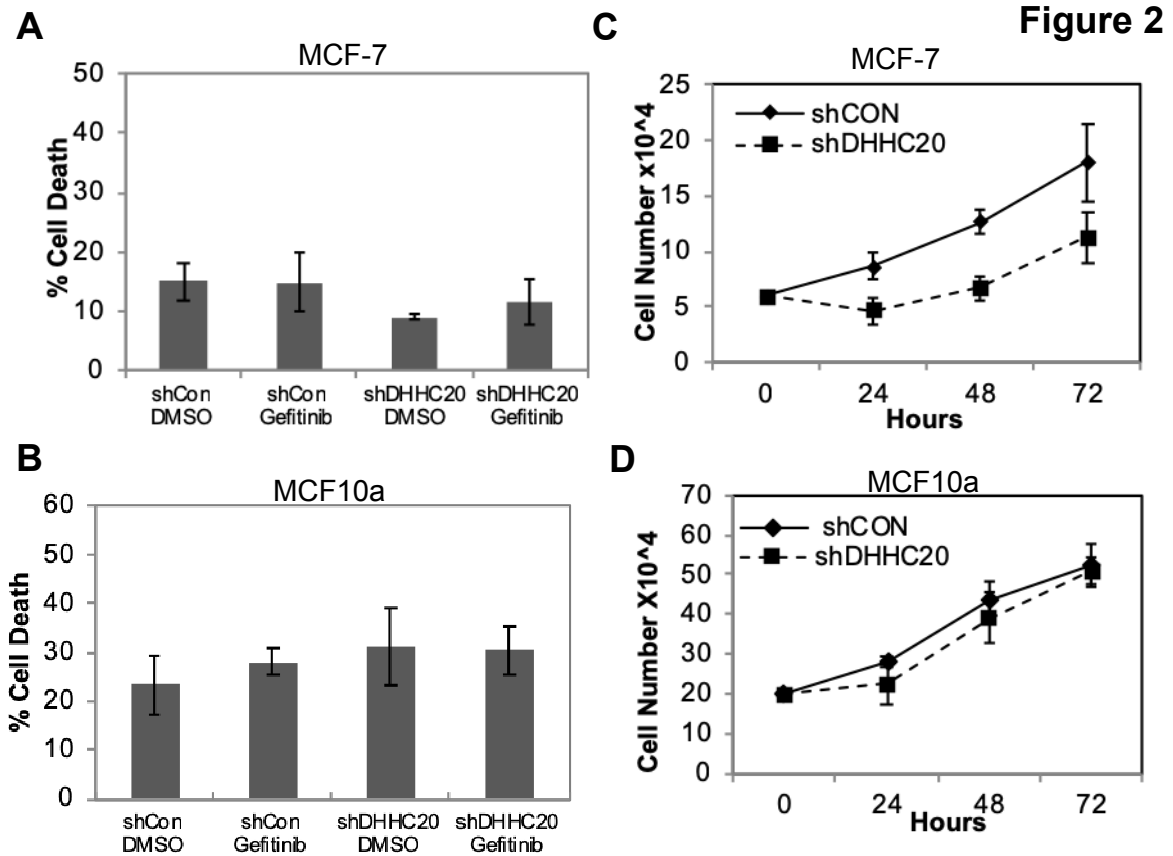


**Figure 2. DHHC20 inhibition increases gefitinib sensitivity in cells with activating mutations and resistance mutations in EGFR.** MCF7 and MCF10A are resistant to gefitinib cytotoxicity in response to DHHC20 silencing. (A, B) shControl and shDHHC20 cells were treated with DMSO or 5  $\mu$ M gefitinib. Cell viability was measured by Trypan Blue staining at 72 hours. (C) Knockdown of DHHC20 in MCF7 (PIK3CA<sup>E545K</sup>) cells slows growth. (D) Knockdown of DHHC20 in the non-transformed MCF10a cells has no effect on cell growth.



## **Increased gefitinib-induced cell death mediated by EGFR<sup>C1025A</sup> requires mutant Kras<sup>G12V</sup>.**

To determine the requirements of gefitinib-induced cell death in shDHHC20 cells, NIH3T3 cells were stably infected with tetracycline-inducible EGFR<sup>WT</sup> or palmitoylation defective EGFR<sup>C1025A</sup>. The level of EGFR<sup>WT</sup> expression was lower than EGFR<sup>C1025A</sup> after 12 hours of induction (Fig. 3A). After 72 hours of induced expression of EGFR<sup>WT</sup> or EGFR<sup>C1025A</sup>, there was no effect on cell viability after 72 hours of gefitinib treatment (Fig. 3B). Since expression of EGFR<sup>C1025A</sup> alone was not sufficient to induce gefitinib sensitivity we asked if oncogenic Kras is required. The mutant Kras<sup>G12V</sup> was stably expressed in NIH3T3 cells together with tetracycline-inducible EGFR<sup>WT</sup> or EGFR<sup>C1025A</sup>. Treatment with gefitinib increased the percentage of cell death to 33.4% in Kras<sup>G12V</sup> cells expressing EGFR<sup>C1025A</sup> compared to 11.0% in cells expressing EGFR<sup>WT</sup> and Kras<sup>G12V</sup> (Fig. 3B). This indicates the combination of oncogenic Kras with palmitoylation defective EGFR<sup>C1025A</sup> is required and sufficient to increase gefitinib-induced cell death. When downstream signaling was examined, we found that cells expressing both Kras<sup>G12V</sup> and EGFR<sup>C1025A</sup> had higher levels of pAKT compared to those with Kras<sup>WT</sup>. This increase in pAKT is inhibited by gefitinib treatment whereas the change in EGFR<sup>C1025A</sup> Kras<sup>WT</sup> is minimal (Fig. 3A). However, the EGFR<sup>C1025A</sup> and Kras<sup>G12V</sup> condition had lower levels of pERK compared to EGFR<sup>C1025A</sup> and Kras<sup>WT</sup> and were reduced upon gefitinib treatment to similar levels in both conditions (Fig. 3A). Therefore, the increase in cell death may be more dependent on the gefitinib-induced changes in AKT activation than ERK.

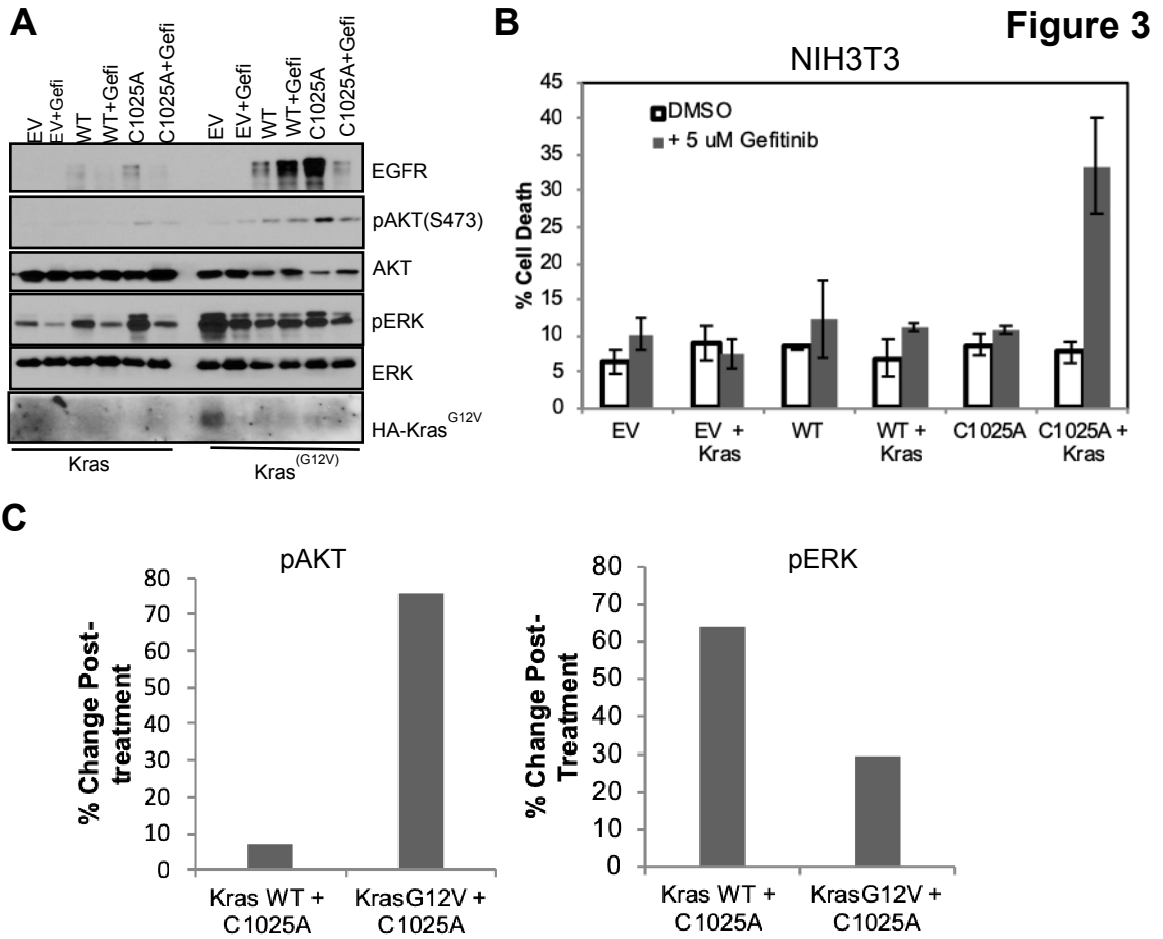


**Figure 3. Mutation of the palmitoylated cysteine 1025 of EGFR in combination with Kras<sup>G12V</sup> increases gefitinib sensitivity.** (A) NIH3T3 cells stably expressing inducible full length EGFR<sup>WT</sup> or EGFR<sup>C1025A</sup> or empty vector control (EV) with Kras<sup>WT</sup> (left) or Kras<sup>G12V</sup> (right). Immunoblotting with EGFR shows induced expression of EGFR<sup>WT</sup> and EGFR<sup>C1025A</sup>, and immunoblotting with HA shows expression of HA-tagged Kras<sup>G12V</sup>. (B) Induced expression of EGFR<sup>C1025A</sup> in NIH3T3 stably expressing Kras<sup>G12V</sup> increased gefitinib-induced cell death. Cells were treated with doxocycline (1µg/ml) every 24 hours for 72 hours and with DMSO or 5 µM Gefitinib at 24 hours post-seeding. Cell viability was measured by Trypan Blue staining at 72 hours post-treatment (mean +/-StDev).

## **DHHC20 inhibition increases gefitinib sensitivity in cells with the activating and resistance mutations in EGFR.**

Upon examination of the Kras<sup>WT</sup> lung cancer cell line, NCI-H1975, inhibiting DHHC20 increased gefitinib-induced cell death (41.7% vs. 13.4%) (Fig. 4A). The increase of sensitivity of the NCI-H1975 shDHHC20 cell line to gefitinib is quite unexpected since this line harbors an activating mutation L858R and the acquired secondary mutation, T790M, in the kinase domain imparting gefitinib resistance.

To address if the increase in cell death in the gefitinib resistant line is associated with an increase in EGFR sensitivity to gefitinib, we examined EGFR signaling in the shDHHC20 cells. When DHHC20 was silenced in NCI-H1975, cells exhibited increased EGFR, AKT and ERK phosphorylation (Fig. 4B). The increase in signaling suggests that the palmitoyl transferase inhibits the mutant EGF receptor. After treatment of NCI-H1975 shDHHC20 cells with gefitinib, the elevated levels of pEGFR were reduced within 1 hour, suggesting that the increase in EGFR phosphorylation upon DHHC20 inhibition was not caused by decreased dephosphorylation. The simplest explanation for the increased EGFR autophosphorylation upon DHHC20 silencing is the high basal kinase activity of the activating mutation. Similarly, levels of pERK and pAKT decreased after 1 hour and remain low for 24 hours after treatment (Fig. 4B). In the NCI-H1975 shControl cells, the gefitinib treatment increased pAKT and pERK levels as well as total levels of AKT and ERK at 6-24 hours of treatment through a mechanism that is still unclear (Fig. 4B). This suggests that reduction of DHHC20 by shRNA increases the sensitivity of these gefitinib resistant cells to inhibitor treatment.

**Palmitate analog 2-bromopalmitate synergizes with gefitinib to induce cell death in gefitinib resistant cells.**

Silencing DHHC20 by shRNA causes chronic inhibition of DHHC20 and constitutively elevated levels of EGFR signaling. The immediate effects of acute DHHC20 inhibition through pharmacologic inhibition would provide greater insight into the utility of DHHC20 as a therapeutic target. Although currently there is not a specific inhibitor to palmitoyl transferases, the palmitate analog 2-bromopalmitate (2-BP) has been shown to inhibit DHHC domain containing palmitoyl transferases at micromolar concentrations (17). Our previous study showed that 2-BP was sufficient to increase sensitivity of MDA-MB-231 cells to gefitinib-induced cell death (16). We wanted to examine the effect of 2-BP on gefitinib sensitivity in greater detail, specifically on gefitinib resistant cells.

We asked if acute treatment of cancer cells with 2-BP is sufficient to sensitize the gefitinib resistant NCI-H1975 cells to gefitinib-induced cell death in and if the sensitivity is comparable to the wild type EGFR expressing MDA-MB-231 cells. The combination treatment increased cell death compared to either gefitinib or 2-BP alone in both MDA-MB-231 and NCI-H1975 cells. Based on these responses to treatment with gefitinib and 2-BP, we assessed the effects of combining 2-BP and gefitinib using the Chou-Talalay method (18). With half-maximal inhibitory concentrations of gefitinib ( $IC_{50} = 3.5 \mu M$  for MDA-MB-231 and  $12.67 \mu M$  for NCI-H1975) and 2-BP ( $IC_{50} = 11.74 \mu M$  for MDA-MB-231 and  $11.46 \mu M$  for H1975), these compounds were tested alone for effects on MDA-MB-231 and NCI-H1975 cell growth at 1/8X, 1/4X, 1/2X, 1X, 2X, and 4X the  $IC_{50}$  values and at equipotent concentrations at the same ratios in combination. Isobologram analysis of the data at ED50, ED75 and ED90 values showed an additive effect of the

gefitinib/2-BP combination in MDA-MB-231 cells (data not shown), but showed synergy of the gefitinib/2-BP combination in NCI-H1975 cells with CI values of less than 1 (Fig. 4C). Upon examination of downstream signaling in NCI-H1975, we found 2-BP treatment increased pEGFR, pAKT(T308) and pERK consistent with the shDHHC20 condition (Fig. 4D). With gefitinib treatment in combination with 2-BP, pEGFR and pAKT(T308) notably reduced and pERK is modestly reduced in contrast to the MDA-MB-231 in which there was no detectable change between treatment groups. Therefore, the signaling mechanism behind the observed synergy between drugs may be through regulation of combined AKT(T308) and ERK phosphorylation. This shows that targeting DHHC20 may be an effective approach to overcoming EGFR TKI resistance in NSCLC.

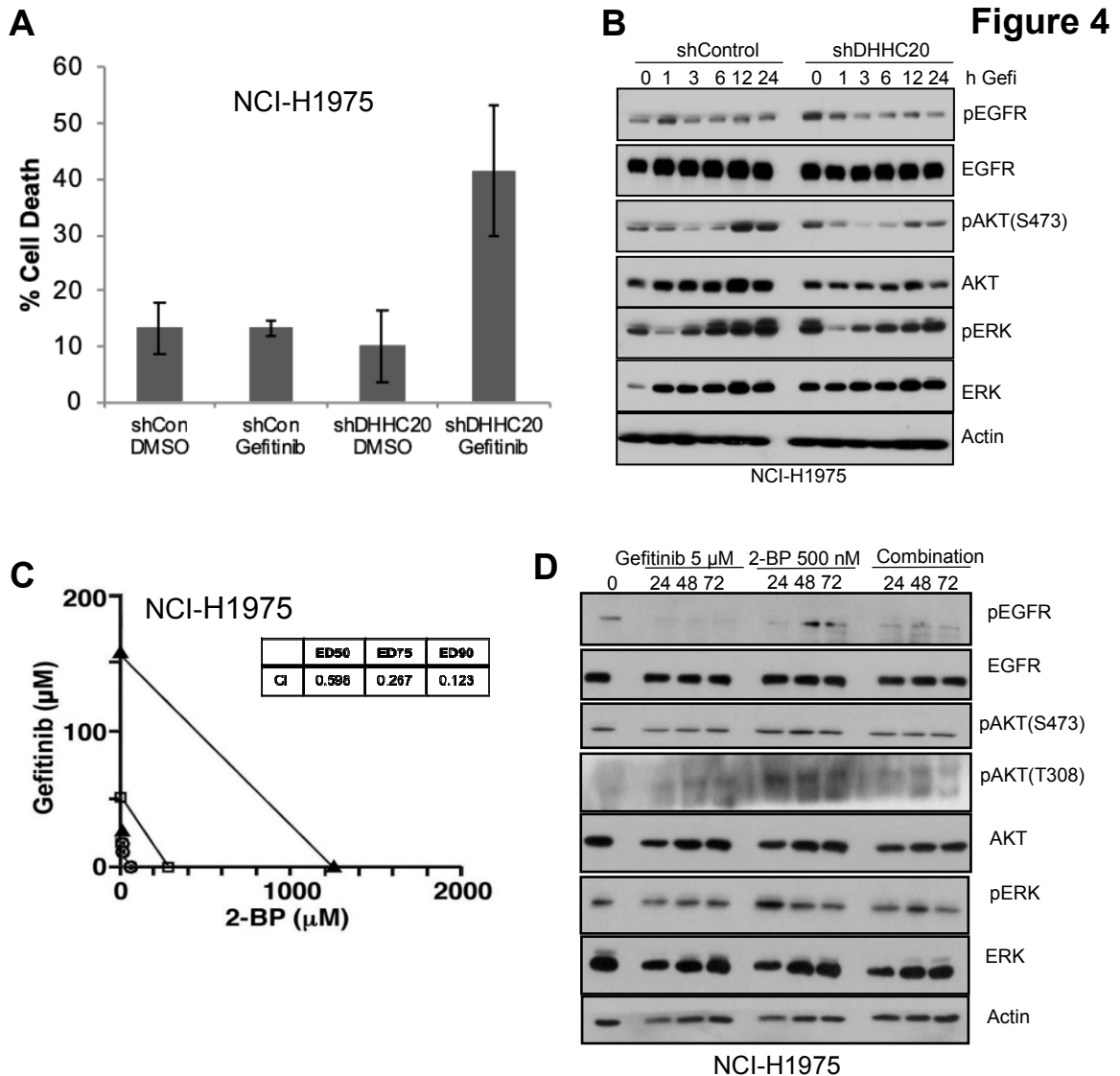


**Figure 4. Palmitoyl transferase inhibitor 2-bromopalmitate synergizes with gefitinib in inducing cell death in gefitinib resistant cells.** (A) shControl and shDHHC20 NCI-H1975 cells were treated with DMSO or 5  $\mu$ M gefitinib. Cell viability was measured by Trypan Blue staining at 72 hours. Gefitinib increases cytotoxicity in H1975 DHHC20 silenced cells. All graphs show mean  $\pm$  StDev. (B) Treatment of NCI-H1975 DHHC20 silenced cells with gefitinib decreases EGFR, AKT and ERK phosphorylation. (C) NCI-H1975 cells were treated with (i) fixed IC<sub>50</sub> ratios of gefitinib alone at 24 hours post-seeding, (ii) fixed IC<sub>50</sub> ratios of 2-BP alone at 24 hours post-seeding, or (iii) Gefitinib in combination with 2-BP. The multiple effect-level isobologram analyses at 72 hours post-treatment are shown for the ED<sub>50</sub> (open circle), ED<sub>75</sub> (closed square) and ED<sub>90</sub> (closed triangle) values. The combination of Gefitinib and 2-BP is synergistic in NCI-H1975 cells. (D) NCI-H1975 cells were treated with 5  $\mu$ M Gefitinib, 500 nm 2-BP or both at 24 hours post-seeding. Cells were harvested after the indicated treatment time points and lysates were immunoblotted with indicated antibodies.

## Discussion

We observe increased gefitinib sensitivity in cells expressing EGFR harboring both activating L858R and a resistance mutation T790M, an acquired secondary mutation that imparts resistance to EGFR TKIs, such as gefitinib. Our results also reveal a requirement for oncogenic Kras for increased inhibitor sensitivity mediated by blocking EGFR palmitoylation in cells with wild type EGFR. Expression of a mutant form of EGFR that is resistant to palmitoylation at cysteine 1025 leads to increased sensitivity to gefitinib-induced cell death, but only in the presence of oncogenic Kras<sup>G12V</sup>. Expression of activated PIK3CA was insufficient to induce sensitivity to gefitinib, confirming the selectivity for Kras<sup>G12V</sup> (Supp. Fig. 1D).

The alterations in EGFR signaling that lead to increased gefitinib-induced cell death are still not entirely clear. Inhibition of DHHC20 in EGFR mutant background increases both pERK and pAKT levels and are both effectively inhibited by gefitinib. One possibility it is the change in signaling from the artificially high levels induced by DHHC20 inhibition or EGFR<sup>C1025A</sup> expression down to the gefitinib inhibited levels that causes the cells to crisis and die. Cells with activated Kras become sensitized to gefitinib with DHHC20 inhibition, but the resulting increase in pERK caused by DHHC20 inhibition is not reduced by gefitinib. It is therefore unclear why the MDA-MB-231 cells become sensitive to gefitinib when DHHC20 is knocked down.

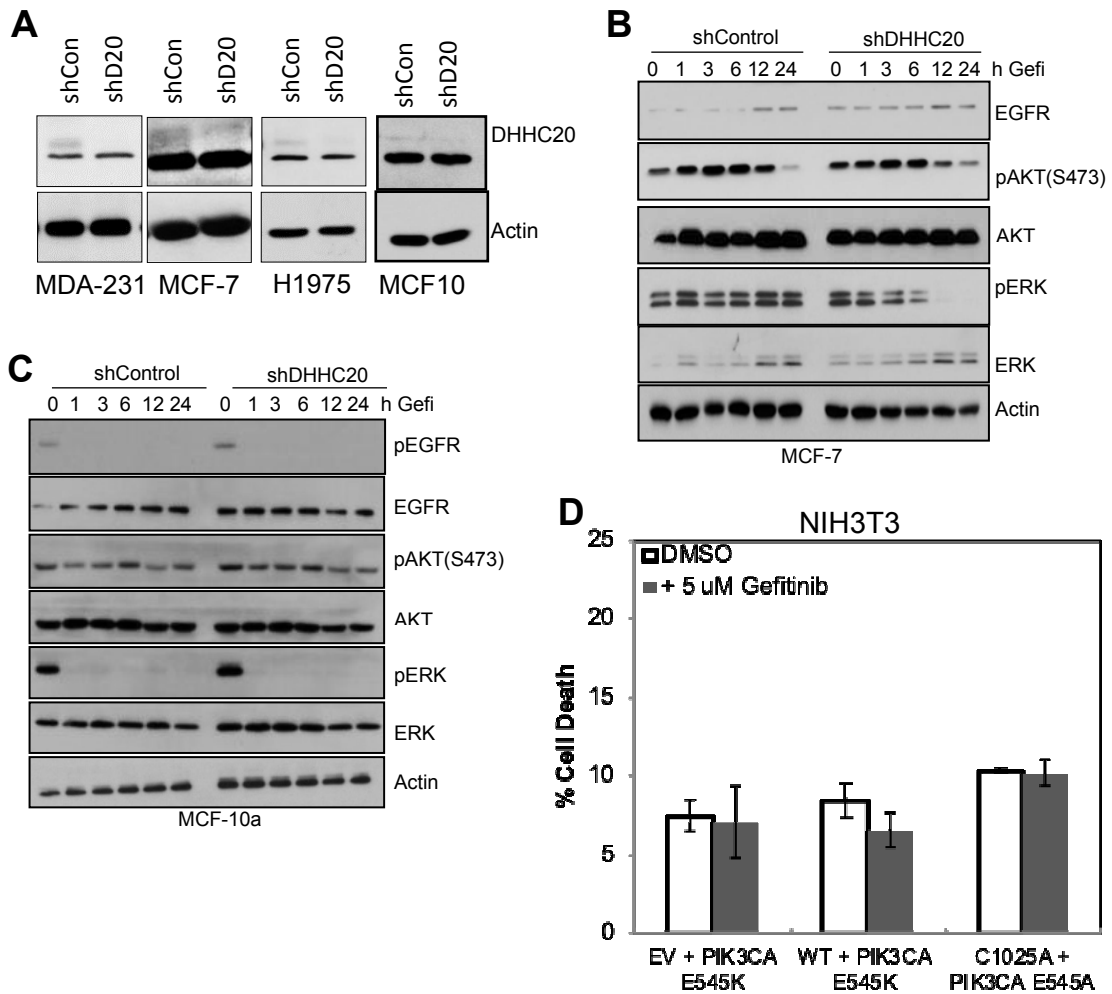
Furthermore, the combined effect of DHHC20 and EGFR inhibition is greater in the cells with mutant EGFR than cells with mutant Kras. The synergy between gefitinib and 2-bromopalmitate (2-BP) in the NCI-H1975 cells compared to the additive effect in MDA-MB-231 cells is particularly surprising. Gefitinib targets EGFR harboring the L858R activating mutation, which increases the affinity of the drug for activated EGFR relative

to ATP, in NCI-H1975. It is therefore not surprising that the gefitinib/2-BP combination treatment is more effective in this cell line than the EGFR wild type cell line, MDA-MB-231. What is surprising is that these cells are resistant to gefitinib because of the T790M secondary acquired resistance mutation. The T790M mutation increases the affinity of the ATP binding pocket for ATP over gefitinib. Due to toxicity, we have been unable to express EGFR<sup>C1025A</sup> in the NCI-H1975 cells or express EGFR<sup>L858R/T790M</sup> also harboring the C1025A mutation in any cell type. We therefore can't conclusively demonstrate that the increased gefitinib sensitivity in the NCI-H1975 cells is through EGFR palmitoylation directly.

Our results reveal two potential vulnerabilities in the EGFR/MAPK pathway mediated by DHHC20 inhibition. First is the gefitinib-induced sensitivity of Kras mutant cancers to inhibition of DHHC20 or blocking EGFR palmitoylation. Oncogenic mutation in Kras is one of the most common mutations in cancer and yet targeting Kras therapeutically has been elusive. Therefore, inducing sensitivity of Kras mutant cells to EGFR inhibitor therapy is an unprecedented alternative approach. The second is the re-sensitization of gefitinib resistant cancer cells by inhibition of DHHC20. While we have not yet shown that this effect is through EGFR, the synergistic effect between 2-BP and gefitinib is striking. The fact we have been unable to express the C1025A mutant with the activating L858R mutant suggests there may be a form of synthetic lethality possibly from hyperactivation of the pathway. Future studies will determine how palmitoylation effects the gate-keeper mutation in the kinase domain and if it is through the C-terminal.



## Supplemental Figure 1



**Supplemental Figure 1.** (A) DHHHC20 expression is silenced using shRNA or sgRNA and the CRISPR/Cas9 system. MDA-MB-231, MCF-7, H1975 MCF10a shControl and shDHHHC20 stable cell lines were generated by lentiviral infection. Immunoblotting with a DHHHC20 specific antibody shows reduction of the DHHHC20 band (arrow). (B) Treatment of MCF7 DHHHC20 silenced cells significantly decreases ERK phosphorylation. (C) Treatment of MCF10A shControl and shDHHHC20 cells decreases EGFR and ERK phosphorylation. (D) Expression of EGFR<sup>C1025A</sup> in NIH3T3 stably expressing PIK3CA<sup>E545K</sup> had no effect on gefitinib-induced cell death. Cells were treated with doxocycline (1µg/ml) every 24 hours for 72 hours and with DMSO or 5µM Gefitinib at 24 hours post-seeding. Cell viability was measured by Trypan Blue at 72 hours post-treatment (mean +/-StDev).

## **Materials and Methods**

### **Cell culture**

MDA-MB-231, MCF7, and NIH3T3 cells (ATCC) were cultured in DMEM containing 10% FBS. NCI-H1975 cells (ATCC) were maintained in RPMI supplemented with 10% FBS. Cells were treated with gefitinib (Selleck Chemicals) and 2-bromopalmitate (2-BP) (Sigma).

### **Immunoblot analysis**

Cell lysates were prepared in 1% Triton-X-100 buffer, including Tris-HCl (pH 7.5) and sodium chloride solution (NaCl). Lysates were analyzed by immunoblotting with the following antibodies: Anti-DHHC20 (HPA014702) and anti-FLAG M2 antibodies were purchased from Sigma-Aldrich. Anti-pY1068-EGFR, EGFR-XP, pERK, ERK, pS473-AKT, pT308-AKT, AKT,  $\beta$ -actin were obtained from Cell Signaling Technologies. Anti-HA antibodies were purchased from Biolegend. Immune complexes were detected with horseradish peroxidase-conjugated secondary antibodies and enhanced chemiluminescence (ECL) (Thermo Scientific).

### **Silencing of Human DHHC20**

The oligonucleotides for shControl and shDHHC20 constructs were synthesized (Integrated DNA Technologies) and inserted into the pLKO.1 vector. shControl encodes the non-targeting sequence of SHC002 (Sigma); the shRNA target sequence of human DHHC20 is 50-GAGCTCTGCGTGTTTACTATT-30. MDA-MB-231, MCF7 and NCI-H1975 cells were transduced with lentivirus encoding shControl or shDHHC20 and selected by puromycin treatment (1 mg/ml) for several passages.

## **Cell Viability**

Cells were treated with gefitinib (5  $\mu$ M) and/or 2-BP (500 nM) for 72 hr, and viability was measured by trypan blue staining. Quantification was done using a 1-way ANOVA with Tukey's multiple comparison post-test.

## **Determination of IC50 Values and Isobologram analysis**

Cells were seeded on a 96-well plate in 100  $\mu$ l growth media at a density of 1500 cells per well. After 24 hours post-seeding, the cells were treated with gefitinib and/or 2-BP for an additional 72 hours. Cell viability was assessed using the alamar blue viability assay (Invitrogen). Triplicate wells for each experiment were analyzed and the experiment was performed three times. The IC50 values were determined by a non-linear regression of the dose-response effect data using Prism for MacOSX (GraphPad Software). Cells were exposed to 1:1 ratios of the respective IC50s for gefitinib and 2-BP at  $\frac{1}{4}$  xIC50,  $\frac{1}{2}$  xIC50, IC50, 2 xIC50, and 4 xIC50. The assessment of synergy was performed using CalcuSyn software (Biosoft). The combination index (CI) was evaluated to assess synergism (CI<1), additive effect (CI~1) or antagonism (CI>>1).

## **Plasmids and generation of stable cell lines**

To generate inducible cell lines, wildtype EGFR and EGFR C1025A cDNA was first subcloned into the inducible pTRIPZ backbone with a puromycin resistance marker and FLAG tag. Empty pTRIPZ, which expresses the rtTA3, puromycin resistance marker, and FLAG tag was used as a negative control. Virus production was performed by transfecting HEK293T cells with the pTRIPZ constructs, psPAX2 and pMD2.G plasmids (Addgene) using TransIT-LT1 (Mirus) according to the manufacturer's instructions. MDA-MB-231 and NIH3T3 were infected with pTRIPZ virus using polybrene and incubated for

24 hours. Post-infection, fresh media was added on infected cells and incubated for an additional 48 hours before selection. Cells infected with the pTRIPZ constructs were selected with 1 µg/ml puromycin for several passages. Expression of EGFR cDNA was induced with 1 µg/ml doxycycline. Lentivirus of human mutant Kras4B(G12V) in pLenti-PGK-hygromycin resistance with an HA tag (Addgene plasmid #35633, [Singh et al. Cell, 2012]) was generated using HEK293T cells, Gag, VSVG and Rev. NIH3T3 cells infected with pTRIPZ constructs and selected with puromycin were subsequently infected with Kras4B(G12V)-HA. NIH3T3 pTRIPZ-plenti-Kras4B(G12V) cells were selected with puromycin (1 µg/ml) and hygromycin (500 µg/ml) together for several passages.

## References

1. Roskoski R Jr. (2014) ErbB/HER protein-tyrosine kinases: Structures and small molecule inhibitors. *Pharmacol Res.*, **87**, 42-59.
2. Walton GM, Chen WS, Rosenfeld MG, Gill GN. (1990) Analysis of deletions of the carboxyl terminus of the epidermal growth factor receptor reveals self-phosphorylation at tyrosine 992 and enhanced in vivo tyrosine phosphorylation of cell substrates. *J Biol Chem.*, **265(3)**:1750-4.
3. Lemmon, MA., Schlessinger J, and Ferguson KM. (2014) The EGFR Family: Not So Prototypical Receptor Tyrosine Kinases. *Cold Spring Harb Perspect Biol.*, **6.4**: a020768.
4. Normanno, N. De Luca A, Bianco C, Strizzi L, Mancino M, Maiello MR, Carotenuto A, De Feo G, Caponigro F, Salomon DS. (2006) Epidermal growth factor receptor (EGFR) signaling in cancer. *Gene*, **366**, 2–16.
5. Siegel, R., Naishadham, D. & Jemal, A. (2013) Cancer statistics, 2013. *Ca Cancer J Clin*, **63**, 11–30.
6. Chen, Z., Fillmore, C., Hammerman, P., Kim, C. & Wong, K.-K. (2014) Non-small-cell lung cancers: a heterogeneous set of diseases. *Nat Rev Cancer*, **14**, 535–546.
7. Jorissen, R. *et al.* Epidermal growth factor receptor: mechanisms of activation and signalling. (2003) *Exp Cell Res*, **284**, 31–53.
8. Fukata Y and Fukata M. Protein palmitoylation in neuronal development and synaptic plasticity. (2010) *Nat Rev Neuro*, **11**, 161-175.

9. Linder, M. & Deschenes, R. Palmitoylation: policing protein stability and traffic. (2007) *Nat Rev Mol Cell Bio*, **8**, 74–84.
10. Young, F., Butland, S., Sanders, S., Sutton, L. & Hayden, M. Putting proteins in their place: Palmitoylation in Huntington disease and other neuropsychiatric diseases. (2012) *Prog Neurobiol*, **97**,220–238.
11. Aicart-Ramos, C., Valero, R. & Rodriguez-Crespo, I. Protein palmitoylation and subcellular trafficking. (2011) *Biochim Biophys Acta*, **1808**, 2981–94.
12. Wang, W., Runkle, K., Terkowski, S., Ekaireb, R. & Witze, E. Protein Depalmitoylation Is Induced by Wnt5a and Promotes Polarized Cell Behavior. *J Biol Chem*, **290**, 15707–15716 (2015).
13. Conibear E, Davis NG. (2010) Palmitoylation and depalmitoylation dynamics at a glance. *J Cell Sci.*, **123**(Pt 23):4007-10.
14. Greaves, J. & Chamberlain, L. DHHC palmitoyl transferases: substrate interactions and (patho)physiology. (2011) *Trends Biochem Sci*, **36**, 245–253.
15. McCormick PJ, Dumaresq-Doiron K, Pluiose AS, Pichette V, Tosato G, (2008) Palmitoylation controls recycling in lysosomal sorting and trafficking. *Lefrancois S. Traffic.*, **9**, 1984-97.
16. Runkle K., Kharbanda A., Stypulkowski E., Cao X-J., Wang W., Garcia B.A., Witze E. Inhibition of DHHC20-Mediated EGFR Palmitoylation Creates a Dependence on EGFR Signaling. (2016) *Mol Cell*, **62**, 385–396.
17. Jennings BC, Nadolski MJ, Ling Y, Baker MB, Harrison ML, Deschenes RJ, Linder ME. (2009) 2-Bromopalmitate and 2-(2-hydroxy-5-nitro-

benzylidene)-benzo[b]thiophen-3-one inhibit DHHC-mediated palmitoylation in vitro. *J Lipid Res.*, **50(2)**:233-42.

18. Chou TC. Drug combination studies and their synergy quantification using the Chou-Talalay method. (2010) Chou TC. *Cancer Res.*, **70(2)**:440-6.

# CHAPTER 4: BLOCKING EGFR PALMITOYLATION SUPPRESSES PI3K SIGNALING AND MUTANT KRAS LUNG TUMORIGENESIS.

Akriti Kharbanda, David Walter, Andrea Guidel, Nancy Schek, David Feldser, Eric S. Witze. Loss of palmitoylated EGFR blocks mutant Kras tumorigenesis through loss of Myc expression. **In Press.** (2019)

## **Abstract**

Non-Small Cell Lung Cancer (NSCLC) is often characterized by mutually exclusive mutations in epidermal growth factor receptor (EGFR) (26%) or KRAS (37%) (1, 2). Here we show that in the presence of oncogenic KRAS, blocking EGFR palmitoylation severely reduces PI3K signaling, Myc expression and decreases cancer cell growth. In vivo, either genetic ablation of the palmitoyl-transferase DHHC20 or expression of a palmitoylation-resistant EGFR mutant blocks tumorigenesis in a KRAS mouse model of lung adenocarcinoma, suggesting that in KRAS mutant cells the PI3K pathway is vulnerable to loss of EGFR palmitoylation. Furthermore, acute inhibition of DHHC20 is sufficient to halt the growth of existing tumors derived from human cells. Inhibition of DHHC20 either genetically in KRAS mutant lung cancer cells increases their sensitivity to PI3K inhibitor treatment, accentuating the clinical potential of this vulnerability. Our findings reveal a molecular mechanism in which palmitoylated EGFR associates with the PI3K regulatory subunit PIK3R1 (p85), recruiting the PI3K heterodimer to the plasma membrane. Blocking palmitoylation increases the association of EGFR with the adaptor Grb2 and decreases EGFR association with p85. The binary switching between MAPK and PI3K signaling, modulated by EGFR palmitoylation, is only observed in the presence of oncogenic KRAS. These findings suggest a mechanism where oncogenic KRAS saturates signaling through unpalmitoylated EGFR,



displacing the PI3K signaling complex. The identification of the palmitoyl-transferase DHHC20 as a vulnerability in EGFR expressing, KRAS mutant cancer could have substantial therapeutic potential.

## Introduction

Non-small cell lung cancers (NSCLC) account for 15% of all cancer related deaths in the United States (3) NSCLCs are characterized by mutually exclusive activating mutations of epidermal growth factor receptor (EGFR) or of *KRAS*. EGFR is one of four members of the ErbB family and is known to facilitate tumorigenesis and cancer progression. EGFR is structurally comprised of an extracellular ligand binding domain, a transmembrane region, a tyrosine kinase domain, and an unstructured C-terminal tail that harbors receptor auto-phosphorylation sites (4). Ligand binding induces activation of the tyrosine kinase domain leading to auto-phosphorylation of tyrosine residues in the C-terminal domain. The phosphorylated tyrosine residues serve as docking sites for adaptor proteins that link the receptor to the downstream signaling pathways RAS/MAPK and PI3K/AKT which promote cell growth and survival. Activating mutations in EGFR increase both MAPK and PI3K signaling and promote oncogenesis. Mutations in *KRAS*, predominantly an amino acid substitution at codon 12 or 13, lead to upregulation of MAPK signaling. However, in the mutant *KRAS* setting tumor growth requires increased PI3K signaling through a mechanism dependent on a *KRAS*-PI3K interaction mediated by the Ras-Binding Domain of PIK3CA (5). Therefore, essential mechanisms are in place to maintain levels of PI3K signaling during tumorigenesis in the mutant *KRAS* background.

Our lab discovered that EGFR is palmitoylated on the C-terminal tail by the palmitoyl-transferase DHHC20 (6). Reduction of DHHC20 increases MAPK signaling by

a mechanism that is independent of EGFR kinase activity suggesting palmitoylation modulates assembly of the MAPK signaling complex on the C-terminal tail. Furthermore, a palmitoylation-defective EGFR point mutant (EGFR<sup>C1025A</sup>) activates downstream MAPK signaling with increased Grb2 receptor association confirming the mechanism is through the palmitoylated cysteine residues. Although MAPK signaling was increased in cells with reduced DHHC20 we observed a cell growth defect in mutant-*KRAS* cells caused by reduced EGFR palmitoylation (7). The mechanism by which unpalmitoylated EGFR is hindering mutant-*KRAS* growth remains unresolved.

Here, we demonstrate that loss of DHHC20 or expression of the palmitoylation-defective EGFR<sup>C1025A</sup> in a mutant-*KRAS* background enhances the *KRAS*/MAPK pathway whilst hindering the PI3K/AKT pathway leading to a reduction in Myc expression and reducing cell proliferation and blocking tumorigenesis. Our results indicate that in cells expressing EGFR and oncogenic *KRAS*, EGFR must be palmitoylated to allow PI3K signal complex formation, downstream signaling and tumorigenesis.

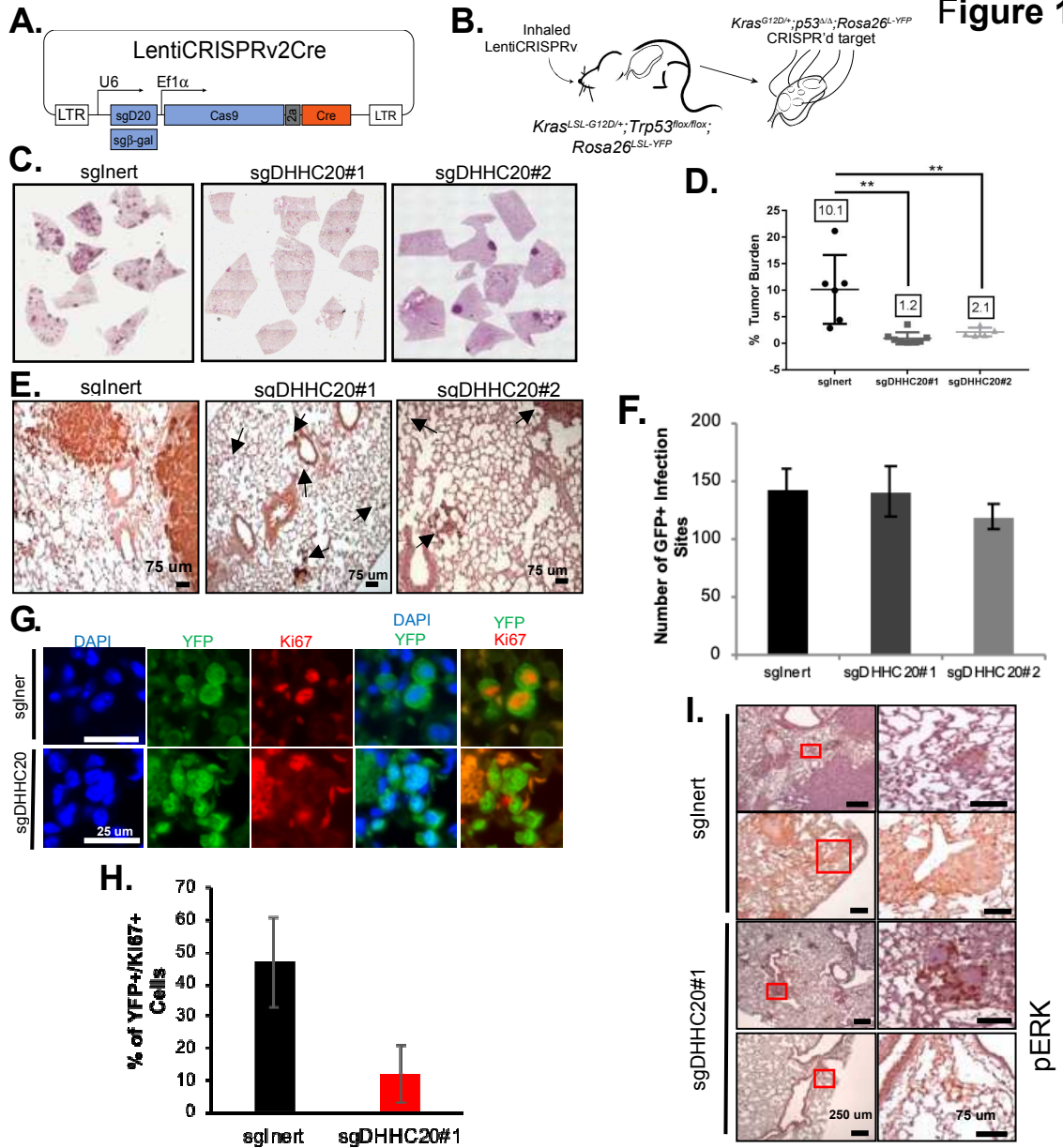
## Results

### DHHC20 inhibition reduces tumor burden in *KRAS*-mutant mice

We have previously demonstrated that inhibition of the palmitoyl-transferase DHHC20 or mutation of the palmitoylation site Cys 1025 on EGFR, induces EGFR receptor activation and thereby presents with increased downstream signaling to MAPK in *KRAS* mutant lung cancer cells SW1573 (*KRAS*<sup>G12V</sup>) (6). We therefore asked if DHHC20 loss affects *KRAS* mediated lung tumorigenesis. To study *KRAS* mutant tumor initiation, we used the genetically engineered *Kras*<sup>LSL-G12D/+</sup>; *p53*<sup>flox/flox</sup>; *Rosa26*<sup>LSL-YFP</sup> (KPY) autochthonous mouse model of lung cancer. In the model, tumors are initiated by

endotracheal delivery of viral particles that transduce lung epithelial cells to express Cre recombinase to activate *Kras*<sup>G12D</sup> and delete *p53* expression. To additionally ablate *DHHC20* expression *in vivo*, we transduced KPY mice with LentiCRISPRv2Cre, a construct that expresses Cre recombinase, Cas9, and a sgRNA targeting *DHHC20* (sgDHHC20#1/#2) or an inert sgRNA targeting  $\beta$ -galactosidase (sgInert) (Fig. 1A, B) (8). Twelve weeks after tumor initiation, animals transduced with LentiCRISPRv2Cre targeting *DHHC20* harbored 10-fold less tumor burden compared to sgInert mice (10.14% vs. 1.16% with a *P*-value= 0.0008) (Fig. 1C, D). Inactivation of *DHHC20* had a durable effect on tumor growth, as 24 weeks post-transduction there was still no increase in tumor burden (Supplemental Fig. 1B). Although significantly fewer tumors emerged when *DHHC20* was targeted, we found a similar frequency of YFP-positive transduction sites in the lungs of each cohort of KPY mice (Fig. 1E, F). We observed airway epithelial cells that were YFP positive and *DHHC20* negative indicating non-tumor cells are viable in the absence of *DHHC20* (Fig. 1E). Consistent with the lack of tumor outgrowth, YFP-labelled sgDHHC20#1 infected cells persisted twelve-weeks post-transduction, but a lower percentage expressed the proliferation-associated antigen Ki67 than tumors initiated with the sgInert expressing vector (Fig. 1H, I). Inhibition of *DHHC20* increases MAPK signaling in human KRAS-driven cancer cells (6). Consistently, we observed a marked increase in phosphorylated Erk in focal areas of the lung tissue of sgDHHC20#1 mice compared to the lung tissue of sgInert mice (Fig. 1J).

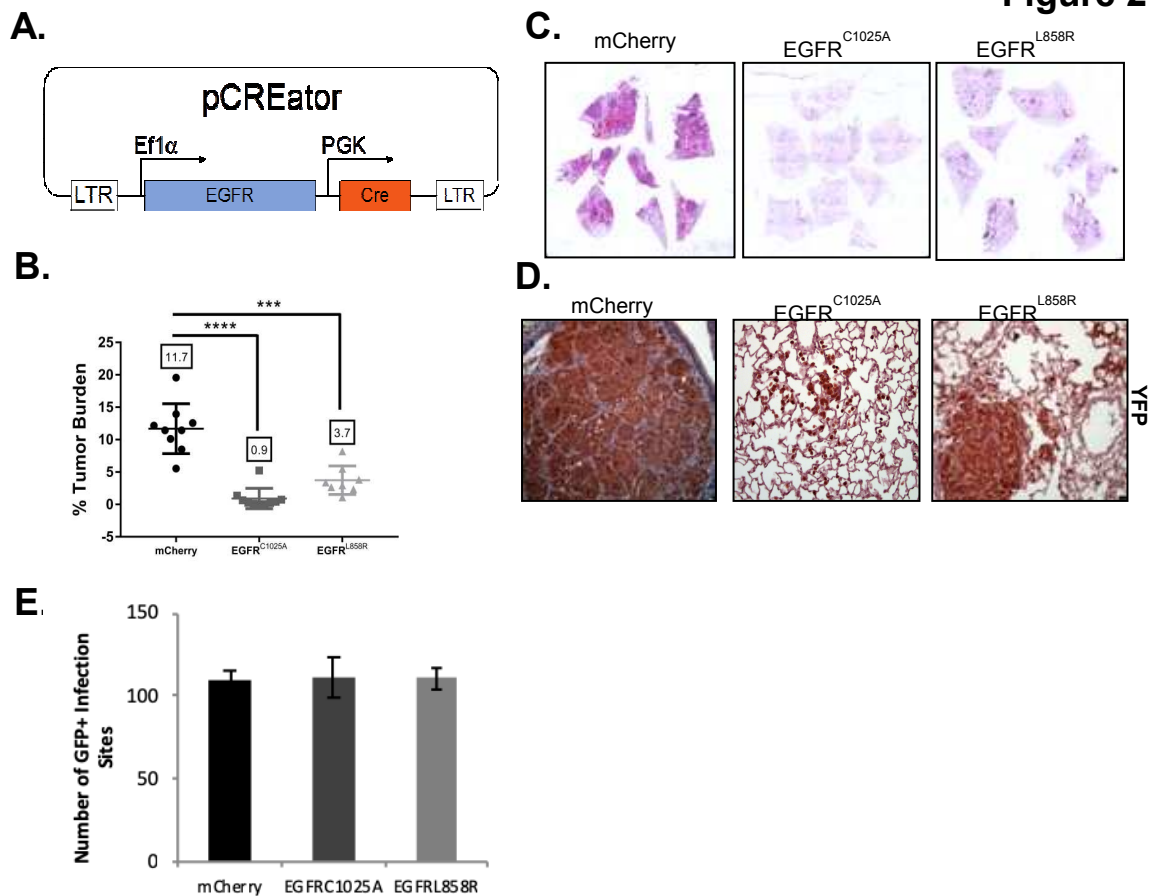
**Figure 1**



**Figure 1. Inhibition of DHHC20 leads to decreased tumour burden in mutant KRAS driven tumorigenesis.**  
**A.** Diagram of the LentiCRISPRv2Cre vector. **B.** Depiction of lentiviral lung tumor induction by intratracheal intubation. **C.** CRISPR of DHHC20 in KRAS<sup>LSL-G12D</sup>; Trp53<sup>lox/flox</sup>; Rosa26<sup>LSL-YFP</sup> (KPY) mice virally introduced to lung leads to a significant decrease in tumour burden. Hematoxylin and Eosin (H&E) 4X stitched images of sglNert, sgDHHC20#1 and sgDHHC20#2 lungs from infected mice. **D.** Average tumor burden (value indicated by boxed number) of sglNert (n=6), sgDHHC20#1 (n=8), and sgDHHC20#2 (n=6) in KRAS<sup>G12D/+</sup>; p53<sup>Δ/Δ</sup>; Rosa26<sup>L-YFP</sup> mice 13 weeks following infection with LentiCRISPRv2Cre, \*\*  $P < 0.05$ , Anova Two-Way. **E.** IHC staining for YFP in lungs from KPY mice 13 weeks after infection with LentiCRISPRv2Cre. Representative images sglNert and sgDHHC20#1 at 20X magnification (arrows indicate sites of infection). **F.** YFP positive regions in 4X stiches of IHC images for sglNert vs. sgDHHC20 were quantified using ImageJ. Graphs represent average number of YFP positive sites  $\pm$ SD of 5 mice per cohort. **G.** Deleting DHHC20 decreases proliferation of YFP positive cells in mouse lung tissue measured by Ki67 immunofluorescence staining. sglNert and sgDHHC20#1. tissue sections were stained for YFP (green), Ki67 (red) and DAPI (blue). All scale bars represent 25μm. **H.** Graph representing the percentage of YFP expressing cells staining positive for Ki67 in lung tissue of 4 mice from each of the sglNert and sgDHHC20#1 cohorts. (A total of 40 fields per cohort were quantified.  $\pm$  s.e.m (n=40), \*\*\*  $P < 0.001$ , Anova Two-Way. **I.** IHC staining for pERK in lungs from KPY mice 13 weeks following infection with LentiCRISPRv2Cre. Right panels show 20X magnification image of region indicated in the red box.

## **The palmitoylation resistant EGFR point mutant blocks KRAS-driven tumor growth.**

As previously discussed, expression of the palmitoylation-deficient EGFR cysteine point mutation, EGFR<sup>C1025A</sup>, also induces EGFR and subsequent MAPK activation. We sought to determine if specific loss of EGFR palmitoylation blocks mutant *KRAS* tumorigenesis *in vivo* phenocopying the result seen with inhibition of DHHC20. To assess whether EGFR<sup>C1025A</sup> is sufficient to block mutant *KRAS* tumorigenesis *in vivo*, we transduced KPY mice with lentiviral vectors to induce oncogenic *Kras*<sup>G12D</sup>, delete *p53* due to Cre-mediated recombination, and stably express either mCherry or palmitoylation- defective EGFR<sup>C1025A</sup> (Fig. 2A). We included expression of oncogenic EGFR<sup>L858R</sup> as a positive-control (Fig. 2A), which has been previously shown to induce synthetic lethality in the presence of mutant *KRAS* in NSCLC cell lines (9-11). EGFR<sup>C1025A</sup> and EGFR<sup>L858R</sup> expressing cohorts stained positively for EGFR compared to the minimal endogenous expression of EGFR in the control cohort (Supplemental Fig. 2A, B). Expression of EGFR<sup>C1025A</sup> or EGFR<sup>L858R</sup> reduced the tumor burden by greater than 10-fold compared to control (0.9%, 3.7% vs. 11.7%) (Fig. 2B, C). Despite the lack of tumor formation in KPY mice with enforced EGFR<sup>C1025A</sup> or EGFR<sup>L858R</sup>, a similar frequency of YFP-positive transduction sites was evident in lungs. (Fig. 2D, E). These results demonstrate that it is the unpalmitoylated form of EGFR that is incompatible with oncogenic *Kras*<sup>G12D</sup>-driven tumor formation, similar to the synthetic lethality observed with expression of EGFR<sup>L858R</sup> in the mutant *KRAS* background (12).

**Figure 2****Figure 2. Specific loss of EGFR palmitoylation blocks KRAS-driven tumour growth.**

**A.** Diagram of pCREator lentiviral EGFR overexpression construct introduced directly to the lung in *KRAS<sup>LSL-G12D</sup>; Trp53<sup>flax/flax</sup>, Rosa26<sup>LSL-YFP</sup>* (KPY) mice via intratracheal intubation. **B.** Average tumour burden of mCherry (n=9), EGFR<sup>C1025A</sup> (n=10), and EGFR<sup>L858R</sup> (n=9) in KPY mice 13 weeks following infection with Lenti-pCREator \*\*\*  $P < 0.001$ , Anova Two-Way. **C.** Expression of EGFR<sup>C1025A</sup> in KPY mice significantly decreases tumour burden compared to expression of the negative control mCherry or expression of the positive control EGFR<sup>L858R</sup>. Hematoxylin and Eosin (H&E) staining at 4X magnification of lungs from mCherry, EGFR<sup>C1025A</sup> and EGFR<sup>L858R</sup> expressing mice. **D.** Images of IHC staining detecting YFP expressing cells in lungs from KPY mice 13 weeks following Lenti-pCREator infection. Representative images of mCherry, EGFR<sup>C1025A</sup> and EGFR<sup>L858R</sup> at 10X magnification. **E.** YFP positive regions in 4X stiches of IHC images of mCherry vs. EGFR<sup>C1025A</sup> or EGFR<sup>L858R</sup> expression were quantified using ImageJ. Graphs represent average number of YFP positive sites  $\pm$ SD of 5 mice per cohort.

## **DHHC20 inhibition reduces PI3K/AKT signaling and Myc expression**

Although the increase in MAPK signaling upon *DHHC20* inactivation *in vivo* is consistent with our previous *in vitro* results, the pro-proliferative function of MAPK signaling is in conflict with the observed inhibition of tumor growth. Similarly, when we examined cell proliferation in KRAS mutant, EGFR positive cancer cell lines, H23 (KRAS<sup>G12V</sup>) and MDA-MB-231 (KRAS<sup>G12D</sup>), we found cell proliferation decreased significantly in both cell lines when *DHHC20* is silenced by shRNA (Fig. 3A, B). We therefore examined PI3K-AKT, a parallel branch of the EGFR signaling pathway and found a marked decrease in AKT phosphorylation at Threonine 308 (T308) when *DHHC20* is inhibited by shRNA (Fig. 3C). T308 is the primary activating phosphorylation site on AKT and is mediated by the PI3K pathway. The PI3K-AKT pathway inactivates glycogen synthase kinase 3 $\beta$  (GSK3 $\beta$ ) via phosphorylation on Ser9, preventing GSK3 $\beta$  mediated Myc phosphorylation and subsequent proteosomal degradation (13, 14). Consistent with a reduction in the PI3K-AKT pathway, *DHHC20* silencing in both MDA-MB-231 and H23 cells decreases GSK3 $\beta$  phosphorylation at Ser9 and severely reduces Myc expression (Fig. 3C). Treating MDA-MB-231 and H23 shDHHC20 cells with MG132, a potent proteasome inhibitor, fully restores Myc expression indicating that inhibiting *DHHC20* promotes Myc proteosomal degradation (Fig. 3D). Similarly, pharmacologic inhibition of GSK3 $\beta$  with CHIR-90021 also restored Myc protein levels, confirming Myc degradation caused by loss of DHHC20 requires GSK3 $\beta$  activity (Fig. 3E). Silencing *DHHC20* did not decrease Myc mRNA levels indicating that the decrease in Myc expression is not a result of changes in Myc transcription (Supplemental Fig. 1A). Finally, we asked if restoring Myc expression could rescue the DHHC20-induced growth defect. Mutating the GSK3 $\beta$  phosphorylation site on Myc (Myc<sup>T58A</sup>) inhibits Myc degradation. When Myc<sup>T58A</sup> was expressed in H23 shDHHC20 cells the growth rate was

fully restored to that of the shCon cells confirming that the reduction in cell growth caused by *DHHC20* inhibition is due to reduced Myc expression (Fig. 3F, G).



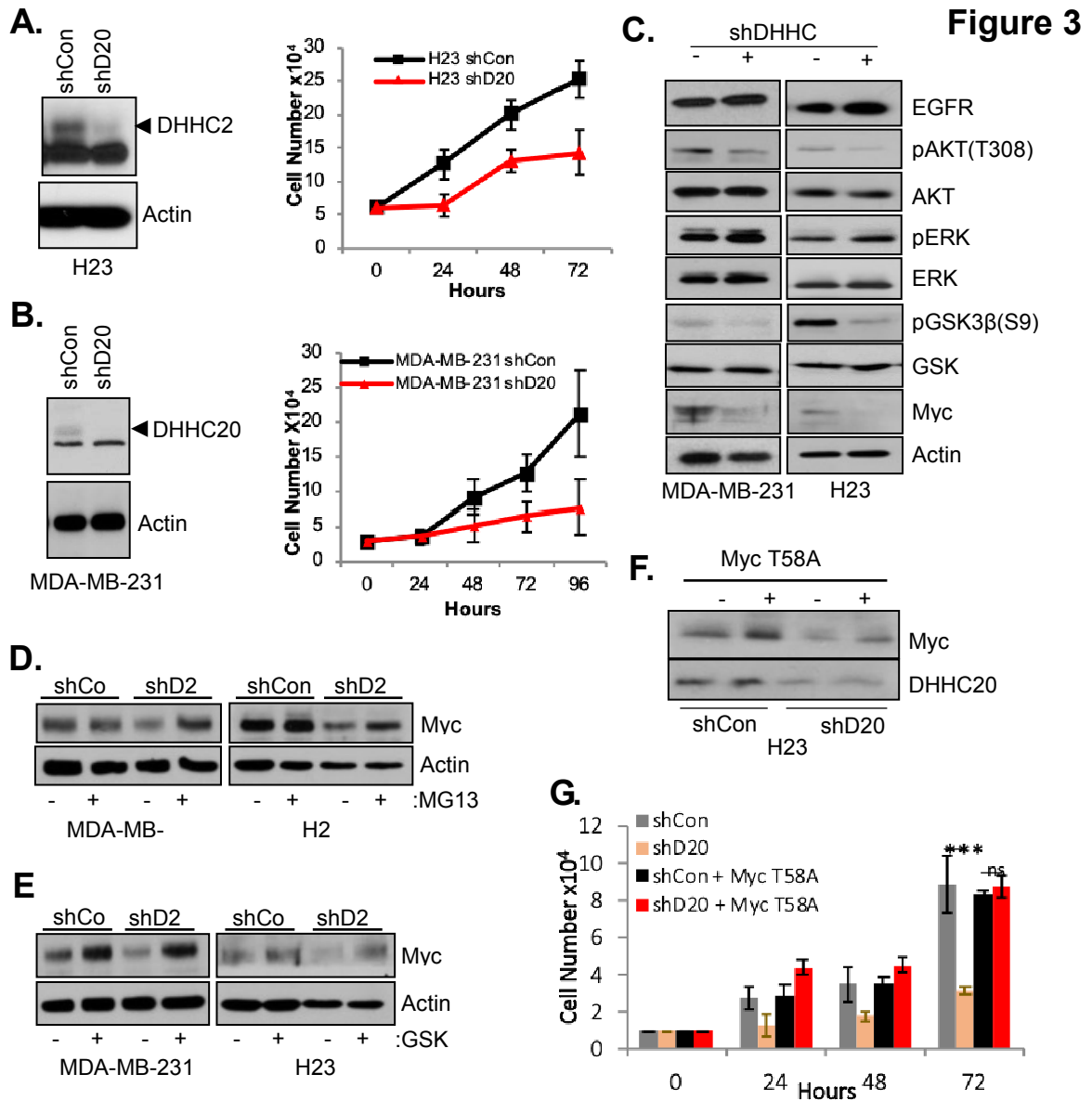


**Figure 3. Inhibition of DHHC20 results in depletion of Myc expression in KRAS mutant cells that is restored by inhibition of the proteasome or GSK3 $\beta$ .**

**A and B.** H23 and MDA-MB-231 cells were stably infected with lentiviruses containing a control scrambled shRNA (shCon) or an shRNA targeting DHHC20 (shD20). Immunoblotting for DHHC20 with anti-DHHC20 antibodies confirms a reduction in DHHC20 expression (left). Silencing DHHC20 decreases cell proliferation in both H23 and MDA-MB-231 cells (right). **C.** Silencing DHHC20 in MDA-MB-231 and H23 cells increases pERK but decreases pAKT and pGSK3 $\beta$  as well as Myc protein expression. **D and E.** Treatment of MDA-MB-231 and H23 shDHHC20 cells with 5  $\mu$ M MG132 (**D**) or 3  $\mu$ M CHIR-99021 (**E**) for 6 hours restored Myc protein levels to shCon levels as determined by immunoblotting with anti-Myc antibody. **F.** Immunoblotting shows that stably transducing H23 shControl (shCon) and shDHHC20 cells (shD20) with the stable Myc<sup>T58A</sup> mutant partially restores Myc protein levels. **G.** Expression of Myc<sup>T58A</sup> in H23 shDHHC20 cells rescues the growth defect from loss of DHHC20. H23 shCon and shD20 cells, and H23 shCon/Myc<sup>T58A</sup> and H23 shD20/Myc<sup>T58A</sup> cells were plated at a density of  $6 \times 10^4$  cells on day 0. Cells were counted once a day for 72 hours. Cell number is expressed as the mean  $\pm$  s.d of three replicates. \*\*\*  $P < 0.001$ , Student's T-Test.

## Palmitoylation-resistant EGFR antagonizes oncogenic KRAS signaling and cell growth

The results thus far suggest PI3K signal activation is inhibited in the presence of unpalmitoylated EGFR. To test this, *EGFR* was silenced by shRNA in MDA-MB-231 and H23 shCon and shDHHC20 cells to restore PI3K signaling and Myc expression (Fig. 4A). We found that when EGFR expression was inhibited phosphorylated AKT and Myc expression were increased and cell growth was completely restored in both MDA-MB-231 and H23 shDHHC20 cells (Fig. 4A, B and C). Therefore, the loss of Myc and the growth defect in *KRAS* mutant cells caused by the DHHC20-loss is dependent on the presence of EGFR (Fig. 4B, C).

We next asked if the unpalmitoylated form of EGFR is the cause of reduced Myc expression when *DHHC20* is silenced. We used a conditional system for expressing wild type EGFR (EGFR<sup>WT</sup>) or EGFR<sup>C1025A</sup>, the palmitoylation-deficient mutant (7). Although, treatment of the cells with doxycycline for 72 hours induced equal levels of EGFR<sup>WT</sup> and EGFR<sup>C1025A</sup>, Myc protein levels were reduced in the EGFR<sup>C1025A</sup>-expressing cells compared to EGFR<sup>WT</sup> (Fig. 4D). Similarly, EGFR<sup>C1025A</sup> expression decreased levels of pAKT(T308) and pGSK3β(S9) compared to EGFR<sup>WT</sup>, phenocopying the results observed with *DHHC20* inhibition (Fig. 4C).

Thus far all the cell contexts examined were in an activated mutant *KRAS* background. We therefore asked if the reduction in cell growth and Myc expression mediated by EGFR<sup>C1025A</sup> specifically requires mutant *KRAS* by measuring Myc levels after inducing EGFR<sup>WT</sup> or EGFR<sup>C1025A</sup> in NIH3T3 cells expressing *KRAS*<sup>WT</sup> or activated *KRAS*<sup>G12V</sup>. When EGFR<sup>C1025A</sup> was induced in the presence of *KRAS*<sup>G12V</sup> there was a decrease in pAKT(T308), pGSK3β(S9) and Myc that was not observed with *KRAS*<sup>WT</sup>

(Fig. 5A). Expression of EGFR<sup>C1025A</sup> in the presence of KRAS<sup>G12V</sup> also decreased cell growth confirming that the mechanism for reducing Myc expression and cell proliferation requires oncogenic KRAS (Fig. 5B).

These results indicate that expression of EGFR<sup>C1025A</sup> in a mutant Kras background is leading to a deficit of PI3K signaling due to lack of access of PIK3R1 to the membrane where it is required to facilitate downstream signaling. The PI3K catalytic subunit p110 $\alpha$ , is also often mutated in lung cancer, but unlike mutant KRAS does not appear to be mutually exclusive with EGFR mutations in NSCLC patients (15, 16). We asked if expressing a constitutively active mutant of p110 in EGFR<sup>C1025A</sup> expressing cells can bypass the requirement of PIK3R1 at the membrane. Co-expression EGFR<sup>WT</sup> or EGFR<sup>C1025A</sup> with either PIK3CA<sup>WT</sup> or the oncogenic mutant PIK3CA<sup>E454K</sup> in NIH3T3 cells (17) had no effect on the levels of pAKT(T308) and pGSK3 $\beta$ (S9) (Fig. 5C). In contrast to the effect seen in KRAS mutant cells, co-expression of EGFR<sup>C1025A</sup> with PIK3CA<sup>E454K</sup> markedly increased Myc expression (Fig. 5C). However, there was no increase in cell proliferation between cells expressing EGFR<sup>C1025A</sup> and those expressing EGFR<sup>WT</sup>, suggesting that the Myc protein is not limiting for cell growth in the mutant PIK3CA<sup>E454K</sup> expressing cells (Fig. 5D). We next examined the lung adenocarcinoma cell line SW1573 which harbors both activating KRAS and PIK3CA mutations. We found that induction of EGFR<sup>C1025A</sup> expression in SW1573 was unable to reduce AKT or GSK3 $\beta$  phosphorylation (Fig. 5E). EGFR<sup>C1025A</sup> expression also had no effect on Myc expression or cell growth, indicating PIK3CA activating mutations are sufficient to restore PI3K signaling, on which the cells are now dependent, and cell growth in mutant KRAS cells expressing unpalmitoylated EGFR (Fig. 5E, F).

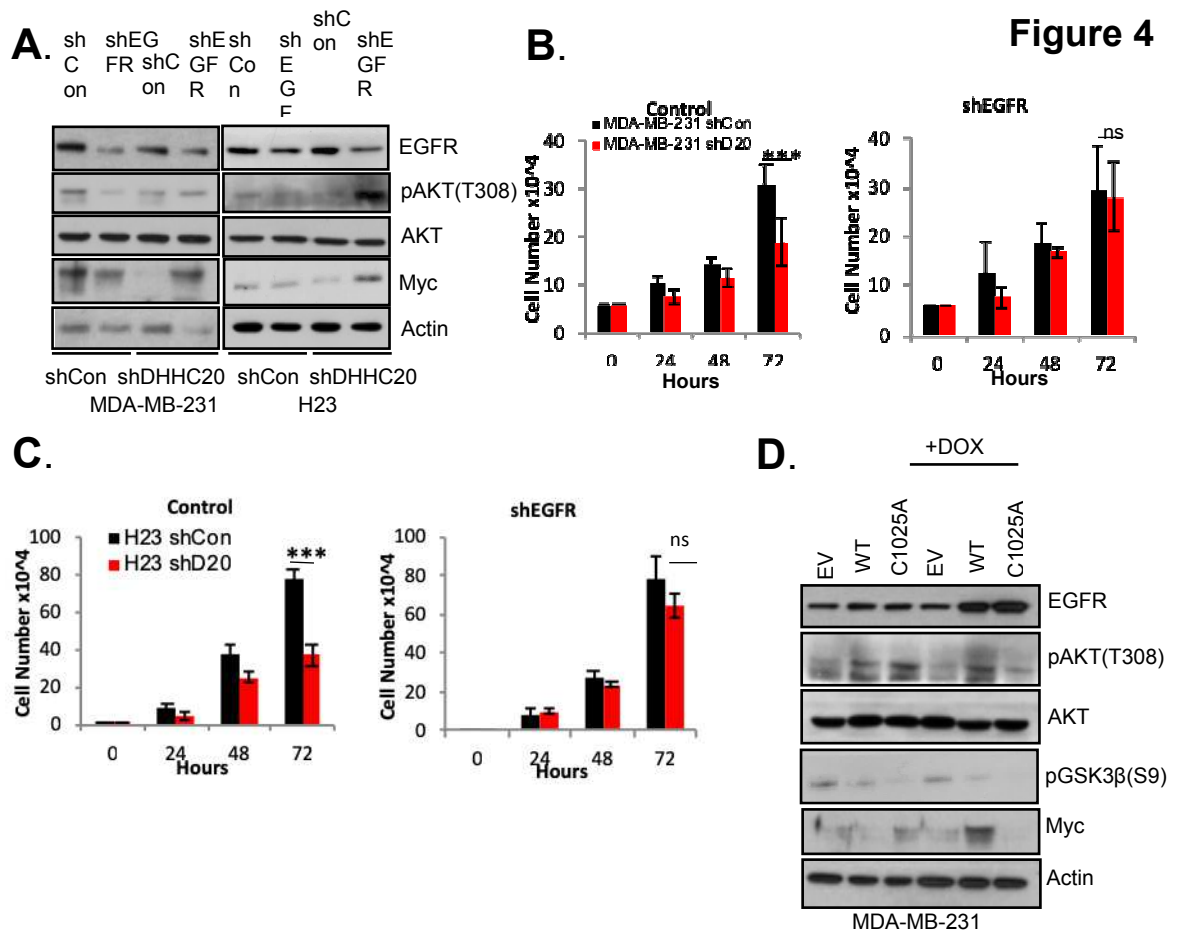


**Figure 4. DHHC20-loss induced depletion of Myc requires the presence of palmitoylated EGFR**

**A.** MDA-MB-231 and H23 shCon and shDHHC20 cells were stably infected with lentiviruses expressing a control scrambled shRNA (shCon) or an shRNA targeting EGFR (shEGFR). Lysates were immunoblotted with the indicated antibodies. EGFR inhibition rescues shDHHC20 induced Myc depletion. **B and C.** Silencing EGFR by shRNA in MDA-MB-231 (**B**) and H23 (**C**) shDHHC20 cells rescues the shDHHC20 (shD20) induced growth defect. Control shRNA (left) shCon (D20); shCon (EGFR) (black) and shCon (EGFR); shD20 (red) cells or EGFR knockdown (right) shEGFR; shCon (D20) (black) and shEGFR; shD20 (red) cells were plated on day 0 and counted after 24, 48 and 72 hours. Cell number is expressed as the mean  $\pm$  s.d of three replicates. \*\*\*  $P < 0.001$ , Student's T-test. **D.** MDA-MB-231 cells expressing inducible EGFR wildtype (WT), EGFR palmitoylation defective mutant cysteine 1025 to alanine (C1025A) or an empty vector control (EV), were treated with doxycycline (1  $\mu$ g/ml) for 15 hours. Lysates were immunoblotted with the indicated antibodies. Expression of EGFR<sup>C1025A</sup> decreased pAKT and pGSK3 $\beta$  as well as Myc expression.

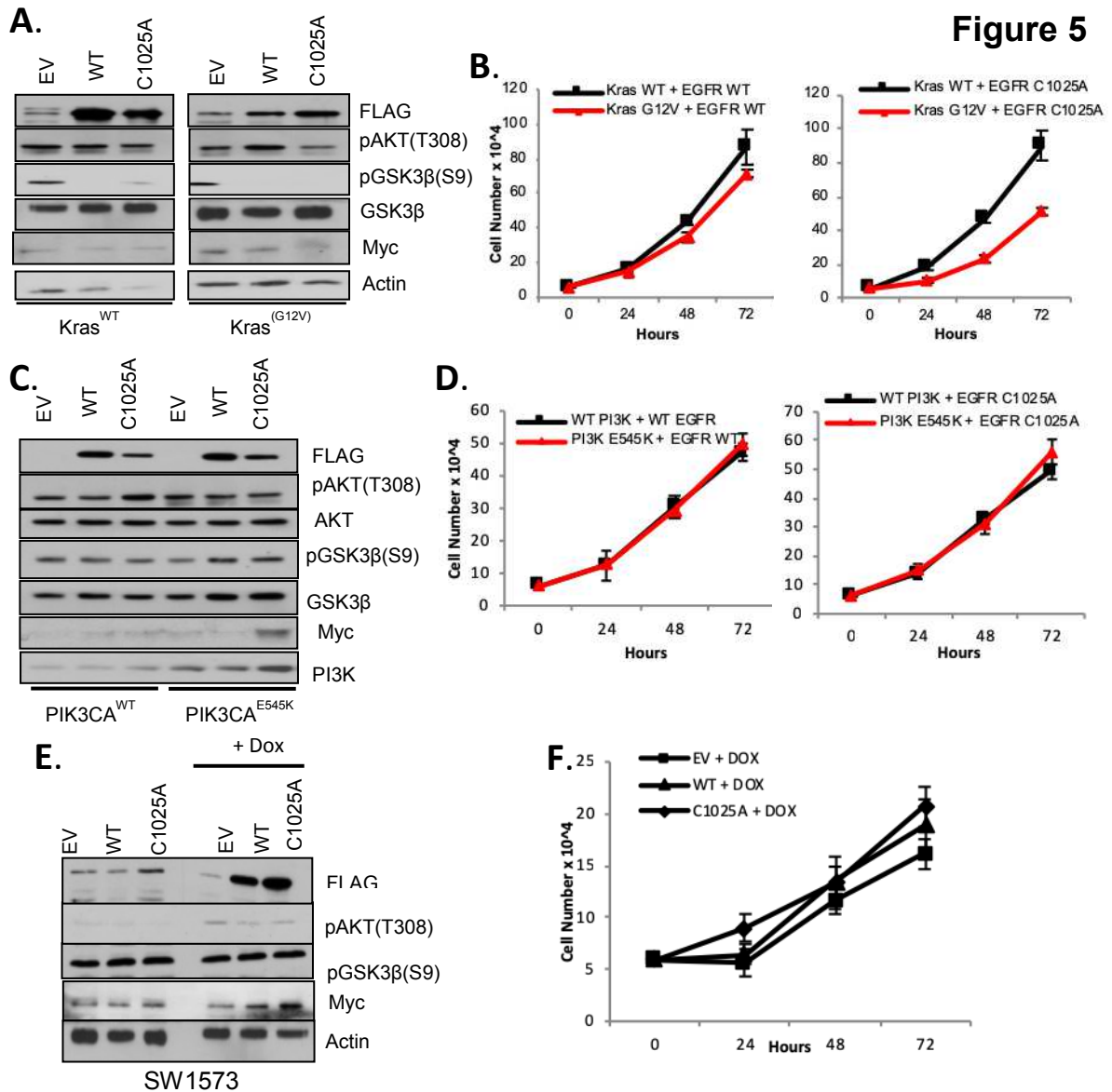


**Figure 5. Presence of mutant KRAS is required to induce loss of PI3K/AKT pathway, Myc expression and reduction of cell growth from loss of EGFR palmitoylation**

**A.** NIH3T3 cells expressing wildtype KRAS (KRAS<sup>WT</sup>) or mutant KRAS (KRAS<sup>G12V</sup>) were stably infected with lentivirus to express doxycycline inducible EGFR<sup>WT</sup> (WT), EGFR<sup>C1025A</sup> (C1025A) or the empty vector (EV). After induction with doxycycline (1 μg/ml) for 15 hours, co-expression of EGFR<sup>C1025A</sup> with KRAS<sup>G12V</sup> decreased pAKT, pGSK3β and Myc expression compared to EGFR<sup>WT</sup> co-expressed with KRAS<sup>G12V</sup>. **B.** Growth curve of NIH3T3 cells co-expressing KRAS<sup>WT</sup> (black squares) or KRAS<sup>G12V</sup> (red triangles) with doxycycline inducible, EGFR<sup>WT</sup> (left) or EGFR<sup>C1025A</sup> (right) or empty vector (data not shown). Co-expression of EGFR<sup>C1025A</sup> with KRAS<sup>G12V</sup> cells (right, red triangles) reduces cell growth compared to cells co-expressing EGFR<sup>WT</sup> with KRAS<sup>WT</sup> (right, black squares) or cells co-expressing EGFR<sup>WT</sup> with KRAS<sup>G12V</sup> (left, red triangles). Cell number is expressed as the mean ± s.d of three replicates. **C.** NIH3T3 cells expressing wildtype PIK3CA (PIK3CA<sup>WT</sup>) or PIK3CA harboring the activating mutation E545K (PIK3CA<sup>E545K</sup>) were stably infected with lentivirus to express doxycycline inducible EGFR<sup>WT</sup>, EGFR<sup>C1025A</sup> or empty vector. After induction with doxycycline (1 ug/ml) overnight, co-expression of EGFR<sup>C1025A</sup> with PIK3CA<sup>E545K</sup> increased Myc protein expression compared to EGFR<sup>WT</sup> co-expressed with

PIK3CA<sup>E545K</sup>. **D.** Growth curve of NIH3T3 cells co-expressing either PIK3CA<sup>WT</sup> (black squares) or PIK3CA<sup>E545K</sup> (red triangles) with doxycycline inducible EGFR<sup>WT</sup> (left), EGFR<sup>C1025A</sup> (right) or empty vector control (data not shown). Co-expression of EGFR<sup>C1025A</sup> or EGFR<sup>WT</sup> with either PIK3CA<sup>WT</sup> or PIK3CA<sup>E545K</sup> (right and left, black squares and red triangles) has no effect on cell proliferation. Cell number is expressed as the mean  $\pm$  s.d of three replicates. **E.** SW1573 cells harboring both mutant KRAS<sup>G12C</sup> and the activating mutation, PIK3CA<sup>K111E</sup>, were stably infected with lentivirus to express doxycycline inducible EGFR<sup>WT</sup>, EGFR<sup>C1025A</sup> or empty vector. After induction with doxycycline (1 ug/ml) overnight, expression of EGFR<sup>C1025A</sup> did increase Myc protein expression compared to EGFR<sup>WT</sup>. **F.** Growth curve of SW1573 cells expressing doxycycline inducible, EGFR<sup>WT</sup> (triangles), EGFR<sup>C1025A</sup> (diamonds) or empty vector (squares). Expression of EGFR<sup>C1025A</sup> (diamonds) does not change cell growth compared to cells expressing EGFR<sup>WT</sup> (triangles) or to cells expressing empty vector (squares). Cell number is expressed as the mean  $\pm$  s.d of three replicates.

## Palmitoylated EGFR recruits PI3K signaling components to the plasma membrane

We reasoned that in the presence of oncogenic KRAS, EGFR palmitoylation is required to promote PI3K complex formation at the membrane, biasing downstream signaling towards PI3K/AKT signaling. The PI3K heterodimer is made up of a regulatory subunit PIK3R1 (p85) and the catalytic subunit PIK3CA (p110 $\alpha$ ) (16). To detect recruitment of signaling components to the membrane, we isolated the membrane fraction of NIH3T3 cells expressing either EGFR<sup>WT</sup> or EGFR<sup>C1025A</sup> together with either KRAS<sup>WT</sup> or Kras<sup>G12V</sup>. Immunoblotting of the membrane fractions revealed an increase in the abundance of the MAPK adapter Grb2 and a decrease in PI3K regulatory subunit p85 in EGFR<sup>C1025A</sup>-expressing cells compared to EGFR<sup>WT</sup>-expressing cells in the presence of Kras<sup>G12V</sup>. The decrease in p85 was not observed in cells expressing EGFR<sup>C1025A</sup> together with Kras<sup>WT</sup> (Fig. 6A). We asked if the preferential binding of EGFR<sup>C1025A</sup> for Grb2 over p85 is also observed in the KRAS mutant cell line. We again found a consistent decrease in p85 and increase in Grb2 association with the plasma membrane in cells expressing EGFR<sup>C1025A</sup> compared to EGFR<sup>WT</sup> (Fig. 6B, C). We then probed the membrane fraction for the presence of KRAS and found that EGFR<sup>C1025A</sup> increased KRAS<sup>WT</sup> membrane association beyond that of EGFR<sup>WT</sup>, but we found equally high levels of KRAS<sup>G12V</sup> at the membrane in all three conditions empty vector, EGFR<sup>WT</sup> and EGFR<sup>C1025A</sup>. This may indicate that the cycling of KRAS between the GTP and GDP bound forms causes a transient association with EGFR<sup>C1025A</sup> allowing both Grb2 and PI3K to associate with EGFR<sup>C1025A</sup> in the presence of wild type KRAS.

Our findings reveal that palmitoylated EGFR is required for PI3K activation and Myc expression in the presence of oncogenic KRAS. As shown, unpalmitoylated EGFR leads to a deficiency of PI3K signaling due to a reduction of p85 at a membrane

complex, but what remains to be determined is how palmitoylated EGFR recruits the PI3K complex and if EGFR engages PI3K directly. We reasoned that EGFR palmitoylation directs PI3K signal complex formation by interacting with the PI3K signaling complex. To measure interactions between PI3K and the palmitoylated form of EGFR, we synthesized biotinylated peptides encompassing Cys 1025, in both palmitoylated and unpalmitoylated forms and incubated them with lysates from PIK3R1 expressing cells (Fig. 6D). PIK3R1 associated with increasing concentrations of palmitoylated peptide, but not the unpalmitoylated peptide or a palmitoylated peptide with a scrambled sequence (Fig. 6D). These results suggest that sequence specific palmitoylated motifs can be recognized as docking sites on proteins that may modulate signal complex formation.



**Figure 6**

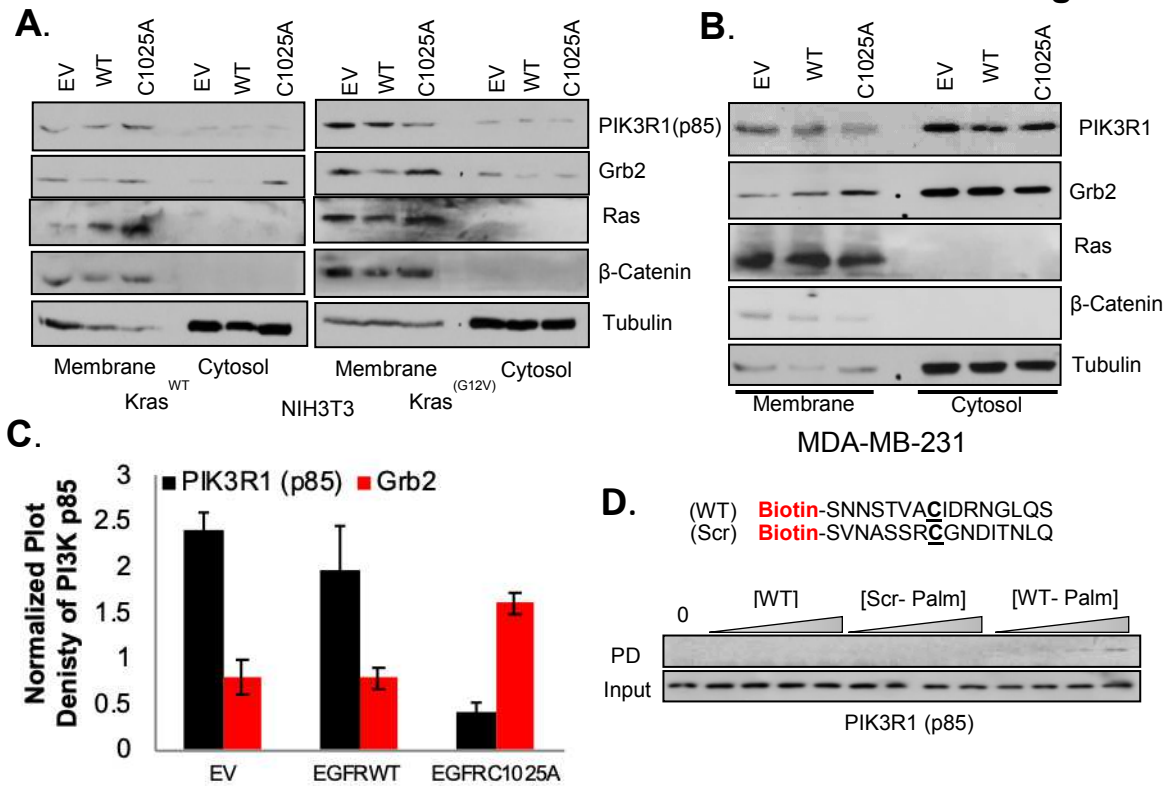


**Figure 6. Expression of unpalmitoylated EGFR in the presence of mutant KRAS leads to loss of PIK3R1 (p85) recruitment to the membrane** **A.** NIH3T3 cells expressing wildtype KRAS (KRAS<sup>WT</sup>) or mutant KRAS (KRAS<sup>G12V</sup>) were stably infected with lentivirus to express doxycycline inducible EGFR<sup>WT</sup> (WT), EGFR<sup>C1025A</sup> (C1025A) or the empty vector (EV). After induction, membrane fractions from NIH3T3 cells expressing mutant KRAS(KRAS<sup>G12V</sup>) and EGFR<sup>C1025A</sup> has reduced levels of PIK3R1 (p85) compared to cells expressing EGFR<sup>C1025A</sup> and KRAS<sup>WT</sup>. α-tubulin and β-catenin were positive controls for cytosolic and membrane enrichment respectively. **B.** The membrane fraction from MDA-MB-231 cells expressing EGFR<sup>C1025A</sup> has reduced levels of PIK3R1 (p85) and increased amounts of Grb2 compared to cells expressing EGFR<sup>WT</sup>. α-tubulin and β-catenin were positive controls for cytosolic and membrane enrichment respectively. **C.** Densitometric quantification of PIK3R1 or Grb2 amounts at the membrane. Density of PIK3R1 or Grb2 bands was normalized to the band density of the loading control β-catenin and expressed as the mean ± s.e.m of seven experiments. **D.** Lysates from NIH3T3 cells expressing WT KRAS or KRAS<sup>G12V</sup> and inducibly expressing empty vector, EGFR<sup>WT</sup> or EGFR<sup>C1025A</sup> cells were subjected to immunoprecipitation with anti-PI3K(p110α). The precipitates were immunoblotted with the indicated antibodies. Lysates not subjected to immunoprecipitation were used as input controls. **E.** Lysates from NIH3T3 cells expressing V5-tagged PIK3R1 were incubated for 15 hours with increasing concentrations of biotinylated peptide encompassing the sequence around either palmitoylated or unpalmitoylated Cys 1025 or a palmitoylated scrambled (Scr) control. Peptides were isolated on streptavidin beads and the washed beads were boiled, and proteins were separated by SDS-PAGE and immunoblotted with anti-PIK3R1. Binding reactions prior to streptavidin pull-down were used as input controls. PIK3R1 interacts with wildtype palmitoylated peptide but not the palmitoylated scrambled peptide or the unpalmitoylated wildtype peptide.

## **Loss of DHHC20 sensitizes KRAS mutant cells to PI3K inhibitors**

The results thus far indicate that blocking EGFR palmitoylation, reduces PI3K signaling. Consequently, KRAS mutant cancer cells are unable to proliferate due to a dependency on higher PI3K signaling needed to balance the hyperactivation of MAPK. Therefore, we hypothesized that KRAS mutant cancer cells where DHHC20 is inhibited by shRNA will be sensitive to elimination of the residual PI3K signaling by treating cells with a PI3K inhibitor. Stable knockdown of DHHC20 in the KRAS mutant SW1573 and H23 cells increases sensitivity to the PI3K inhibitor, BKM120. (Fig. 7A and Supp. Fig. 4A). BKM120, also known as, Buparlisib, is a pan PI3K inhibitor currently in clinical development for various solid tumors. Inhibition by BKM120 proves more effective in inducing cell death than gefitinib in KRAS mutant cells where DHHC20 is inhibited using both stable knockdown and acute doxocycline-induced shRNA driven knockdown, (Fig. 7A, B and Supp. Fig. 4B). Furthermore, prolonged DHHC20 inhibition in SW1573 and H23 cells reduced the IC50 concentrations of BKM120 by 2-fold indicating increased sensitivity of the KRAS mutant cell lines to inhibition of PI3K signaling (Fig. 7C and Supp. Fig. 4A). Relevant to the clinic, simulating acute drug inhibition, knockdown of DHHC20 using doxocycline to induce expression of shRNA targeting DHHC20 in A549-GFP-Luciferase (A549-GL) and H23-GFP-Luciferase (H23-GL) cells reduced the IC50 concentrations of BKM120 by 3- and 5-fold, respectively. (Fig. 7D and Supp. Fig 4B). These results corroborate the finding that KRAS mutant cells become sensitive to the loss of PI3K signaling when EGFR is not palmitoylated. This facet of the mechanism can be translated to the clinic by developing a pharmacologic inhibitor of DHHC20 to use in combination with a PI3K inhibitor.

### **Inhibition of DHHC20 blocks growth of established KRAS-mutant lung tumors**

To determine the potency of targeting DHHC20 in existing tumors we generated xenografts using the KRAS-mutant cell line, A549, expressing GFP and luciferase and doxocycline-inducible shRNA targeting a control scrambled sequence or DHHC20. Doxocycline treatment was initiated when tumors reached 100 mm<sup>3</sup> in size, and was administered every day for 10 days. Tumor growth was measured by luciferase imaging. Induction of shRNA targeting DHHC20 abrogated the growth of all xenograft tumors by day 2 of treatment whereas induction of shRNA targeting control scrambled was unable to inhibit tumor growth. (Fig. 7 E, F) . These results set up a strong rationale for developing specific small molecule inhibitors to the enzyme DHHC20.

**Figure 7**

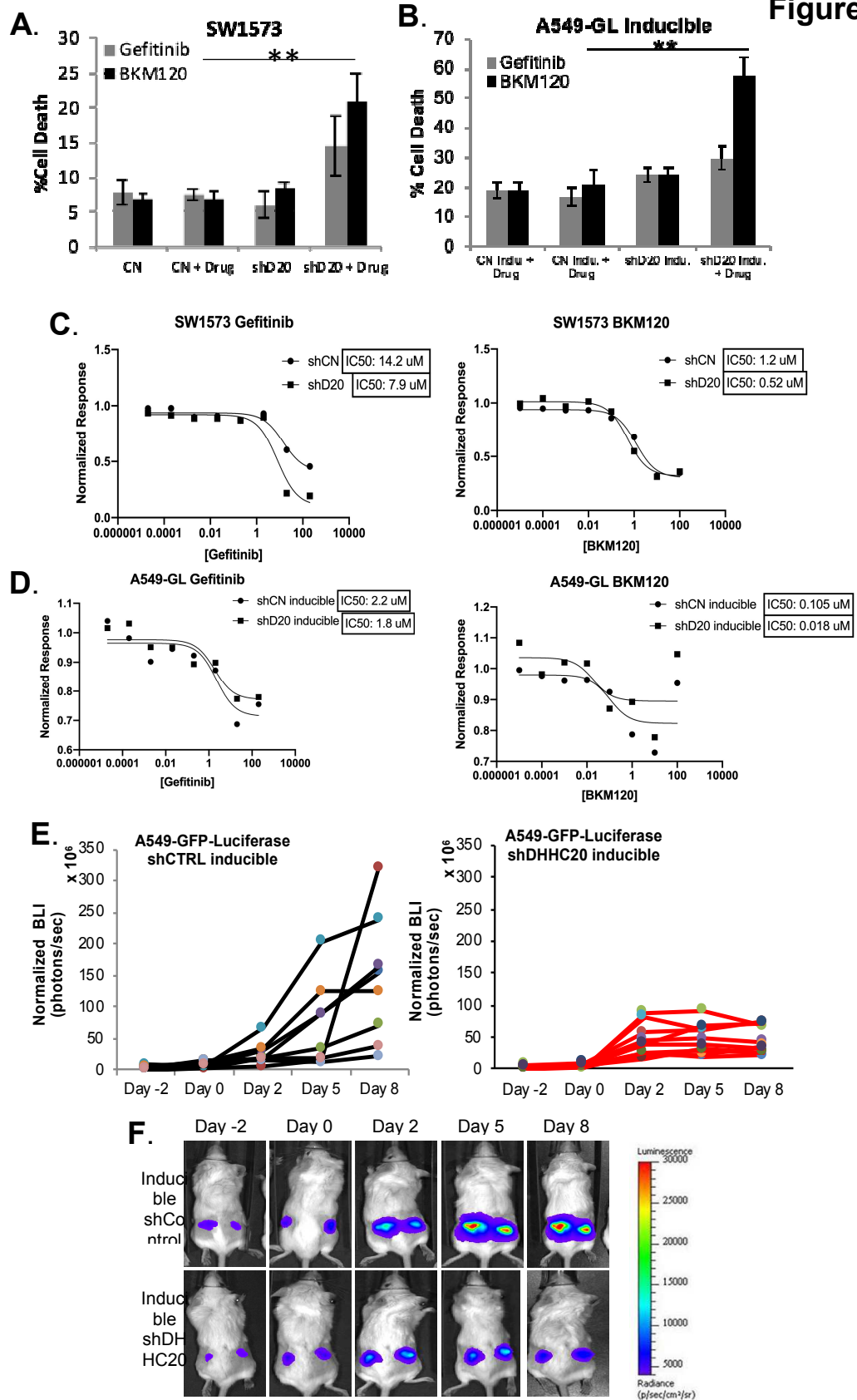


**Figure 7. Loss of DHHC20 sensitizes KRAS mutant cells to PI3K inhibitors**

**A and B.** Gefitinib (5  $\mu$ M) (gray) and BKM120 (500 nM) (black) treatment increases cytotoxicity in DHHC20 silenced SW1573 cells and inducibly silenced A549-GFP-Luciferase (A549-GL) cells (mean  $\pm$ StDev). \*\*  $P < 0.05$  **C and D.** Dose-response curves for SW1573 shCN and shDHHC20 and A549-GL with inducible shRNA against a control scrambled sequence (shCN) and shD20 cells treated with either Gefitinib or BKM120 at various doses for 72 h (n=3) to determine IC<sub>50</sub> differences. \*\*\*  $P < 0.001$  for all IC<sub>50</sub> pairs, Two-Way Anova.  $R^2$  value =0.98. **E.** Tumor volume of each shControl xenograft (left, black) and each shDHHC20 xenograft (right, red) represented as the day 0 normalized bioluminescence intensity (photons/sec). n=10. **F.** Bioluminescence images of A549-GL xenograft bearing mice. Representative image of one shControl and one shDHHC20 mouse through all days of measurement.

## Discussion

Taken together, our findings indicate that in a mutant KRAS background the PI3K heterodimer associates with palmitoylated EGFR at the plasma membrane to activate PI3K/AKT signaling. As a result, there is an increase in Myc expression that activates pro-proliferative transcription programs supporting cancer cell growth (Fig. 9A, left). Using a genetically engineered mouse model for Kras driven lung cancer, we find that in the absence of this mechanism tumorigenesis is blocked.

Our previous studies on EGF stimulation of shDHH20 cells showed that without EGF stimulation there is high basal Erk phosphorylation and increased AKT is dependent on ligand stimulation. EGF stimulation also increases EGFR palmitoylation at C1025, but phosphorylation at Y1068, the main Grb2 binding site that mediates MAPK signaling is reduced considerably when C1025 is palmitoylated (6). This suggests EGF stimulation mediated EGFR palmitoylation at C1025 antagonizes MAPK signaling. The studies presented here examine the consequence of losing EGFR palmitoylation in either a wild type or oncogenic KRAS setting. In a wild type KRAS setting there is an increase in KRAS at the membrane upon expression of EGFR<sup>C1025A</sup>, but the rapid cycling of KRAS activity allows association of the PI3K complex at the membrane. However, in the mutant KRAS setting, KRAS is locked in the active GTP bound state, therefore when EGFR is not palmitoylated there is constitutive binding of Grb2, and hyperactivation of the KRAS/MAPK pathway downstream. Under these conditions, PI3K is unable to interact with EGFR to form a stable signaling complex and the PI3K/AKT signaling cascade is impeded. As a result, GSK3 $\beta$  is active and promotes rapid degradation of Myc leading to a loss of pro-proliferation signals and attenuation of cancer cell growth (Fig. 9A, right).

Recent studies show that cancer cells are dependent on signaling mechanisms for undergoing oncogenic transformation that are dispensable in normal cells (5). For example, mutations in the Ras binding domain of PIK3CA have no discernible effects on mouse development or cell homeostasis but this mutation reduces oncogenic KRAS driven tumor formation and maintenance through a loss of PI3K signaling (5). This demonstrates that oncogenic KRAS requires interaction with PIK3CA for downstream signaling to MAPK and PI3K to initiate tumorigenesis. We find a similar requirement for EGFR palmitoylation to maintain PI3K signaling during KRAS driven tumorigenesis since expressing EGFR<sup>C1025A</sup> has no effect on Myc expression in cells with wild type KRAS. Additionally, our previous studies showed that although knockdown of DHHC20 reduces cell proliferation of the breast cancer cell line MDA-MB-231, knockdown of DHHC20 has no effect on the growth of the normal breast epithelial cell line MCF10A (7).

The growth defect in the shDHHC20 cells is restored by shEGFR indicating unpalmitoylated EGFR is itself inhibitory in the presence of oncogenic KRAS. In general, the mechanism of PI3K activation by EGFR is unclear as EGFR lacks the canonical PI3K binding motif (pYXXM) present in other receptor tyrosine kinases and it has been proposed another adaptor like Gab1 mediates PI3K signaling by EGFR (18). We propose an alternative mechanism where cells expressing EGFR may be dependent on DHHC20 mediated palmitoylation to sustain PI3K signaling in the presence of oncogenic KRAS.

Our findings show that reducing DHHC20 levels blocks tumor formation in a KRAS-mutant GEMM and arrests growth of existing human KRAS-mutant tumors. One would predict that low DHHC20 levels in KRAS-mutant NSCLC tumors would predict improved prognosis of survival of patients. Our experimental data is validated by the

analysis of large lung adenocarcinoma patient datasets revealing a strong correlation between low DHHC20 expression and improved probability of survival (Supplemental Fig. 3A) (19). This clinical impact is strengthened by the improved efficacy of pan-PI3K inhibitor, Buparlisib, induced by DHHC20 inhibition. Buparlisib monotherapy has resulted in modest efficacy in the clinic so far, thereby, the focus of clinical trials rests in combination therapy. These findings reveal DHHC20, an enzyme, as a susceptible drug target for use in combination with clinically available PI3K inhibitors as a strategy for targeted treatment of KRAS-driven adenocarcinoma.



## A. Model

## Figure 8

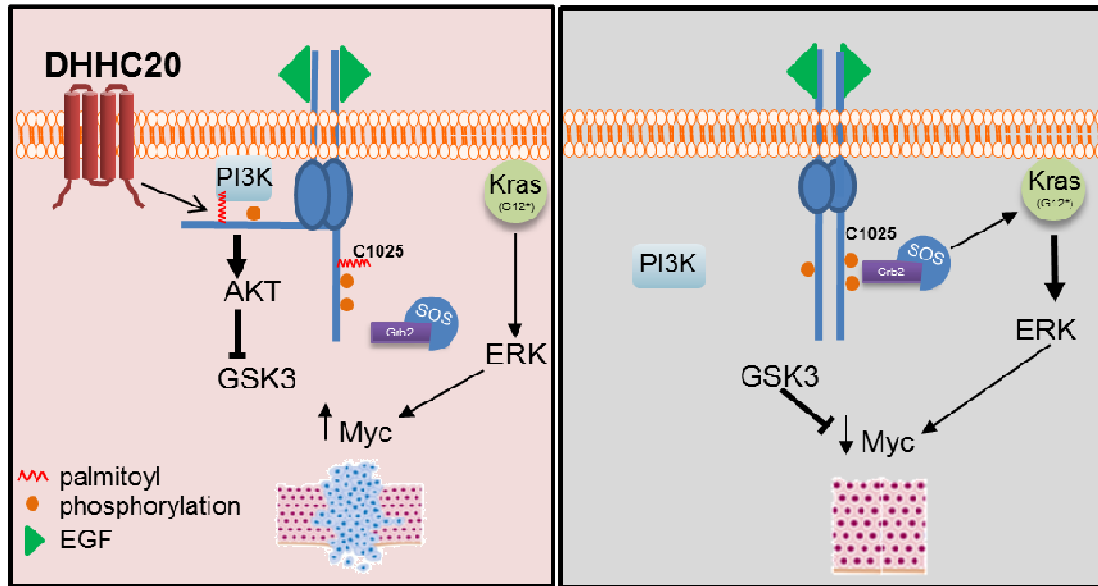
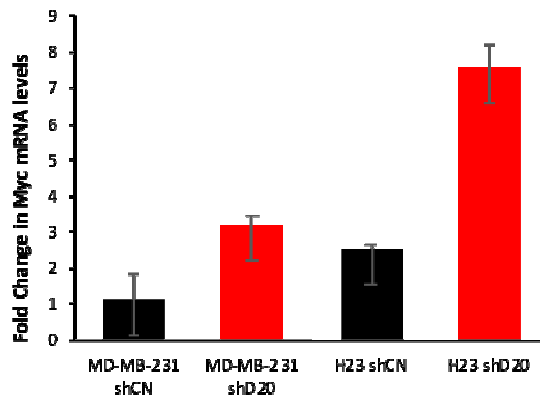


### Figure 8. Mechanistic Model

A. Model: EGFR palmitoylation (Left) promotes PI3K/AKT signaling leading to stable Myc production and cell proliferation. Loss of EGFR palmitoylation (Right) promotes binding of Grb2-SOS leading to hyperactivation of KRAS/MAPK, but impedes PI3K/AKT signaling, causing Myc depletion and reduced cell proliferation.

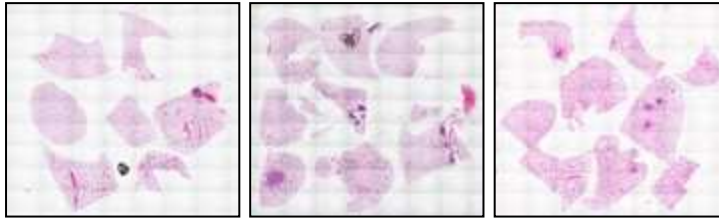
## Supplemental Figure 1

**A.**



**B.**

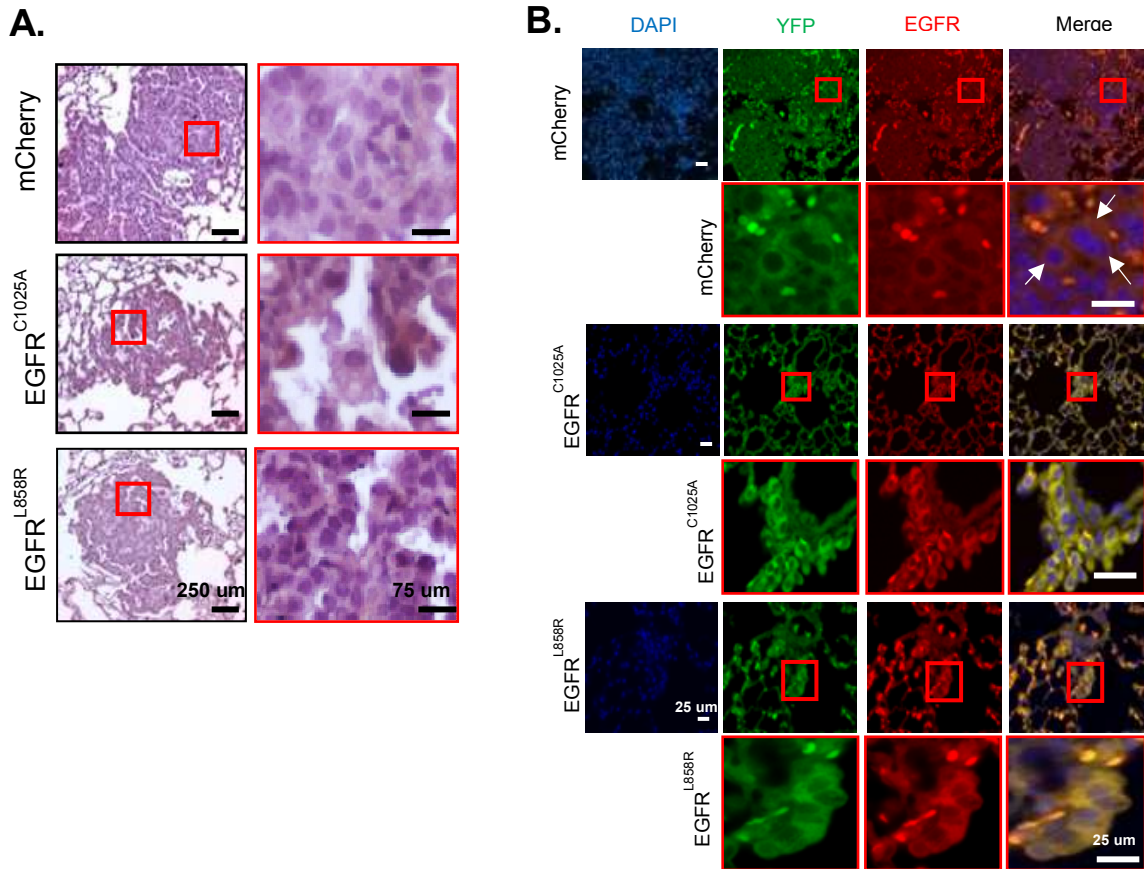
crDHH20#1 at 24 weeks post-infection



### Supplemental Figure 1.

**A.** Fold change in Myc mRNA levels in MDA-MB-231 and H23 shCon versus shDHH20 (shD20) cells. Graph represents average calculated fold change  $\pm$  s.d of 6 replicates. **B.** Hematoxylin and Eosin (H&E) 4X stitched images of 3 sgDHH20#1 mice lungs 24 weeks post-infection. Tumour burden does not increase after 24 weeks. Control mice had to be sacrificed at 13 weeks due to extensive tumour burden.

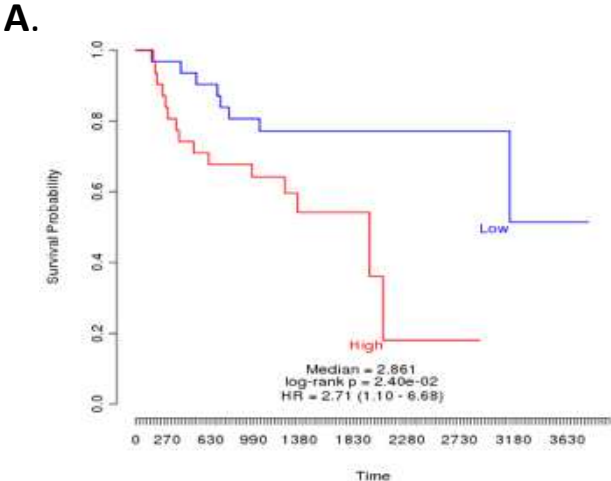
## Supplemental Figure 2



### Supplemental Figure 2.

**A.** IHC images of lungs stained for EGFR from KPY mice 13 weeks following Lenti-pCreator-Cre infection. Representative images mCherry (top), EGFR<sup>C1025A</sup> (middle) and EGFR<sup>L858R</sup> (bottom) at 10X magnification. Red square shows 20X magnification image of indicated region. **B.** mCherry, EGFR<sup>C1025A</sup> and EGFR<sup>L858R</sup> cohort tissue sections were stained for YFP (green), EGFR (red) and DAPI (blue). Red square shows 20X magnification image of indicated region.

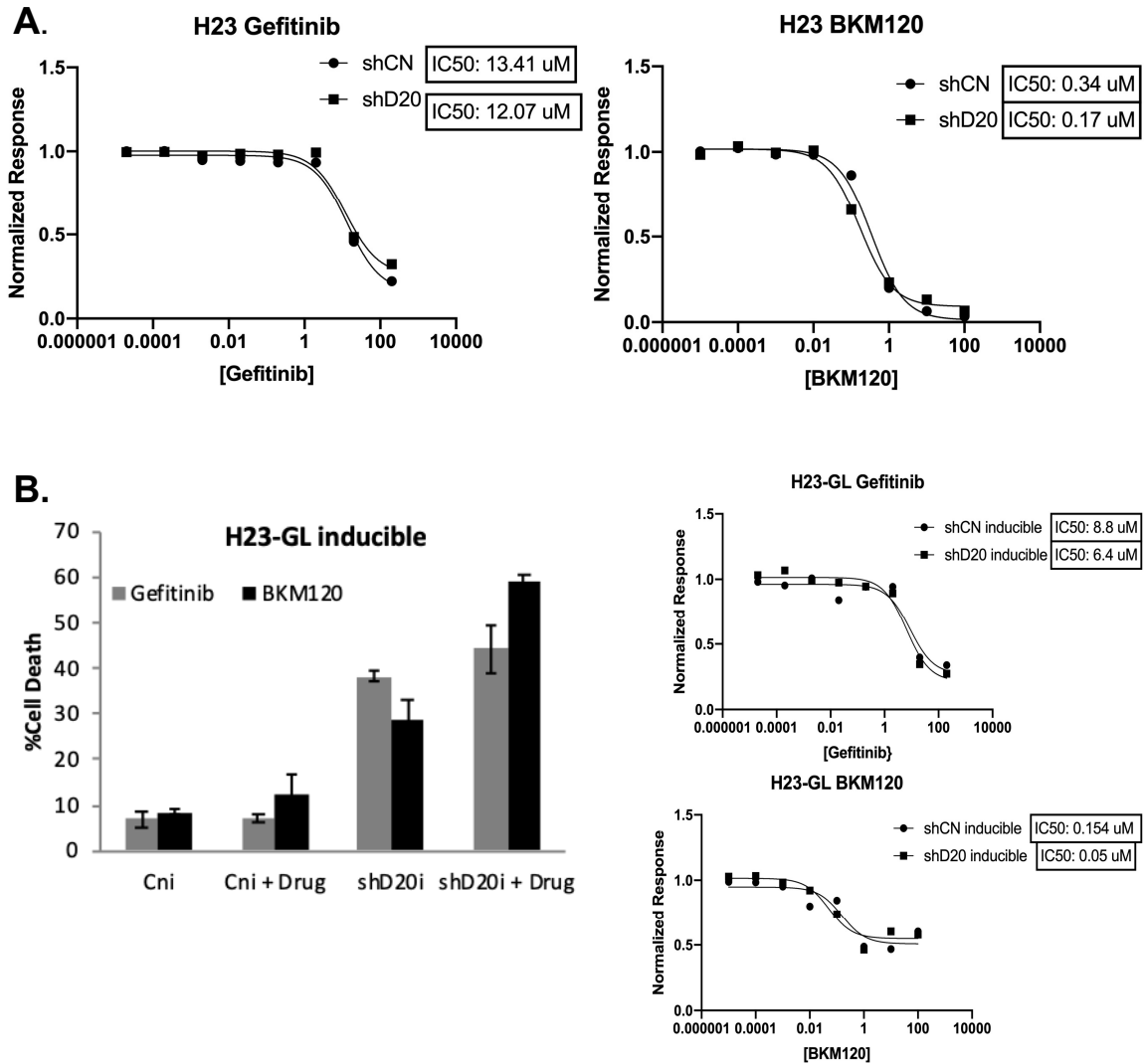
Supplemental Figure 3



**Supplemental Figure 3.**

**A.** Representative KM plot for survival probability of low vs. high DHHC20 expression from triple-negative breast cancer (TNBC) patients. Meta-Z Score = 2.03 from 16 different data sets. **B.** Representative KM plot for survival probability of low vs. high DHHC20 expression from lung adenocarcinoma. Meta-Z Score = 3.03 from 16 different data sets.

## Supplemental Figure 4



**Supplemental Figure 4. A.** Dose-response curves for H23 shCN and shDHHC20 treated with either Gefitinib or BKM120 at various doses for 72 h (n=3) to determine IC50 differences. **B.** Gefitinib (5  $\mu$ M) (gray) and BKM120 (500 nM) (black) treatment increases cytotoxicity in inducibly silenced H23-GL cells (mean  $\pm$  StDev). Dose-response curves H23-GL with inducible shRNA against a control scrambled sequence (shCN) and shD20 cells treated with either Gefitinib or BKM120 at various doses for 72 h (n=3) to determine IC50 differences.

## Materials and Methods

### Cell culture

MDA-MB-231 and NIH3T3 cells (ATCC) were cultured in DMEM containing 10% FBS. H23 and SW1573 cells (ATCC) were maintained in RPMI supplemented with 10% FBS. GSK3 $\beta$  inhibitor (CHIR-99021), Gefitinib, and BKM120 was purchased at Selleck Chemicals. 2-Bromopalmitate (2-BP) was purchased at Sigma Aldrich.

### Silencing of Human DHHC20

The oligonucleotides for shControl and shDHHC20 constructs were synthesized (Integrated DNA Technologies) and inserted into the pLKO.1 vector. shControl encodes the non-targeting sequence of SHC002 (Sigma); the shRNA target sequence of human DHHC20 is 50-GAGCTCTGCGTGTTTACTATT-30. MDA-MB-231 and H23 cells were transduced with lentivirus encoding shControl or shDHHC20 and selected by puromycin treatment (1 mg/ml) for several passages.

### Plasmids and Generation of Stable Cell Lines

Human mutant Myc<sup>T58A</sup> from pLV-tetO with an HA tag (Addgene plasmid #19763) (20) was gateway cloned into the pLX304 backbone with a blasticidin resistance marker and V5 tag (Addgene). Lentivirus of pLX305-MycT58A was generated using HEK293T cells with Gag, VSVG and Rev plasmids using TransIT-LT1 (Mirus) according to manufacturer's instructions. H23 cells that were transduced with lentivirus encoding shControl or shDHHC20 and selected by puromycin treatment were subsequently infected with MycT58A-V5. H23 shControl or shDHHC20 and Lenti-pLX304-MycT58A were selected with puromycin (1  $\mu$ g/ml) and blasticidin (10  $\mu$ g/ml) together for several passages. To generate inducible cell lines, wildtype EGFR and EGFR<sup>C1025A</sup> cDNA was

first subcloned into the inducible pTRIPZ backbone with a puromycin resistance marker and FLAG tag. Empty pTRIPZ, which expresses the rtTA3, puromycin resistance marker, and FLAG tag was used as a negative control. Virus production was performed by transfecting HEK293T cells with the pTRIPZ constructs, psPAX2 and pMD2.G plasmids (Addgene) using TransIT-LT1 (Mirus) according to the manufacturer's instructions. MDA-MB-231 and NIH3T3 were infected with pTRIPZ virus using polybrene and incubated for 24 hours. Post-infection, fresh media was added on infected cells and incubated for an additional 48 hours before selection. Cells infected with the pTRIPZ constructs were selected with 1 µg/ml puromycin for several passages. Expression of EGFR cDNA was induced with 1 µg/ml doxycycline overnight before proceeding with experiments. Lentivirus of human KRAS4B(WT) or mutant KRAS4B(G12V) in pLenti-PGK-hygromycin resistance with an HA tag (Addgene plasmid #35633) (20) was generated using HEK293T cells with Gag, VSVG and Rev plasmids using TransIT-LT1 (Mirus) according to manufacturer's instructions. NIH3T3 cells infected with pTRIPZ constructs and selected with puromycin were subsequently infected with KRAS4B(WT)-HA or KRAS4B(G12V)-HA. NIH3T3 pTRIPZ-plenti-KRAS4B (WT) or (G12V) cells were selected with puromycin (1 µg/ml) and hygromycin (500 µg/ml) together for several passages. Lentivirus of human mutant PI3KCA-E545K in pcw107-PGK-puromycin resistance (Addgene plasmid #64605) (21) generated using HEK293T cells with Gag, VSVG and Rev plasmids using TransIT-LT1 (Mirus) according to manufacturer's instructions. NIH3T3 cells infected with pTRIPZ constructs and selected with puromycin were subsequently infected with PI3KCA-E545K.

### **Immunoblot analysis**

Cell lysates were prepared in 1% Triton-X-100 buffer, including Tris-HCl (pH 7.5) and sodium chloride solution (NaCl). Lysates were analyzed by immunoblotting with the following antibodies: Anti-DHHC20 (HPA014702) antibody was purchased from Sigma-Aldrich. Anti-EGFR-XP, pERK, ERK, pS473-AKT, pT308-AKT, AKT, pGSK3 $\beta$ (Ser9), GSK3 $\beta$ , PI3K(p110 $\alpha$ ), PIK3R1 (p85), Ras,  $\beta$ -catenin and  $\beta$ -actin were obtained from Cell Signaling Technologies. Anti-Myc and  $\alpha$ -tubulin were purchased from Santa Cruz. Immune complexes were detected with horseradish peroxidase-conjugated secondary antibodies and enhanced chemiluminescence (ECL) (Thermo Scientific).

### **Membrane Fractionation**

Cell lysates were prepared in hypotonic lysis buffer including Tris-HCl (pH 8), magnesium chloride (MgCl<sub>2</sub>), potassium chloride (KCl) and dithiothreitol (DTT). Lysates were disrupted using passage through 25-gauge needle. Lysates were subject to centrifugation at 800 xg for 10 min at 4C to pellet nuclei. The resulting supernatant was then subject to centrifugation with a tabletop ultracentrifuge at 42000 rpm for 1 hour at 4C. The resulting supernatant was kept as the cytosolic fraction and pellet contained the membrane fraction. Membrane fraction was resuspended in 1% NP-40 lysis buffer including Tris-HCl (pH 8), sodium chloride (NaCl), sodium dodecyl sulfate (SDS) and glycerol. Sample loading buffer was added to the membrane samples and the samples were boiled for 8 minutes followed by western analysis and immunoblotting.

### **Drug Proliferation Assays**

Cells were plated in a solid white 96-well plate at 5000 cells per well in 90  $\mu$ l of 10% FBS RPMI media. Serial dilutions of gefitinib and BKM120 were made in media and 10  $\mu$ l of



the diluted compounds were transferred to the cells. After 72 hours, cell viability was measured by CellTiter-Glo (Promega) according to manufacturer's instructions. Luminescent readout was normalized to DMSO-treated control cells and empty wells. Data was analyzed by nonlinear regression curve fitting on Prism 8 and IC50 values were reported.

### **Myc qPCR**

Total RNA was isolated using the RNeasy Extraction Kit (Quiagen). To quantify Myc expression levels, equal amounts of cDNA were synthesized using the SuperScript™ III First-Strand Synthesis System (Invitrogen) and mixed with the Power SYBR Green PCR master mix (Applied Biosystems, Carlsbad, CA) and 5 pmol of both forward and reverse primers. GAPDH was amplified as an internal control.

### **Primers pairs used for qPCR**

The sequences of the human primers used for qPCR, listed from 5' to 3', were:

Gene	Forward and reverse primers' sequence
------	---------------------------------------

---

MYC	CCTACCCTCTCAACGACAGC	CTCTGACCTTTTGCCAGGAG
-----	----------------------	----------------------

B-Actin	AATCTGGCACCACACCTTCTAC	ATAGCACAGCCTGGATAGCAAC
---------	------------------------	------------------------

---

### **Peptide streptavidin pull-down**

Cell lysates were made as described above. Lysates were incubated with various concentrations of biotinylated scrambled-palmitoylated, unpalmitoyled C1025 containing EGFR C-terminal tail, and palmitoylated C1025 containing EGFR C-terminal tail peptides dissolved in DMSO overnight at 4 degrees Celsius. The streptavidin agarose beads

(Thermo Scientific) were washed three times with aforementioned lysis buffer. Lysates with peptides were incubated with 20 $\mu$ l of the prewashed streptavidin agarose beads for 2 hours at 4 degrees Celsius with rotation. The beads-lysate-peptide mix was spun down at 6000 x g for 1 minute. The beads were washed 3 times with cold lysis buffer. Loading sample buffer containing  $\beta$ -mercaptoethanol was added to beads and the beads were then boiled for 10 minutes at 100 degrees Celsius. The boiled sample was centrifuged at 16000 x g for 1 minute and supernatant was collected for western blotting.

### **Vector design and production**

LentiCRISPRv2Cre is described in D. Walter et al. *Can. Res.*, 2017 (10) and is available from Addgene (#82415). DHHC20 sgRNAs were designed to target exons in the first one-third of the gene using the CRISPR Design Tool (<http://crispr.mit.edu/about>) to minimize off-target effects in the mouse genome. DHHC20 sgRNAs were cloned into LentiCRISPRv2Cre vector by Golden Gate assembly using BsmBI (New England Biolabs R0580S). The sgRNAs used for targeting Cas9 are: DHHC20 1, 5'-CACCGAGTACGTGGAACCTTTGCGCTGTTT-3' and DHHC20 2, 5'-CACCGGCGCTGCTGCCAACGCGTGGGTTT-3'. The sensor assay reporter was generated by synthesizing sgRNA targets in series and cloning them upstream of mCherry in the pCHK-mCherry vector using Gibson assembly as discussed in D. Walter et al. *Can. Res.*, 2017. (10) pCreatorBsmBI was constructed by synthesis of a gene block encoding a KpnI cloning site, the eukaryotic elongation factor short promoter (EFS) followed by a 2xBsmBI golden gate cloning site, P2a peptide sequence, and CreNLS. The fragment was obtained from Genescript and cloned into pUC57mini vector. The KpnI-ClaI fragment of the gene block was subsequently subcloned into the vector backbone portion of a KpnI-ClaI digested pLentiCRISPRv2Cre to create pCreatorBsmBI.

mCherry and EGFR mutants were PCR amplified with primers containing BsmBI tails and appropriate restriction sequences for Golden Gate cloning such that the 5' (left) overhang is 5'-CACC-3', and the 3' (right) overhang is 5'-ATCC-3' after BsmBI digest.

### **Lentivirus production**

HEK293 FT cells were transfected with LentiCRISPRv2Cre or pCreator EGFR WT, C1025A, L858R, and  $\Delta 8.2$ , and VSV-G plasmids in a 4:3:1 ratio using polyethylenimine. Twenty-four hours after transfection, the media were replaced with fresh DMEM supplemented with 25 mmol/L HEPES (Gibco 15630-080) and 3 mmol/L caffeine (Sigma C0750). Lentivirus-containing supernatant was collected from the cells at 48 and 72 hours following transfection, filtered through 0.45- $\mu$ m filters (Thermo Scientific 723-2545), and centrifuged at 107,000  $\times$ g. The viral pellet was soaked in 100- $\mu$ L PBS for 16 hours at 4°C, triturated, vortexed for 15 minutes at 4°C, and finally centrifuged at 16,000  $\times$  g for 30 seconds to remove insoluble debris. Lentivirus was then aliquoted and frozen at -80°C for later use. Lentivirus was titered on Green-Go cells, an NIH3T3 derivative harboring an integrated Cre-dependent GFP reporter. These cells are validated for reporter activity by flow cytometry during viral titration. A total of  $2 \times 10^5$  cells were plated in 6-well plates, and 24 hours later lentivirus was added at 10, 1, and 0.1  $\mu$ L per well. Cells were analyzed by flow cytometry for GFP expression 48 hours following infection, and viral titer was calculated accordingly.

### **Animal work**

*KRAS*<sup>LSL-G12D</sup>, *p53*<sup>flox/flox</sup>, *Rosa26*<sup>LSL-YFP</sup> (KPY) mice are maintained on a mixed C567B6/129Sv4 background and were treated as previously described (22). Mice were given lentivirus at  $6 \times 10^4$  pfu per mouse by intratracheal intubation at 6–10 weeks of age as described previously (23). Mouse lungs were harvested at 12 weeks.

## **Histologic analysis**

Tumor number was counted on hematoxylin and eosin–stained slides. Tumor area was quantified using ImageJ software. Tumor burden percentage was calculated as tumor area over total lung area multiplied by 100.

## **Immunohistochemistry (IHC) and Immunofluorescence (IF)**

Mouse tissues were fixed in 10% neutral buffered formalin (Fisher Scientific 23-245-685) for 16 hours and dehydrated in a series of ethanol washes up to 100%. Samples were paraffin embedded and sectioned at 4- $\mu$ m thickness. For IHC, slides were deparaffinized in xylene and rehydrated with a series of ethanol washes. Antigen retrieval was performed using citrate buffer (Electron Microscopy Sciences 62706-10) and slides were stained using antibodies against GFP that cross-react with YFP (1:200, Abcam), pERK (1:500, CST) and EGFR-XP (1:200, CST). Primary antibody was incubated on slides for 16 hours at 4°C, and biotinylated secondary antibody (Vector Laboratories) was incubated at room temperature for 1 hour. ABC reagent and ImmPACT DAB were prepared as directed (Vector Laboratories PK-4001 and SK-4105). Slides were analyzed on a Leica DMI6000B inverted microscope. For IF, slides were again deparaffinized in xylene and rehydrated with a series of ethanol washes. Antigen retrieval was performed using citrate buffer (Electron Microscopy Sciences 62706-10) and slides were stained using antibodies against GFP (1:200, Abcam), Ki67 (1:200, Abcam) and EGFR-XP (1:200, CST) and counterstained with DAPI using Fluoro-Gel II with DAPI (EMS Catalog #17985-50). Detection was by Alexa 488nm or Alexa 594nm conjugated secondary antibodies (Molecular Probes, Eugene, OR). Slides were analyzed on a Leica DMI6000B inverted microscope.

## **NSCLC Xenografts**

Four- to 6 week SCID beige mice (CB17.Cg-Prkdc<sup>scid</sup>Lyst<sup>bg-J</sup>/CrI) purchased from Charles River were injected subcutaneously with  $5 \times 10^6$  cells in 1:1 solution with matrigel in both flanks. Mice with established A549-GFP-Luciferase tumors ( $100\text{mm}^3$ ) were treated intraperitoneally each day with doxocycline (20 mcg in 0.5 cc water) to induce expression of shRNA targeting either a control scramble sequence or DHHC20. Tumors were measured on day -2, 0, 5, and 8 using in vivo bioluminescent imaging. To image, mice were anesthetized and intraperitoneally injected with D-Luciferin (GoldBio LUCNA-1G) in PBS at 150mg/kg. Luminescent signals were acquired 15 minutes post-injection with the IVIS Spectrum (Caliper Life Sciences). Analysis was done using Living Image 4.5 (Perkin Elmer).

## **Statistics**

Statistical analyses were performed using Prism software version 7.0 (GraphPad). Experiments are reported as mean  $\pm$  SD or SEM as noted in the legends. Data were analyzed using a 2-tailed Student's t-test for comparison between 2 data sets. Multiple comparisons were analyzed by 1-way ANOVA and 2-way ANOVA, followed by Tukey's multiple-comparison correction. A P-value of less than 0.05 was considered statistically significant.

## **Study Approval**

All experiments involving live animals were performed in compliance with the guidelines set forth in the Public Health Service Policy on the Humane Care and Use of Laboratory Animals. Mice were housed in a pathogen-free facility at the American Association for Laboratory Animal Science–accredited Animal Facility at the University of Pennsylvania

Perelman School of Medicine. All studies were performed under protocols approved by the Institutional Animal Care and Use Committee (IACUC) at the University of Pennsylvania Perelman School of Medicine (#804774).

## References

1. Cancer Genome Atlas Research Network. Comprehensive molecular profiling of lung adenocarcinoma. *Nature*. **511**, 543–550 (2014).
2. Westcott PM, Halliwill KD, To MD, Rashid M, Rust AG, Keane TM, Delrosario R, Jen KY, Gurley KE, Kemp CJ, Fredlund E, Quigley DA, Adams DJ and Balmain A. The mutational landscapes of genetic and chemical models of KRAS-driven lung cancer. *Nature*. **517**, 489–492(2015).
3. Jemal A, Siegel R, Ward E, Hao Y, Xu J, Murray T and Thun MJ. Cancer statistics. *CA Cancer J Clin*. **2**, 71 (2008).
4. Seshacharyulu P, Ponnusamy MP, Haridas D, Jain M, Ganti AK, and Batra SK. Targeting the EGFR signaling pathway in cancer therapy. *Expert Opin Ther Targets*. **16**, 15-31 (2012).
5. Castellano E, Sheridan C, Thin M Z, Nye E, Spencer-Dene B, Diefenbacher ME, Moore C, Kumar MS, Murillo MM, Grönroos E, Lassailly F, Stamp G and Downward J. (2013). Requirement for interaction of PI3-kinase p110 $\alpha$  with RAS in lung tumor maintenance. *Can Cell*. **24(5)**, 617-630 (2013).
6. Runkle KB, Kharbanda A, Stypulkowski E, Cao XJ, Wang W, Garcia BA and Witze ES. Inhibition of DHHC20-Mediated EGFR Palmitoylation Creates a Dependence on EGFR Signaling. *Mol Cell*. **62**, 385-396 (2016).
7. Kharbanda A, Runkle KB, Wang W and Witze ES. Induced sensitivity to EGFR inhibitors is mediated by palmitoylated cysteine 1025 of EGFR and requires oncogenic KRAS. *Biochem Biophys Res Commun*. **493(1)**, 213-219 (2017).
8. Walter D.M., Venancio O, Buza EL, Tobias JW, Deshpande C, Gudiel AA, Kim-Kiselak C, Cicchini M, Yates TJ and Feldser DM. Systematic In Vivo Inactivation

- of Chromatin-Regulating Enzymes Identifies Setd2 as a Potent Tumour Suppressor in Lung Adenocarcinoma. *Can Res.* **77(7)**, 1719-1729 (2017).
9. Scheffler M, Bos M, Gardizi M, König K, Michels S, Fassunke J, Heydt C, Künstlinger H, Ihle M, Ueckerth F, Albus K, Serke M, Gerigk U, Schulte W, Töpelt K, Nogova L, Zander T, Engel-Riedel W, Stoelben E, Ko YD, Randerath W, Kaminsky B, Panse J, Becker C, Hellmich M, Merkelbach-Bruse S, Heukamp LC, Büttner R and Wolf J. *PIK3CA* mutations in non-small cell lung cancer (NSCLC): Genetic heterogeneity, prognostic impact and incidence of prior malignancies. *Oncotarget.* **6(2)**, 1315-1326 (2015).
  10. Walter D.M., Venancio O, Buza EL, Tobias JW, Deshpande C, Gudiel AA, Kim-Kiselak C, Cicchini M, Yates TJ and Feldser DM. Systematic In Vivo Inactivation of Chromatin-Regulating Enzymes Identifies Setd2 as a Potent Tumour Suppressor in Lung Adenocarcinoma. *Can Res.* **77(7)**, 1719-1729 (2017).
  11. Ambrogio, C., Barbacid, M. and Santamaria, D. In vivo oncogenic conflict triggered by co-existing KRAS and EGFR activating mutations in lung adenocarcinoma. *Oncogene.* **36(16)**, 2309-2318 (2017).
  12. Unni, AM, Lockwood WW, Zejnullahu K, Lee-Lin SQ and Varmus H. Evidence that synthetic lethality underlies the mutual exclusivity of oncogenic KRAS and EGFR mutations in lung adenocarcinoma. *Elife* (2015).
  13. Alessi, DR, Andjelkovic M, Caudwell B, Cron P, Morrice N, Cohen P, and Hemmings BA. Mechanism of activation of protein kinase B by insulin and IGF-1. *EMBO.* **23**, 6541-6551 (1996).
  14. Gregory MA, Qi Y and Hann SR. Phosphorylation by glycogen synthase kinase-3 controls c-myc proteolysis and subnuclear localization. *J Biol Chem.* **278(51)**, 51606-51612 (2003).



15. Okudela K. et al. PIK3CA mutation and amplification in human lung cancer. *Pathol Int.* **57**, 664–671 (2007).
16. Hollestelle A, Elstrodt F, Nagel JH, Kallemeijn WW, and Schutte M. Phosphatidylinositol-3-OH kinase or RAS pathway mutations in human breast cancer cell lines. *Mol Cancer Res.* **5**, 195–201 (2007).
17. Scheffler M, Bos M, Gardizi M, König K, Michels S, Fassunke J, Heydt C, Künstlinger H, Ihle M, Ueckerth F, Albus K, Serke M, Gerigk U, Schulte W, Töpelt K, Nogova L, Zander T, Engel-Riedel W, Stoelben E, Ko YD, Randerath W, Kaminsky B, Panse J, Becker C, Hellmich M, Merkelbach-Bruse S, Heukamp LC, Büttner R and Wolf J. *PIK3CA* mutations in non-small cell lung cancer (NSCLC): Genetic heterogeneity, prognostic impact and incidence of prior malignancies. *Oncotarget.* **6(2)**, 1315-1326 (2015).
18. Mattoon DR, Lamothe B, Lax I and Schlessinger J. The docking protein Gab1 is the primary mediator of EGF-stimulated activation of the PI-3K/Akt cell survival pathway. *BMC Biol.* **2**, 24 (2004).
19. Gentles A., Newman AM, Liu CL, Bratman SV, Feng W, Kim D, Nair VS, Xu Y, Khuong A, Hoang CD, Diehn M, West RB, Plevritis SK, and Alizadeh AA. The prognostic landscape of genes and infiltrating immune cells across human cancers. *Nat Med.* **21**, 938-945 (2015).
20. Stadfield M, Maherali N, Breault DT, and Hochedlinger K. Defining molecular cornerstones during fibroblast to iPS cell reprogramming in mouse. *Cell Stem Cell.* **2(3)**, 230-240 (2008).
21. Martz CA, Ottina KA, Singleton KR, Jasper JS, Wardell SE, Peraza-Penton A, Anderson GR, Winter PS, Wang T, Alley HM, Kwong LN, Cooper ZA, Tetzlaff M, Chen PL, Rathmell JC, Flaherty KT, Wargo JA, McDonnell DP, Sabatini DM, and

Wood KC. Systematic identification of signaling pathways with potential to confer anticancer drug resistance. *Sci Signal.* **7(357)**, (2014).

22. Jackson EL, Olive KP, Tuveson DA, Bronson R, Crowley D, Brown M and Jacks T. The differential effects of mutant p53 alleles on advanced murine lung cancer. *Cancer Res.* **65**, 10280–10288 (2005).

23. DuPage M., Dooley AL and Jacks T. Conditional mouse lung cancer models using adenoviral or lentiviral delivery of Cre recombinase. *Nat Protoc.* **4**, 1064–1072 (2009).

## CHAPTER 5: DISCUSSION

### Overview

The origins of this thesis lie in our discovery that the receptor tyrosine kinase, EGFR, is palmitoylated on the C-terminal tail which was discovered in a breast cancer cell line overexpressing EGFR and, to some extent, overexpressing the palmitoyltransferase, DHHC20. From this initial discovery rose the overarching question: what is the regulatory role of EGFR palmitoylation in tumorigenesis? Upon study, the research question became: what is the mechanism by which loss of EGFR palmitoylation hinders tumorigenesis, specifically KRAS-driven tumorigenesis? Into this set of questions, we tried to incorporate one of the main drivers of cancer research: can EGFR palmitoylation be manipulated to develop a new therapeutic strategy?

EGFR palmitoylation occurs at three critical cysteines, Cys1025, Cys1034 and Cys1122, on the C-terminal tail. We have determined that palmitoylation of the C-terminal tail inhibits receptor activity, perhaps as a negative feedback mechanism or as mitigation of access activity upon ligand binding. Upon the loss of palmitoylation, EGFR is activated with or without EGF stimulation indicating that palmitoylation is an activity suppressant. Mutation of Cys1025 and Cys1122 alone or in combination increases the phosphorylation and thereby activity of EGFR. Loss of EGFR palmitoylation at Cys1122 exhibited increased presence of EGFR at the membrane, sustained phosphorylation of EGFR in response to EGF, and endocytotic dysregulation indicating that palmitoylation at Cys1122 is involved in promoting receptor turnover. However, mutation of Cys1025 significantly increases the binding of the adapter protein, Grb2, to EGFR, leading to the RAS/MAPK pathway. Thereby, we focused our energy towards understanding the signaling mechanism in the presence of the Cys1025 mutation (EGFR<sup>C1025A</sup>).

These results specifically showed that the EGFR<sup>C1025A</sup> and EGFR<sup>C1122A</sup> mutation alone or in combination increase the phosphorylation of EGFR and subsequently ERK, and one particular phosphorylation site of AKT (Ser473). However, upon further inspection, we discovered that the Thr308 phosphorylation of AKT, directly downstream of PI3K, decreases upon expression of the EGFR<sup>C1025A</sup> mutation. Therefore, we found that loss of EGFR palmitoylation in a mutant KRAS setting specifically leads to an increase in the MAPK signaling cascade, but also a significant decrease in PI3K/AKT signaling. With further study, we discovered that due to this decreased PI3K/AKT signaling, GSK3 $\beta$  remains active and promotes rapid degradation of Myc, the critical cell proliferation associated transcription factor. Now we understand mechanistically why loss of EGFR palmitoylation leads to disrupted cell growth; the degradation of Myc leads to a loss of pro-proliferative transcription and subsequent loss of cancer cell growth. Structurally, we found that the regulatory subunit of PI3K (p85) specifically associates with palmitoylated EGFR and p85 is required to be in the vicinity of the membrane to interact with catalytic subunit of PI3K, p110 $\alpha$ . Thereby, on the loss of EGFR palmitoylation in a mutant KRAS setting, PI3K is unable to form a stable signaling complex at the membrane in the vicinity of EGFR, but there is constitutive binding of Grb2 to EGFR and hyperactivation of the KRAS/MAPK pathway. We speculate that KRAS mutant cancer cells require balanced activity of both the MAPK and PI3K cascade to proliferate through Myc stabilization. Moderate disruption of PI3K signaling from loss of EGFR palmitoylation leads to a significant growth defect of tumor cells. We hypothesized that further inhibition of the remaining PI3K activity would kill the cancer cells. As such, we found that inhibiting DHHC20 with either stable knockdown or acute inducible knockdown in mutant KRAS cells induced sensitivity to the clinically used PI3K inhibitor, BKM120. Finally, we showed that DHHC20 ablation or expression of

EGFR<sup>C1025A</sup> in a mutant KRAS-driven mouse model blocks tumorigenesis. This correlation is consistent with our findings that DHHC20 ablation in KRAS driven mouse model drastically blocks tumorigenesis. These findings reveal that loss of EGFR palmitoylation from inhibition of DHHC20 makes the untreatable KRAS-driven adenocarcinoma susceptible to treatment with a clinically available inhibitor against PI3K, such as BKM120.

Additional data suggests that DHHC20 inhibition may make KRAS-driven adenocarcinoma susceptible to EGFR inhibition as well as PI3K inhibition. We found that inhibition of DHHC20 or expression of the EGFR<sup>C1025A</sup> point mutant leads to increased sensitivity to gefitinib-induced cell death in the KRAS mutant MDA-MB-231 cells. Gefitinib is a potent TKI and functionally, blocks EGFR kinase activity by binding to the ATP binding site. Currently, the alterations in EGFR signaling that lead to increased or decreased sensitivity to gefitinib is still not entirely clear. Inhibition of DHHC20 in wildtype KRAS MCF-7 and non-transformed MCF-10a cells had no effect on gefitinib sensitivity. This result prompted the question: is this phenotype of increased gefitinib sensitivity upon loss of EGFR palmitoylation dependent on the presence of mutant KRAS? In addressing this question, we discovered that expression of the palmitoylation-resistant EGFR<sup>C1025A</sup> mutant in NIH3T3 cells leads to increased sensitivity to gefitinib-induced cell death, but only in the presence of oncogenic KRAS<sup>G12V</sup>, whereas expression of mutant PI3KCA did not change the sensitivity to gefitinib. This suggests that the phenotype of increased gefitinib sensitivity when EGFR palmitoylation is lost is dependent on the presence of specifically mutant KRAS. We were unable to determine the mechanism by which loss of EGFR palmitoylation is causing sensitivity to gefitinib and why this requires the presence of mutant KRAS. As we previously observed, inhibition of DHHC20 or expression of EGFR<sup>C1025A</sup> activates the receptor and further

increases MAPK signaling that is already high due to the presence of mutant KRAS. Thereby, inhibition of DHHC20 or loss of EGFR palmitoylation may be making KRAS mutant cells dependent on EGFR signaling and this may be one reason for the increased gefitinib sensitivity. The cells now dependent on EGFR signaling and artificially high levels of MAPK signaling could be sensitive to an EGFR inhibitor, such as gefitinib, that is inhibiting MAPK levels causing the cells to crisis and die. However, we did not observe a decrease in MAPK levels upon gefitinib treatment suggesting that the increased sensitivity is not due to the cells newfound dependency on EGFR signaling.

More intriguingly, we found that cells harboring both the EGFR activating L858R and drug resistant T790M mutant, H1975 cells, exhibit a synergistic effect when treated with gefitinib and 2-bromopalmitate (2-BP). 2-BP is a palmitate analogue that has the ability to block palmitoyltransferases by competing out the palmitic acid. Although sufficient to inhibit DHHC enzymes, 2-BP is not specific to DHHC20 and requires high doses to cause an effect. The EGFR<sup>L858R</sup> mutation is uniquely sensitive to gefitinib, but upon prolonged treatment, the cells acquire the secondary EGFR<sup>T790M</sup> mutation, aptly named the gatekeeper mutation, which is strongly resistant to gefitinib. Therefore, inhibition of DHHC20 is resensitizing gefitinib-resistant cells to gefitinib. However, we were unable to express EGFR<sup>C1025A</sup> in H1975 cells or express EGFR<sup>L858R/T790M</sup> in cells with the EGFR<sup>C1025A</sup> mutation due to severe toxicity. Therefore, we could not claim that the increased gefitinib sensitivity in the H1975 cells is directly dependent on the loss of EGFR palmitoylation. Our palmitoylated EGFR mass spectrometry studies also identified a potentially modified cysteine in the kinase domain, cysteine 751. However, the data acquired from the acyl-biotin exchange method followed by mass spectrometry was unclear as to if the modification was palmitoylation or another cysteine modification, such as nitrosylation, due to the complete protection of thioester linkages to

hydroxylamine (HAM) treatment at that site. Regardless, this site could regulate conformational changes based on the presence or lack of a fatty acid chain, which will in turn effect the kinase activity of the receptor. A modification at cysteine 751 could add to the conformational changes associated with the gatekeeper mutation that cause an increase in the affinity of ATP again leading to drug resistance. If the cysteine 751 is in fact palmitoylated, loss of this palmitoylation could cause the gatekeeper mutation to be ineffective leading to a return in sensitivity to gefitinib. Many future studies are required to determine how potential palmitoylation in the kinase domain effects the gatekeeper mutation or if palmitoylation of the C-terminal tail is indirectly affecting the kinase domain. However, the resensitization of a drug-resistant cell line to a tyrosine kinase inhibitor by inhibition of a palmitoyltransferase is therapeutically compelling and warrants further scientific examination.

The work described in this thesis demonstrates a novel mechanism of tyrosine kinase receptor, specifically EGFR, regulation through DHHC20-mediated palmitoylation of the C-terminal tail. Sequence analysis has identified that other receptors implicated in tumorigenesis, such as HER2 in breast cancer and FLT3 in leukemia, have critical cysteines in the C-terminal tail that could be palmitoylated. ABE analysis and metabolic labeling followed by click chemistry of HER2 and FIT3 confirm that these receptors are palmitoylated, but the critical cysteines are yet to be determined (unpublished data, Witze Laboratory). Additionally, unpublished data from the Witze Laboratory demonstrates that in fact many receptors are palmitoylated on the C-terminal tail by specific DHHC enzymes, such as insulin receptor (INSR) by DHHC19 and vascular endothelial growth factor receptor (VEGFR) by DHHC13. Furthermore, other groups have shown that DHHC13 palmitoylates melanocortin-1 receptor (MC1R) and inhibition of MC1R palmitoylation by expression of a cysteine point mutation in vivo leads to a loss

of mouse coat color and follicular degeneration **(1)**. Therefore, palmitoylation could be involved in regulating the signaling faculty of these receptors as well as EGFR. Potentially, disruption of the palmitoylation of these receptors, such as FLT3, may be detrimental to the cancers dependent on these receptors. As such, there is a necessity to further study the palmitoylation of receptors and to identify the responsible palmitoyltransferases. Furthermore, as determined, loss of palmitoylation activates EGFR, which induces synthetic lethality in the presence of mutant KRAS. Many groups are searching for targets of synthetic lethality specifically in the incurable mutant KRAS cancers. We have shown that activating EGFR is a means to induce synthetic lethality in mutant-KRAS adenocarcinoma, however, it is challenging to therapeutically activate a protein. We have also identified the enzyme responsible for palmitoylating EGFR demonstrated in this thesis to be DHHC20. We have observed that pharmacologic inhibition of DHHC20 in KRAS-driven adenocarcinoma allows therapeutic efficacy of readily available inhibitors, such as BKM120 and gefitinib. Taken together, the work in this thesis sets up a strong precedence to develop small molecule inhibitors specific to DHHC20 to potentially eradicate the aggressive KRAS-driven adenocarcinoma.

## **Challenges**

### **Studying the Comprehensive Loss of EGFR Palmitoylation or DHHC20**

The true extent of the regulatory abilities of EGFR palmitoylation could be studied through complete loss of EGFR palmitoylation. In order to allow complete loss of EGFR palmitoylation, a triple mutation of all three critical cysteines must be expressed. The EGFR<sup>C1025A</sup> or EGFR<sup>C1122A</sup> reduced EGFR palmitoylation compared to wild type EGFR when expressed in HEK293T cells, but the double mutation is not sufficient to completely eliminate palmitoylation. The EGFR ABE followed by mass spectrometry



directly showed that both Cys1025 and Cys1034 sites exist as palmitoylated and unpalmitoylated, which is understandable as palmitoylation is a reversible modification. However, Cys1122 was never identified by the mass spectrometry as palmitoylated due to experimental technicality as the peptide containing Cys1122 was too large to be measured. Cys1122 was shown to be palmitoylated by generating the EGFR<sup>C1122A</sup> mutation and performing an ABE to show a decrease in overall EGFR palmitoylation. Unfortunately, the EGFR<sup>C1034A</sup> mutation was only detected by immunofluorescence (IF) as expressed in a small number of cells that seemed to be dying. These cells contained extremely high levels of phosphorylated ERK as seen by IF and taken together with the deteriorating morphology of the cells, these indications suggested that EGFR<sup>C1034A</sup> expressing cells were unable to progress through mitosis. As a result, we could not perform many studies concerning signaling effects using the EGFR<sup>C1034A</sup> mutant.

Given the immediate deteriorating phenotype observed upon the minimal expression of EGFR<sup>C1034A</sup>, we speculated that Cys1034 may be a primary palmitoylation site. Many kinases have a priming phosphorylation site that is required to be phosphorylated before other sites can be phosphorylated, including but not limited to cyclin-dependent kinase 2 (CDK2), Interferon-gamma factor 1 receptor (IGF1R) and protein kinase b (PKB), which are required to be phosphorylated in an activation segment with a conserved arginine and aspartate (thus named RD kinases) preceding phosphorylation for catalytic activity **(2)**. Similarly, we believe that there are priming palmitoylation sites; cysteines that require palmitoylation before any other cysteines can be palmitoylated. As such, if Cys1034 is in fact a prime site for palmitoylation, then upon expression of the EGFR<sup>C1034A</sup> perhaps neither Cys1025 nor Cys1122 would be able to get palmitoylated leaving EGFR completely unpalmitoylated. Given this potential understanding of Cys1034, we hypothesized that a complete loss of EGFR

palmitoylation is detrimental to the cell due to unstainable ERK activity. As we could not express EGFR<sup>C1034A</sup>, it was impossible to generate a viable triple mutant of EGFR Cys1025, Cys1122 and Cys1034.

A further hurdle arises in the fact that the wildtype, endogenous receptor is still being produced upon the expression of the aforementioned point mutants. The expression of the EGFR<sup>C1025A</sup> mutant is exogenous. EGFR<sup>C1025A</sup> receptor can homodimerize with other EGFR<sup>C1025A</sup> receptors, losing palmitoylation at Cys1025 completely, or with wildtype, endogenous EGFR receptors. Whether one monomer of EGFR<sup>C1025A</sup> has the capacity to impair the palmitoylation of its potentially wildtype monomer pair in a dominant negative manner remains unstudied. To study this, tagged EGFR<sup>C1025A</sup> and tagged wildtype EGFR can be co-expressed in HEK293T cells followed by a tag specific immunoprecipitation of the respective EGFR receptors, an ABE, and the SDS-PAGE analysis of the ABE samples. Western analysis using antibodies against the different tags will indicate the palmitoylation or lack thereof of the wildtype receptor upon association with the EGFR<sup>C1025A</sup> receptor. Regardless, the expressed wildtype receptor still has the capacity to homodimerize with other wildtype EGFR receptors or heterodimerize with other ERBB family members, such as HER2 (ERBB2) **(3)**. Upon the expression of a palmitoylation point mutant, these wildtype receptors will be normally palmitoylated and may compensate for the signaling capacity lost by the expressed unpalmitoylated receptors. Consequently, the growth defect and hindered signaling phenotype we observe upon expression of EGFR<sup>C1025A</sup> may be a subdued result given the compensation from the normally palmitoylated wildtype EGFR. As such, generating and expressing a triple palmitoylation EGFR mutant will still not phenotypically represent a complete loss of EGFR palmitoylation. To fully understand how palmitoylation regulates EGFR or even other receptors, we will have to find a way to completely inhibit

the specific palmitoylation of the receptors. One possible way to eliminate EGFR palmitoylation would be to inhibit the enzyme responsible, in this case DHHC20. However, other complications will follow this route.

We observed that shRNA knockdown of DHHC20 was never complete. As a result, knockdown of DHHC20 is also insufficient to produce a complete loss of EGFR palmitoylation. Knockout of the DHHC20 gene using the CRISPR/Cas9 system can be a method to overcome incomplete loss of DHHC20. However, with complete loss of DHHC20, there may be compensatory palmitoylation activity from other palmitoyltransferases. Expression analyses show that many other DHHC enzymes are expressed in lung tissue and cells, including DHHC5 and DHHC21 at the plasma membrane. In fact, almost all tissue types express multiple DHHCs both at the RNA and protein level (4, 5). Upon complete loss of DHHC20, expression of these other palmitoyltransferases could become amplified to subsequently be recruited to palmitoylate EGFR as a mechanism of signaling recovery especially in transformed cells.

To fully study the requirement of DHHC20, a DHHC20 conditional knockout mouse must be generated. There are no studies as of yet that have generated a DHHC20 knockout mouse and therefore, developmental phenotypes have not been observed and it remains unknown whether loss of DHHC20 is embryonic lethal. There are very few in vivo studies that have been performed involving any DHHC enzyme. The few examples that exist include studies with a targeted DHHC11 knockout mouse or a mouse that generates a spontaneous DHHC21 mutation. The DHHC11 knockout mice are viable and present with simply a decreased threshold for an auditory response (6). The DHHC21 mutant mouse that generate the aptly named *dep* (depilated) mutation

present with disoriented hair follicles and damaged hair **(7)**. Therefore, to determine the requirement of DHHC20 in vivo in the context of development or tumorigenesis, creation of a complete or conditional DHHC20 knockout mouse is a future necessity in this field.

### **Discrepancies in AKT Phosphorylation**

As mentioned, we originally found that the EGFR<sup>C1025A</sup> mutation increases the phosphorylation of EGFR and subsequently ERK, and AKT phosphorylation at Ser473. However, we then discovered that expression of EGFR<sup>C1025A</sup> decreases the phosphorylation of AKT at Thr308, which is directly downstream of PI3K. The Thr308 phosphorylation site of AKT has proven to be the initial site of AKT phosphorylation allowing AKT activity, however, the second phosphorylation at Ser473 allows for complete activation of AKT. The human AKT family of proteins consists of three major isoforms, AKT1, AKT2, and AKT3. Studies have shown that AKT1 and AKT3 have phosphorylation sites on both Thr308 and Ser473, whereas AKT2 apparently can only be phosphorylated at Thr308, suggesting that these isoforms are differentially regulated and are not redundant. Furthermore, these studies show that phosphorylation at Thr308 is critical for AKT function as all isoforms must be phosphorylated at Thr308 at the least **(8)**. Other studies have shown that key phosphatases, such as PP2A, are preferentially targeted to dephosphorylate AKT at Thr308 rather than Ser473, again indicating that AKT phosphorylation at Thr308 is critical for AKT activity **(9)**. Some studies have gone as far as to say that phosphorylation of AKT at Thr308 is a more reliable in vivo biomarker to predict tumor response to therapeutics. These studies found that the phosphorylation of Thr308 correlates with poor survival in NSCLC and acute myeloid leukemia, but there was no such correlation with AKT phosphorylation at Ser473. One group performed a detailed and quantitative examination of the activation of AKT in

normal and patient-matched tumor tissue from NSCLC patients. The concluded that Thr308 phosphorylation of AKT was a better predictor than Ser473 phosphorylation of AKT for poor overall survival in NSCLC and more importantly, Thr308 phosphorylation is a stronger indicator of AKT activity in tumor samples **(10)**. Our results were contradictory in terms of AKT activation as we saw an increase in Ser473 phosphorylation originally but then saw a drastic decrease in Thr308 phosphorylation. Taking these studies together with the context of our study, we determined that the loss of Thr308 phosphorylation upon loss of EGFR palmitoylation more accurately determined the activity of AKT as the observed phenotype alluded to a loss of AKT activity.

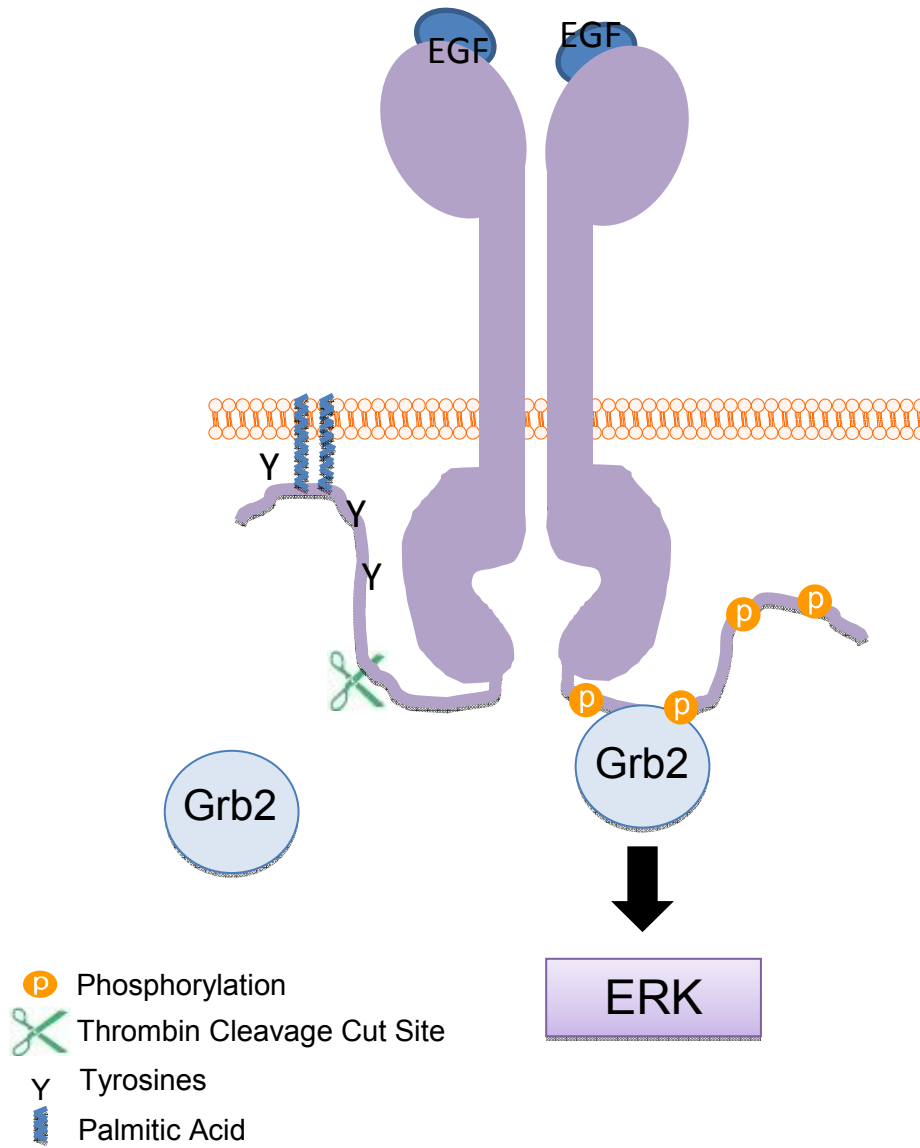
### **Spatial Functionality of Palmitoylation**

A palmitic acid moiety is a large hydrophobic entity. As can be assumed, this moiety will have steric or spatial consequences on the cellular surroundings. Furthermore, palmitic acid is strongly hydrophobic indicating that the palmitic acid moiety cannot reside in the hydrophilic cytoplasm and must be situated in hydrophobic surroundings, such as the plasma membrane or a pocket of a protein. In fact, upon discovery, palmitoylation was thought to specifically function as a modification that allowed proteins to anchor into the plasma membrane. Many integral and peripheral membrane proteins require palmitoylation to increase their hydrophobicity and localize to the membrane from the golgi apparatus; a well-known example is the membrane localization of the RAS protein isoforms **(11)**. More recently, in the nanoparticle realm, researchers have created a superhydrophobic coating material for the nanoparticles by modifying already hydrophobic zinc oxide with palmitic acid, generating a surface on which water will form a complete spherical droplet identified as superhydrophobic **(12)**.

Thereby, the scientific community has identified palmitoylation as a means to generate hydrophobicity in proteins allowing them to associate with membrane compartments.

Given this understanding of palmitoylation, we originally hypothesized that the palmitoylated C-terminal tail of EGFR is associating or “pinning” the tail to the plasma membrane. The C-terminal tail of EGFR is canonically depicted in crystal structures and in subsequent images as unstructured, extending away from the plasma membrane and the kinase domain. As such, we thought that the palmitic acid moiety could be adding structure to the C-terminal tail by promoting peripheral association with the plasma membrane, allowing the existing hydrophobic palmitic acid to bury itself into the hydrophobic lipid bilayer. We tested this hypothesis by adding a thrombin cleavage site at the start of the C-terminal tail of EGFR and performing a membrane isolation with and without the presence of DHHC20. Upon cleavage of the tail in the presence of DHHC20, there was a strong presence of the C-terminal tail in the membrane fraction which was partially lost when DHHC20 was removed from the equation (Refer to Page 64). This experiment suggested that in part the palmitoylated C-terminal tail of EGFR is associated with the plasma membrane. However, to accurately determine if the palmitoylated C-terminal tail is associated with the membrane, a crystal structure of EGFR in the presence of palmitoylation must be isolated. If so, the proposed inhibitory (to EGFR downstream activity) function of palmitoylation of the C-terminal tail can be understood because if the C-terminal tail is looped into the plasma membrane, scaffolding and other signaling proteins will have no access to the necessary binding motifs (Figure 1).

Figure 1



**Discussion Figure 1:** Model showing C-terminal tail looped into the plasma membrane disrupting access of scaffolding and other signaling proteins to the necessary binding motifs.

The result aforementioned indicated that upon the loss of DHHC20, there is still some presence of C-terminal tail in the membrane fraction (Refer to Page 64). As discussed above, we know that DHHC20 inhibition using shRNA is not a complete inhibition. As such, there may still be palmitoylated EGFR present contributing to that result. Ideally, this experiment can be advanced by adding a thrombin cleavage site to the beginning of the C-terminal tail of a triple palmitoylation mutant EGFR. This experiment will show that the unpalmitoylated EGFR C-terminal tail can no longer associate with the plasma membrane. However, as discussed, we were not able to generate a triple palmitoylation mutant of EGFR. Furthermore, the result aforementioned indicated that not all of the expressed EGFR C-terminal tail was isolated in the membrane fraction because the amount of full-length EGFR expressed was higher than the level of isolated C-terminal tail (Refer to Page 64). Firstly, the result will show only the cleaved C-terminal tails in the membrane fraction signifying that this could be a technical issue of the experiment in that the thrombin enzyme may not be efficient enough to cleave all EGFR molecules expressed. Secondly and more likely, the result indicates that not all palmitoylated C-terminal tails are anchored to the plasma membrane. The palmitic acid moiety may adjust the C-terminal tail in another manner.

As we progressed through the study, we determined that in fact there may be another structural function of palmitoylation. Recent studies have shown that some proteins have hydrophobic pockets where specifically acyl-moieties can interact. An example that has already been mentioned is the myristoylated N-terminal tail of the Src kinase, c-Abl. The myristoyl group can penetrate into a deep pocket in the kinase domain of c-Abl formed by a congregation of hydrophobic amino acid side chains. This loop of the N-terminal tail and myristoyl binding to the pocket is necessary to generate a critical inhibitory conformation of c-Abl. The residues that make up the myristate binding



pocket in c-Abl are conserved in the Abl paralog, Arg. In fact, the general structure of this kinase domain base incorporating the hydrophobic pocket is conserved amongst the Src kinases, suggesting that acylated moieties on these other kinases may interact with hydrophobic binding sites in the kinase domains. **(13,14)**. Recently, a group showed that a polypeptide conjugated to a small-molecule ligand binds to the enzyme glycogen phosphorylase a (GPa) at a hydrophobic binding site on the surface of the protein composed of hydrophobic amino acids **(15)**.

Given these examples of the existence of hydrophobic binding sites on proteins, we speculated that the EGFR kinase domain could also have a hydrophobic binding site where the C-terminal palmitoyl groups can interact. Groups in the EGFR dynamics field have shown that there are several states of tyrosine kinase activation. There is an inactive monomer and dimer state, a catalytically competent dimer that precedes phosphorylation and finally, an active conformation post-phosphorylation. These demonstrated that the inactive and catalytically competent states are defined by the presence of hydrophobic “spines” within the kinase domain composed of hydrophobic amino acid side chains. In particular, there is a small hydrophobic core that is formed by the structural helices required to maintain the kinase in the inactive conformation. Activation of the receptor requires conformational changes that specifically disrupt these hydrophobic spines and cores. **(16,17)** As we have determined that palmitoylation of the C-terminal tail is inhibitory to the activation of EGFR, it is possible that palmitoylation allows the C-terminal tail to loop and interact with these hydrophobic cores in the kinase domains keeping the receptor in the inactive conformation. Furthermore, as mentioned, we identified a cysteine in the kinase domain that has the capacity to be acylated. Although the palmitoylation of this cysteine, Cys751, was not experimentally confirmed, the presence of a modified cysteine furthers the notion that the kinase domain has a

deep hydrophobic capacity. Therefore, the palmitoylated EGFR C-terminal tail could be associating with the kinase domain. Further study of the EGFR structure in the presence of palmitoylation will shed light on this possibility.

Finally, we also speculated that the palmitic acid moiety on the C-terminal tail could be motif to which other proteins can interact. Other proteins might have a similar hydrophobic binding pocket as the above-mentioned examples. These proteins could have an affinity to the palmitic acid moiety on the C-terminal tail and thereby promote interaction with the receptor. One of the primary functions of palmitoylation is to modulate protein-protein interactions. Therefore, the requirement of palmitoylation for the necessary recruitment of interacting proteins to modulate signaling is extremely feasible and, as we have discovered, is occurring.

### **PI3K-Receptor Complex Formation**

PI3K/AKT signaling is one of the main component cascades downstream of EGFR. PI3K is composed of two subunits, the catalytic p110 subunit and the regulatory p85 subunit, which mediates binding to the receptor. The regulatory subunit, p85, has two SH2 domains that must be phosphorylated in order to induce the catalytic activity of p110 and initiate the remaining cascade. It is known that PI3K p85 binds to ERBB3 and ERBB4 directly at a recognized C-terminal tail motif, a phosphorylated Tyr-X-X-Met (PYXXM) motif **(18)**. Interestingly, EGFR (ERBB1) and ERBB2 do not contain the PYXXM motif on the C-terminal tail. Thus far, it has been shown that p85 interacts with EGFR indirectly through the adaptor protein, GAB1 (GRB2-associated binder), which bind the scaffold protein Grb2 **(19)**. It has also been proposed that PI3K is activated perhaps directly upon formation of EGFR heterodimers with other ERBB family members. We believe that we have found another mechanism by which p85 perhaps

interacts directly with EGFR or in the least, allows recruitment of p85 to the vicinity of EGFR in order to make necessary interactions.

We discovered that p85 preferentially binds to a generated palmitoylated C-terminal tail peptide of EGFR. Moreover, immunoprecipitation of p85 shows an interaction with wildtype EGFR that is completely lost upon expression of the palmitoylation-deficient EGFR<sup>C1025A</sup> mutation. We have seen that inhibition of EGFR palmitoylation significantly decreases PI3K/AKT signaling. Taken together, these data suggest that p85 in part requires the presence of palmitoylation on the C-terminal tail to be able to activate the pathway, although much more work is required to confirm this direct association. Work done on early signaling dynamics of EGFR in response to EGF stimulation shows that PI3K phosphorylation levels increase rapidly within 10-20 seconds of EGF stimulation followed by equilibration. Contrastingly, GAB1 show slower but more sustained increases in phosphorylation of relevant sites. Interestingly, the phosphorylation timing of the key phosphorylation sites on the C-terminal tail drastically differs from the rapid phosphorylation of PI3K. Specifically, the phosphorylation of the EGFR tyrosines take upwards to 80 seconds of EGF stimulation to reach the levels equivalent to PI3K phosphorylation at 10 seconds. **(20)** This indicates that something else on EGFR that is unconnected to the phosphorylation sites is allowing activation of PI3K prior to activation of the receptor or even GAB1. If PI3K is phosphorylated before GAB1 is phosphorylated, then GAB1 cannot be the only adaptor that is allowing activation of PI3K. This work adds precedence to the discovery that p85 binds to the palmitoylated EGFR tail early and this interaction could allow activation of PI3K.

Interestingly, it is well-studied that RAS interacts with PI3K at a RAS-binding domain (RBD) in p110. This binding and the subsequent stimulation of the PI3K pathway

is specific to the GTP-bound form of RAS. **(21)** Disruption of the RAS-PI3K interaction in progressed KRAS-driven NSCLC. showed partial regression suggesting the requirement of this interaction in the maintenance of KRAS-driven NSCLC. However, these data could not prove that this interaction was required for tumor initiation or development **(22)**. Very recently, another group showed that the RAS-PI3K interaction is required for the tumor onset and maintenance of EGFR-driven NSCLC despite the lack of presence of mutant KRAS **(23)**. Thus, the PI3K pathway is activated by interaction with RAS in both mutant-KRAS and mutant-EGFR settings. The background of most of our studies has been the presence of mutant KRAS. By inhibition EGFR palmitoylation in a mutant KRAS background, we discovered a significant loss of PI3K signaling. Given the studies discussed above, it would follow that activation of PI3K from its interaction with active RAS should compensate for the loss of PI3K signaling from unpalmitoylated EGFR. However, the above studies show that the interaction between RAS and PI3K is specifically between RAS and the RBD of the p110 subunit. These studies indicate, as it is not explicitly demonstrated, that the catalytic p110 subunit can be activated by its interaction with RAS and no longer requires the regulatory p85 subunit. However, we speculate that activity of PI3K, whether it be through interaction with a receptor or RAS, requires association with p85. This speculation can explain the drastic loss of PI3K signaling that we have observed upon the loss of EGFR palmitoylation. As there is no longer efficient recruitment of p85 due to the loss of palmitoylation, there is no PI3K signaling even from the interaction of RAS and p110. In order to demonstrate this speculation, RAS-p110 binding studies in the presence and absence of p85 need to be performed. However, given our results, we have revealed that loss of EGFR palmitoylation drastically affects recruitment of p85 to the vicinity of its activator and thus hinders PI3K activation.

## Challenges of In Vivo Genetic Manipulation

For scientists in cancer research field, in order to understand how cancer develops and metastasizes throughout the body and to discover more effective ways to diagnose and treat cancer, it is critical to conduct live animal research. Using live animals, we can understand how the active immune system and metabolism will affect the efficacy of manipulating a specific target. There are many advantages of using mice over other live animals or model organisms. For instance, their genome is 99% similar to that of the human genome and their small size allows for large scale/high throughput studies in a cost-efficient manner. To best recapitulate the genetics and histology of human tumors, genetically engineered mice models (GEMMs) were developed. In the most recent GEMMs, oncogenes are activated and/or tumor-suppressor genes are inactivated somatically at a chosen time and in a tissue-specific manner with expression of CRE recombinase. These GEMMs have become valuable tools to study the pathways and mechanisms underlying human disease on a cellular and molecular level; complex processes, such as cancer initiation, progression, metastasis formation, and the involvement of the tumor microenvironment. Thereby, studies using GEMMs have also been crucial to enable the development of novel targeted treatments.

However, like many scientific methods, GEMMs also have limitations and technical challenges. A major limitation of germline GEMMs is that development and validation of these models is time-consuming and laborious. For example, introducing a novel germline mutation into an existing multi-allelic mouse model requires extensive breeding and genotypic validation after each round. We were lucky enough to have a readily available GEMM that ideally served the purposes of the work in this thesis. This mouse model is called the  $Kras^{LSL-G12D/+}; Trp53^{flox/flox}; Rosa26^{LSL-YFP}$ . In this model,

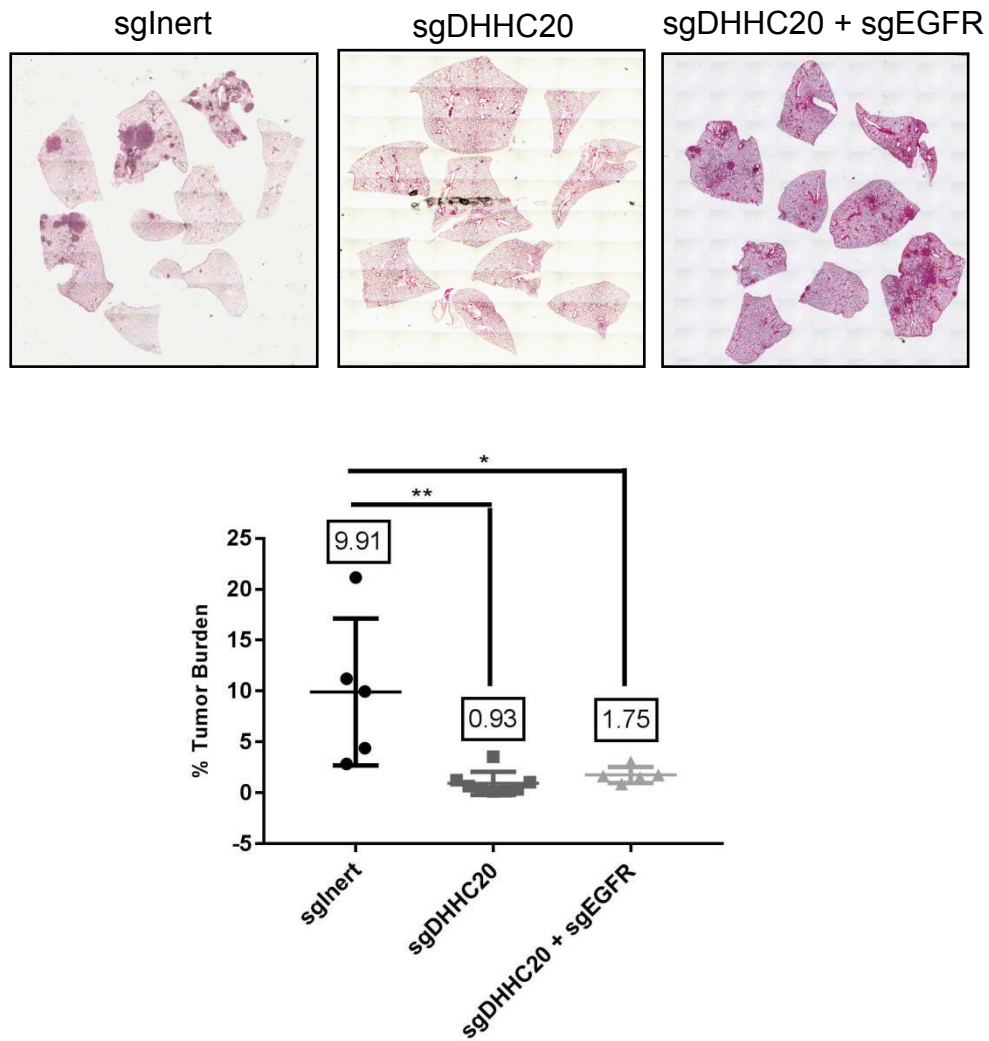
expression of Cre recombinase is induced virally in the lung to turn on expression of KrasG12D, delete the *p53* gene and turn on expression of the YFP reporter in the same cell. This model recapitulates the initiation and progression of mutant KRAS lung adenocarcinoma.

We manipulated the viral plasmid housing the promoter driven Cre recombinase by introducing gene components of the CRISPR/Cas9 system driven by a EF1alpha promoter and a guideRNA (sgRNA) targeting the DHHC20 gene driven by a U6 promoter. Thereby, the virus generated using this CRISPR-Cre plasmid can be used to infect lung cells subsequently deleting DHHC20 in the same cells that have KRAS<sup>G12D</sup> expressed and *p53* deleted. Using the CRISPR/Cas9 system brought upon its own set of challenges. Primarily, Cas9 enzymes have the ability to cut the wrong genes even when driven by a nucleotide guided sequence preceding the sgRNA producing potential off-target cleavage events. To minimize these events, we generated two very specific sgRNAs targeting DHHC20 and validated these sgRNAs in cell lines prior to introduction into the mice. Deletion of DHHC20 using both sgRNAs resulted in a drastic decrease in mutant KRAS tumorigenesis measured by analysis of tumor burden in the lung.

In cell lines, we were able to test the requirement of the presence of EGFR when DHHC20 is deleted to produce the growth defect phenotype in a KRAS mutant background. Ideally, we sought to recapitulate this result in vivo. We generated a plasmid that contained the CRISPR/Cas9 system, Cre recombinase and sgRNAs targeting both DHHC20 and EGFR. We expected that deletion of EGFR and DHHC20 would rescue the tumor burden similar to the results observed in vitro. However, we did not observe a significant return of tumor growth upon deletion of both EGFR and DHHC20 (Figure 2). On further inspection, we determined that this result was due to

limitations of the CRISPR/Cas9 system with two sgRNAs. As the sgRNAs are driven by the same promoter, placement of the sgRNAs with respect to the promoter seems to affect the efficiency of the guide. As the sgRNA targeting DHHC20 was placed right next to the promoter, the CRISPR/Cas9 system was more efficient in deleting DHHC20 and could not effectively delete the EGFR gene. Furthermore, the length of the EGFR gene is significantly larger (4 kb) than that of DHHC20 (<1 kb). The CRISPR/Cas9 system has limitations on the length of the gene that can be deleted efficiently. However, deletions of up to 60kb in length have been generated **(24)**.

**Figure 2**



**Discussion Figure 2:** Deletion of EGFR and DHHHC20 does not rescue KPY tumor burden unlike in vitro, where inhibition of EGFR and DHHHC20 rescued the cell growth defect seen upon loss of DHHHC20.



To confirm deletion of DHHC20 in the lung tissue upon introduction of the Viral-CRISPR/Cre, immunohistochemistry (IHC) and immunofluorescence (IF) using the available antibodies to DHHC20. Unfortunately, there are no antibodies against mouse DHHC20 and the available antibodies against human DHHC20 have not been tested for use in IHC or IF. As a result, DHHC20 could not be detected by even in the control lung tissue. Therefore, we could not determine by IHC or IF that DHHC20 was deleted in the experimental cohort. Furthermore, the lack of tumor lesions in the DHHC20 deleted cohort made it difficult to stain anything. To step around this challenge, we stained lung tissues from the control cohort and DHHC20 deleted cohort with antibodies against pERK. Given our in vitro results showing an increased expression of pERK upon inhibition of DHHC20 in KRAS mutant cells, we expected that the small tumor lesions that we observed in the DHHC20 deleted lung tissues would stain higher for pERK than the control tissue. In fact, that was the result we observed. Taking the drastic phenotype of lost tumor burden and the increased expression of pERK in the DHHC20 deleted lung tissues, we determined that the CRISPR/Cas9 system efficiently deleted DHHC20. We faced a similar challenge with the overexpression vector that we generated. This plasmid contains Cre recombinase gene driven by the PGK promoter and gene encoding wildtype EGFR or EGFR<sup>C1025A</sup> or EGFR<sup>L858R</sup> driven by an Actin promoter. This viral vector was named pCREator. We observed that expression of EGFR<sup>C1025A</sup> drastically reduced lung tumor burden more than even expression of EGFR<sup>L858R</sup>, which has been shown previously to hinder mutant KRAS tumorigenesis. The pCREator viral vectors were tested and validated for EGFR and Cre expression in vitro. However, to validate the phenotype in vivo, we had to show expression of human EGFR in the EGFR overexpressing cohorts. Antibodies against human EGFR were used to detect

overexpression of EGFR via IF but the overexpression was more difficult to determine using IHC.

Another challenge we faced was quantifying the infection efficiency of both the CRISPR-Cre and the pCREator viruses. The phenotype of a drastic loss in tumor burden that we see upon deletion of DHHC20 or expression of EGFR<sup>C1025A</sup> could be result of unequal infection between the control and the experimental viruses. Therefore, it was critical to prove that the viruses infect cells at the same efficiency. Each virus was generated and titered before being introduced into the mice. Viral titers are calculated by performing a plaque-forming assay using different volumes at 10-fold dilutions of the generated virus. Plaques formed are counted and the virus is given a titer of plaque-forming units (PFU) per milliliter. The mice cohorts were given equivalent amounts of virus (60000 PFU/ml) according to the calculated titer. However, equivalent amount of virus does not equate with the efficiency of the virus or the infection rate. To approximately determine if the different viruses being compared had a similar infection rate, the Rosa26<sup>LSL-YFP</sup> reporter in the mouse model was utilized. Each cell in the lung infected with any of the viral vectors will express Cre recombinase and Cre will remove the stop cassette flanked by the loxP sites in the Rosa26 gene, thereby turning on expression of yellow fluorescent protein (YFP) that can be easily detected by IHC and IF. After IHC staining using antibodies against YFP, we counted the YFP positive spots in each cohort of mice representing infection locales. In the control cohort, a tumor was counted as one infection site. Similarly, in the DHHC20 deleted or EGFR<sup>C1025A</sup> expressing cohorts, each visible lesion was considered one infection site. We observed that between the control and experimental cohorts, there were an equivalent number of YFP positive sites. Taking this data, we determined that the viral vectors had approximately the same infection rate.

The GEMM and the genetic manipulation using viral vectors represents the effects of DHHC20 deletion or expression of EGFR<sup>C1025A</sup> on tumor initiation as DHHC20 is deleted at the same time that KRAS<sup>G12D</sup> is expressed and *p53* is deleted. Therefore, the question still remains whether loss of DHHC20 effects the progression of mutant KRAS cancer. It will be more clinically relevant to determine if the loss of DHHC20 effects tumor progression, whether that be regression or stability, as patients often present with already progressed disease. To study cancer progression, we chose to use mice xenografts generated by subcutaneous transplantation of human KRAS mutant lung cancer cell lines into which we stably introduced doxocycline-inducible shRNA targeting DHHC20. In this model, human mutant KRAS cancer can be generated followed by induction of the DHHC20 shRNA using doxocycline treatment to test if inhibition of DHHC20 in an established tumor can cause regression. There are several advantages of the xenograft model. Xenografts utilize human cells or tissue allowing the study of the complex genetic and epigenetic abnormalities that exist in human disease. Results from xenografts are acquired in a few weeks whereas GEMM often take months to a year to develop and test. Finally, xenografts can be used to help in the development and to quickly test the efficacy of targeted molecular therapies. **(25)** Although we have not yet acquired results from this model, we have been able to generate viable xenografts and have optimized doxocycline treatment for the mice to obtain the most efficient expression of the inducible shRNA against DHHC20. This model will be critical in the future to test the small molecule inhibitors against DHHC20 that we are aiming to eventually develop.

## Future Ideas

### Universality of Palmitoylation

Throughout the course of this thesis work, many enlightening facets of palmitoylation and its newfound role in regulation of receptor signaling have been discovered. However, there is much more work to be done to understand the full molecular scope of palmitoylation and its role in regulating signaling cascades. As we have discovered, palmitoylation seems to be inhibitory for EGFR activity as when we remove palmitoylation, EGFR is hyperactivated. As aforementioned, work done in the Witze lab demonstrates that many other receptor tyrosine kinases have cysteines on the C-terminal tails and in fact, we have found that receptor involved in critical signaling cascades, such as the insulin receptor (IR) and fms-like tyrosine kinase 3 (FLT-3) in the hematopoietic environment, are palmitoylated. Often, the innate sources of disease initiation and progression are a mutation in the receptor rendering it hyperactive or subsequent distortions in the signaling cascades downstream of these receptors. For example, a FLT-3 internal tandem duplication (ITD) mutation renders FLT-3 and the subsequent cascades downstream, primarily PI3K/AKT and MAPK, constitutively hyperactive. These distortions drive generation and progression of acute myeloid leukemia (AML). FLT-3 inhibitors are currently first line therapy for AML patients with the FLT3-ITD mutation. However, as with many TKIs, prolonged treatment can generate secondary mutations causing drug resistance. **(26)** As such, there is a need to study alternate mechanism of receptor signaling control and manipulating palmitoylation may be a new therapeutic approach. Our work on palmitoylation of various receptors and how it affects the activity of these receptors is being continued. As these receptors are expressed in different cell types, such as FLT-3 in hematopoietic cells, and different

locations, it is likely that different DHHC enzymes palmitoylate different receptors and much work is needed to identify these enzyme-substrate pairs. Additionally, the 23 DHHC enzymes palmitoylate thousands of protein substrates in the cell. Thus, there must be a mechanism of substrate recognition that is also to be determined. Taken together, this future work may identify a potential universal function of receptor palmitoylation that can be manipulated to treat a plethora of signaling dependent diseases.

### **Temporal Dynamics of Palmitoylation**

Another primary question that arose after the discovery that EGFR is palmitoylated was the temporal dynamics of palmitoylation with respect to phosphorylation. In other words, the connection between palmitoylation, given that it is inhibitory for EGFR activity, and phosphorylation, which transmits activity of the receptor, remains unclear. Palmitoylation is reversible indicating that there is an on/off rate. To determine the on/off rate of EGFR palmitoylation, a pulse-chase experiment with 17-ODYA metabolic labeling followed by click chemistry at various time points can be used. We have crudely determined that the total wildtype EGFR population, in active or inactive conformation, is palmitoylated before ligand stimulation. Ligand stimulation induces a modest increase in the level of palmitoylation, which then gradually return to basal levels. By isolating specifically phosphorylated EGFR and performing an ABE, we observed that dual palmitoylated/phosphorylated EGFR exists at some given time and this receptor is turned over as dually palmitoylated/phosphorylated. However, we still do not know if ligand binding and/or phosphorylation of the receptor induces palmitoylation as a means to inhibit the activity or if palmitoylation is temporarily displaced by phosphorylation. Ideally, the temporal dynamics of palmitoylation could be determined

using immunofluorescence and live cell imaging if an antibody to palmitoylated EGFR were developed. Currently, we are attempting to isolate phosphorylated EGFR at early timepoints after ligand stimulation and performing the ABE assays to measure the amount of dual palmitoylated/phosphorylated EGFR over time.

### **Development of Inhibitor against DHHC20**

The foremost proposal for the future is the development of an inhibitor against DHHC20. DHHC20 is an enzyme that has the capacity to be inhibited. Furthermore, DHHC20 resides on the plasma membrane allowing accessibility to compounds. On the plasma membrane, DHHC20 has transmembrane loops that are exposed in the extracellular matrix and in the context of lung adenocarcinoma, DHHC20 is overexpressed. As such, it is possible to take a monoclonal antibody approach to inhibiting DHHC20, specifically in cancer cells. Monoclonal antibodies interact with a larger region of the target molecule's surface, allowing for better discrimination between closely related targets and providing higher affinity. This high specificity that can be established using monoclonal antibodies is the basis for their lack off-target toxicity, which is a major concern with small-molecule drugs. However, this approach will require that the exposed loops have a functional responsibility for the protein. As of yet, our DHHC20 sequence studies suggest that the residues on the loop are largely responsible for protein shape as opposed to having a functional purpose. Furthermore, these residues seem to be conserved across all DHHC enzymes further indicating their role in simply connecting secondary structures. Without a distinct target region, generating a monoclonal antibody specifically targeting DHHC20 is difficult. Thereby, a monoclonal antibody against DHHC20 may not be the ideal therapeutic approach.

Current inhibitors of palmitoylation have been limited to 2-bromopalmitate (2-BP), cerulenin, and tunicamycin. The most commonly used is 2-BP, which is a non-metabolizable palmitate analog with a bromide group. The exact mechanism of action of 2-BP is not fully understood, but it is speculated that it binds to palmitoyl-transferases and the bromide prevents the transfer of 2-BP to the substrate. It has been shown that 2-BP inhibits palmitoylation in cells and activity of DHHC proteins in vitro using an established palmitoyl-acyltransferase (PAT) activity assay **(27)**. However, 2-BP inhibits all DHHC enzymes without specificity. Furthermore, 2-BP also inhibits fatty acid CoA ligase and many other enzymes involved in lipid metabolism. Cerulenin and tunicamycin are even more non-specific inhibitors of palmitoylation. Cerulenin is mainly used to inhibit fatty acid synthesis and tunicamycin is mainly used to inhibit N-glycosylation. A group has developed a high throughput screen (HTS) for inhibitors of palmitoylation. High-throughput screening (HTS) involves the screening of an entire compound library directly against the drug target or in a cell-based assay, whose activity is dependent upon the target. In this cell-based assay, membranes isolated from MCF-7 cells were used as the source of PAT activity. The substrates for the activity included fluorescently-labeled peptides mimicking myristoylated and palmitoylated proteins, such as c-Src, or farnesylated and palmitoylated proteins, such as N- and H-RAS, to evaluate the ability of screened compounds to inhibit palmitoylation in vitro. **(28)** Five compounds inhibited palmitoylation of either the myristoylated/palmitoylated or farnesylated/palmitoylated peptides. As cell membranes were used in this case as the source of PAT activity, this assay did not demonstrate that the inhibitors reduced palmitoylation by directly blocking DHHC proteins as opposed to any other acyltransferases. Another group used four different purified DHHC enzymes with larger protein fragments as substrates for in vitro PAT assays to evaluate if these compounds can inhibit DHHC-mediated palmitoylation

of protein substrates. Furthermore, the level of DHHC inhibition of these inhibitors was compared to that of 2-BP. They found that compound V (CV), behaved similarly to 2-BP as it inhibited all four of the tested DHHCs. They also unfortunately discovered that, unlike 2-BP, inhibition by CV is reversible and requires a higher concentration of inhibitor compared to 2-BP. **(29)** As such, CV is still not clinically viable and is not specific to individual DHHCs. However, this study has now provided a candidate that can be used as a starting point to rationally reduce compound libraries for HTS and can be manipulated with structural/side-chain substitutes focused on enhancing potency and specificity.

The crystal structure of DHHC20 was recently isolated providing necessary structural insight into direct and indirect binding sites of the enzyme potentiating structural-aided drug design **(30)**. Now we can collaborate with the Banerjee group that discovered the structure of DHHC20 to isolate a DHHC20 crystal with CV docked to provide understanding of the enzyme-inhibitor binding location. Our *in vitro/in vivo* mechanism of action studies allow the development of a high-throughput compound screen (HTS) (similar to that used to isolate CV) to identify potential inhibitory small molecules. HTS are fairly effective in quickly discovering new compounds, however, HTS is only as effective as the assay format chosen for the output. This assay is dependent upon the biology of the drug target protein, the equipment and financial infrastructure in the laboratory, whether an inhibitor or activator molecule is needed, and the scale of the compound screen. Another important factor to consider when designing an assay is the pharmacological relevance of the assay. Relevant cell types and conditions must be used to understand the effect of the screened compounds on the biological disease state. Furthermore, the assay must be reproducible so that multiple compounds can be screened with comparable results across the experiments. Lastly,



each assay should control for the organic solvents, such as ethanol or DMSO, in which inhibitors are dissolved.

Currently, we are developing a cell-based assay that is dependent on the specific presence and activity of DHHC20. In basic, we are designing a fluorometric assay using expression of differentially tagged ERK and Myc in human mutant KRAS cancer cells based on the mechanism we have postulated in this thesis. We have access to multiple compound libraries from the screening core at the university and a library available through the National Institute of Health (NIH). Here, we can use the structure of CV upon binding to DHHC20 to help predict where modifications could be added to provide increased potency or selectivity and to prune or tailor the extensive compound libraries. Compounds that activate ERK and lose Myc expression will be selected for secondary screening. In the colorimetric assay, we will be able to see the strengthening of the color attributed to ERK and the diminishing of the color attributed to Myc. Subsequently, we will design a DHHC20 activity assay for the secondary screening of selected compounds to identify those that directly inhibit DHHC20 activity. In this *in vitro* assay, purified DHHC20 and palmitoyl-CoA will be incubated with a EGFR C-terminal tail peptide with present cysteines. DHHC20 will not be able to transfer the palmitoyl-CoA to the substrate cysteine in the presence of compounds that will inhibit DHHC20. Then we will have to test the efficacy of these compounds in inhibiting other DHHC enzymes to solidify specificity to DHHC20. When a few compounds are isolated, we can test the preclinical efficacy in our already designed and used experiments described in this thesis. Additionally, we have an established mouse model in which we will be able to test lead compounds *in vivo*.

## Concluding Remarks

The palmitoylation field is fairly new in the realm of scientific study especially in the context of cancer. As such, there is much to do before the scientific community will understand the cellular magnitude of palmitoylation. This thesis challenges the canonical understanding of receptor signaling dynamics by showing that a seemingly inconsequential post-translational modification can assert control on disease defining signaling proteins, such as EGFR. Furthermore, loss of EGFR palmitoylation by inhibition of DHHC20 has the capacity to block mutant KRAS tumorigenesis. Inhibiting EGFR palmitoylation activates the receptor and active EGFR is incompatible with the presence of mutant KRAS described as synthetically lethal. In other words, this thesis has discovered and validated a novel therapeutic target that blocks the growth of KRAS-driven adenocarcinoma, which is the most difficult form of NSCLC to treat. We believe that using a DHHC20 inhibitor in combination with clinically available inhibitors to EGFR or PI3K can lead to regression of KRAS-driven NSCLC and perhaps complete remission. It is our hope that the work in this thesis will inspire further study of the uncharted functions of protein palmitoylation and of the deep mechanistic dynamics of tyrosine kinase receptor regulation still not fully understood.

## References

1. Chen S, Zhu B, Yin C, et al. Palmitoylation-dependent activation of MC1R prevents melanomagenesis. *Nature*. **549(7672)**:399-403, 2017.
2. Nolen B1, Taylor S, Ghosh G. Regulation of protein kinases; controlling activity through activation segment conformation. *Mol Cell*. **15(5)**:661-75, 2004.
3. Spears, M. & Bartlett, J.M. Human epidermal growth factor receptor dimerization analysis in breast cancer diagnosis: potential for improving testing accuracy and treatment selection. *Mol. Diagn. Ther.* **13**: 359–365, 2009.
4. Uhlen M et al. Towards a knowledge-based Human Protein Atlas. *Nat Biotechnol*. 2010.
5. Human Protein Atlas available from [www.proteinatlas.org](http://www.proteinatlas.org)
6. Oku S, Takahashi N, Fukata Y, Fukata M. In silico screening for palmitoyl substrates reveals a role for DHHC1/3/10 (zDHHC1/3/11)-mediated neurochondrin palmitoylation in its targeting to Rab5-positive endosomes. *J Biol Chem*. **288(27)**:19816-29, 2013.
7. C. Mayer, Thomas & Kleiman, Norman & C. Green, Margaret. Depilated (dep), a Mutant Gene That Affects the Coat of the Mouse and Acts in the Epidermis. *Genetics*. (**84**):59-65, 1976.
8. Vanhaesebroeck B, Alessi DR. The PI3K-PDK1 connection: more than just a road to PKB. *Biochem J*. **346(3)**:561-76, 2000.
9. Kuo YC, Huang KY, Yang CH, Yang YS, Lee WY, Chiang CW. Regulation of phosphorylation of Thr-308 of Akt, cell proliferation, and survival by the B55alpha regulatory subunit targeting of the protein phosphatase 2A holoenzyme to Akt. *J Biol Chem*. **283(4)**:1882-92, 2008.

10. Vincent EE, Elder DJ, Thomas EC, et al. Akt phosphorylation on Thr308 but not on Ser473 correlates with Akt protein kinase activity in human non-small cell lung cancer. *Br J Cancer*. **104(11)**:1755-61, 2011.
11. Rocks O, Peyker A, Kahms M, Verveer PJ, Koerner C, Lumbierres M, Kuhlmann J, Waldmann H, Wittinghofer A, Bastiaens PI. An acylation cycle regulates localization and activity of palmitoylated Ras isoforms. *Science*. **(5716)**:1746-52, 2005.
12. Agrawal, Nikhil, Munjal, Sandeep, Ansari, Mohd Zubair and Khare, Neeraj. Superhydrophobic palmitic acid modified ZnO nanoparticles. *Ceramics International*. 2017.
13. Hantschel O1, Nagar B, Guettler S, Kretzschmar J, Dorey K, Kuriyan J, Superti-Furga G. A myristoyl/phosphotyrosine switch regulates c-Abl. *Cell*. **112(6)**:845-57, 2003.
14. Nagar B1, Hantschel O, Young MA, Scheffzek K, Veach D, Bornmann W, Clarkson B, Superti-Furga G, Kuriyan J. Structural basis for the autoinhibition of c-Abl tyrosine kinase. *Cell*. **112(6)**:859-71, 2003.
15. Balliu A1, Baltzer L1. Exploring Non-obvious Hydrophobic Binding Pockets on Protein Surfaces: Increasing Affinities in Peptide-Protein Interactions. *Chembiochem*. **18(14)**:1396-1407, 2017.
16. Shih AJ, Telesco SE, Choi SH, Lemmon MA, Radhakrishnan R. Molecular dynamics analysis of conserved hydrophobic and hydrophilic bond-interaction networks in ErbB family kinases. *Biochem J*. **436(2)**:241-51, 2011.
17. Kornev AP, Haste NM, Taylor SS, Eyck LF. Surface comparison of active and inactive protein kinases identifies a conserved activation mechanism. *Proc Natl Acad Sci U S A*. **103(47)**:17783-8, 2006.

18. Soltoff SP, Carraway KL, Prigent SA, Gullick WG, Cantley LC. ErbB3 is involved in activation of phosphatidylinositol 3-kinase by epidermal growth factor. *Mol Cell Biol.* **14(6)**:3550-8, 1994.
19. Mattoon DR, Lamothe B, Lax I, Schlessinger J. The docking protein Gab1 is the primary mediator of EGF-stimulated activation of the PI-3K/Akt cell survival pathway. *BMC Biol.* **(2)**:24, 2004.
20. Reddy RJ, Gajadhar AS, Swenson EJ, Rothenberg DA, Curran TG, White FM. Early signaling dynamics of the epidermal growth factor receptor. *Proc Natl Acad Sci U S A.* **113(11)**:3114-9, 2016.
21. Castellano E, Downward J. RAS Interaction with PI3K: More Than Just Another Effector Pathway. *Genes Cancer.* **2(3)**:261-74, 2011.
22. Castellano E, Sheridan C, Thin MZ, et al. Requirement for interaction of PI3-kinase p110 $\alpha$  with RAS in lung tumor maintenance. *Cancer Cell.* **24(5)**:617-30, 2013.
23. Murillo MM, Rana S, Spencer-Dene B, Nye E, Stamp G, Downward J. Disruption of the Interaction of RAS with PI 3-Kinase Induces Regression of EGFR-Mutant-Driven Lung Cancer. *Cell Rep.* **25(13)**:3545-3553, 2018.
24. Pelletier S, Gingras S, Green DR. Mouse genome engineering via CRISPR-Cas9 for study of immune function. *Immunity.* **42(1)**:18-27, 2015.
25. Richmond A, Su Y. Mouse xenograft models vs GEM models for human cancer therapeutics. *Dis Model Mech.* **1(2-3)**:78-82, 2008.
26. Fathi AT, Chen YB. Treatment of FLT3-ITD acute myeloid leukemia. *Am J Blood Res.* **1(2)**:175-89, 2001.

27. Varner AS, Ducker CE, Xia Z, Zhuang Y, De Vos ML, Smith CD.  
Characterization of human palmitoyl-acyl transferase activity using peptides that mimic distinct palmitoylation motifs. *Biochem J.* **(373)**:91–9, 2003.
28. Ducker CE, Griffel LK, Smith RA, et al. Discovery and characterization of inhibitors of human palmitoyl acyltransferases. *Mol Cancer Ther.* **(7)**:1647-59, 2005.
29. Jennings BC, Nadolski MJ, Ling Y, et al. 2-Bromopalmitate and 2-(2-hydroxy-5-nitro-benzylidene)-benzo[b]thiophen-3-one inhibit DHHC-mediated palmitoylation in vitro. *J Lipid Res.* **50(2)**: 233-42, 2009.
30. Rana MS, Kumar P, Lee CJ, Verardi R, Rajashankar KR, Banerjee A. Fatty acyl recognition and transfer by an integral membrane S-acyltransferase. *Science.* **359(6372)**, 2018.